Selective Hydrogenation of Acetylene over Pd, Au, and PdAu Supported Nanoparticles

By

Michael P. Walker

A dissertation submitted to the
Faculty of Graduate and Postdoctoral Studies
in partial fulfillment of the requirements
for the degree of Masters in Chemistry

University of Ottawa
Ottawa, Ontario

© Michael Walker, Ottawa, Canada, 2014

Abstract

The removal of trace amounts of acetylene in ethylene streams is a high-volume industrial process that must possess high selectivity of alkyne hydrogenation over hydrogenation of alkenes. Current technology uses metallic nanoparticles, typically palladium or platinum, for acetylene removal. However, problems arise due to the deactivation of the catalysts at high temperatures as well as low selectivities at high conversions.

Pore expanded MCM-41 is synthesized via a two-step strategy in which MCM-41 was prepared via cetyltrimethylammonium bromide (CTMABr) followed by the hydrothermal treatment with N,N-dimethyldecylamine (DMDA). This material was washed with ethanol to remove DMDA, or calcined to remove both surfactants. PE-MCM-41 based materials were impregnated with palladium, gold, and palladium-gold nanoparticles. The removal of DMDA had an effect on both the conversion and selectivity, in which they were found to drop significantly. However, by using the bimetallic PdAu catalysts, higher selectivity could be achieved due to increased electron density.

Table of Contents

Chapter 3-Experimental & Instrumentation

Chapter 4-Results and Discussion

Chapter 5- Conclusion and Future Work

List of Figures

Chapter 2

Chapter 3

Chapter 4

List of Tables

Chapter 2

Chapter 4

List of Abbreviations

APTES	3-aminopropyltriethoxysilane
Au-PE-MCM-41-W	Gold PE-MCM-41 water washed catalyst
Au-PE-MCM-41-Et	Gold PE-MCM-41 ethanol washed catalyst
Au-PE-MCM-41-CR	Gold PE-MCM-41 calcined reduced catalyst
BET	Brunauer-Emmett-Teller
BJH	Barret-Joyner-Halenda
CTAB	Cetyltrimethylammonium bromide
$CTMA^+$	Cetyltrimethylammonium ions
DMAP	(N, N-dimethyl-3-aminopropyl) trimethoxysilane
DMDA	N, N-Dimethyldecylamine
d_p	Pore Size
E_a	Activation Energy
eV	Electron Volts
Fau	Faujasite
FTIR	Fourier Transform Infrared Spectroscopy
GC	Gas Chromatography
ICP	Inductively Coupled Plasma
IR	Infrared Radiation
KJS	Kruk-Jaroniec-Sayari
MCM-41	Mobil Composition of Matter Number 41
MCM-48	Mobil Composition of Matter Number 48
MCM-50	Mobil Composition of Matter Number 50
PdAu-PE-MCM-41-W	Palladium-Gold PE-MCM-41 water washed catalyst
PdAu-PE-MCM-41-Et	Palladium-Gold PE-MCM-41 water washed catalyst
PdAu-PE-MCM-41-CR	Palladium-Gold PE-MCM-41 water washed catalyst

Pd-PE-MCM-41-W	Palladium PE-MCM-41 Water Washed Catalyst
Pd-PE-MCM-41-Et	Palladium PE-MCM-41 Ethanol Extracted Catalyst
Pd-PE-MCM-41-CR	Palladium PE-MCM-41Calcined Reduced Catalyst
PE-MCM-41	Pore expanded Mobil Composition of Matter 41
PE-MCM-41-W	Pore Expanded MCM- 41Water Washed
PE-MCM-41-Et	Pore Expanded MCM-41 Ethanol Washed
PE-MCM-41-CR	Pore Expanded MCM-41 Calcined Reduced
ppb	Parts Per Billion
ppm	Parts Per Million
S_A	Surface Area
SBA-15	Santa Barbara Amorphous Number 15
SBA-1	Santa Barbara Amorphous Number 1
SEM	Scanning Electron Microscopy
STEM	Scanning Transmission Electron Microscopy
TCD	Thermal Conductivity Detector
TGA	Thermogravimetric Analysis
TMAOH	Tetramethylammonium hydroxide
TOF	Turnover Frequency
TOS	Time on steam
TPR	Temperature Programmed Reduction
UV	Ultra Violet
V_P	Pore Volume
XRD	X-Ray Diffraction
XPS	X-Ray Photoelectron Spectroscopy

Acknowledgements

First, I would like to thank my supervisor, Dr. Abdelhamid Sayari for providing me with the opportunity to work in his group and to discover a new field of solid state and materials chemistry. I am deeply grateful to him for all the motivation, advice, direction, and freedom he has provided me with.

Secondly, I would like to thank Dr. Pryiabat Dash for his time spent helping me, showing me around the lab, and helping me understand my project. His guidance and experience are invaluable to me.

I would also like to thank Dr. Yong Yang for all his help and guidance surrounding the characterization techniques of my samples.

I thank the Canadian Center for Electron Microscopy at McMaster University, particularly Dr. Glynis de Silveira, for running scanning transmission electron microscopy on my catalysts.

I also need to thank Dr. Nimal De Silva for the determination of my metal loadings of my catalysts through ICP analysis.

My colleagues also need to be thanked: Asieh Ahmadalinezhad, Ritesh Tailor, Alexis Theriault, Mohamed Abboud, Nansi Fakhri, Govind Sethia, and Walaa Baslyman. Thank you all for your friendship, help, and invaluable experience throughout my time here.

I also need to thank my family, particularly my mother, Dawn, and my brother, Daniel for all their love, patience, and support during my time in Ottawa.

Chapter 1: Introduction and Motivation

Porous materials have been widely used as adsorbents, catalysts, or drug delivery systems since the 1990's in a wide range of processes. They possess high surface areas, pore sizes, and pore volumes while maintaining high hydrothermal and mechanical stability. Porous solids are typically defined by their pore size, pore size distribution, and the structural arrangement of the pores.

Ordered mesoporous materials represent a very important class of molecular sieves that are made up of arrays of long ordering, tuneable textural properties (pore volume, surface area, etc), and controllable pore size and a narrow pore size distribution. The structure of the pores is periodic and the pore size distribution is narrow with the pore size being between 2-50 nm. Since the discovery of mesoporous silica by Mobil Corporation, there has been a vast number of papers published based on their controlled synthesis, characterization, and applications. The demand for porous solids with specific frameworks and surface properties has been rapidly expanding due to exhibited control on several properties of the material. This has led to developments in catalysis, sustained drug release, electronic sensors, and bioceramics. Even though there has been development in many areas with regards to new processes for porous materials, a greater understanding of how they work is still desired.

The work at hand is concerned with developing monometallic and bimetallic supported catalysts for the selective hydrogenation of acetylene. There are issues pertaining to the selective hydrogenation of acetylene, which include selectivity, activity, and lifetime of catalysts. In order to address these issues, the use of Pd, Au, and PdAu supported

nanoparticles on different pore-expanded MCM-41 silicas were used. There are also several other objectives and questions that needed to be understood and answered.

1. To prepare pore-expanded MCM-41 and the palladium, gold, and palladium-gold supported nanoparticles.
2. The catalysts and the pore-expanded MCM-41 silica need to be characterized through various techniques, as described below
3. The catalytic reactions need to be run in order to determine the conversion, selectivity, and turnover frequency of the catalysts.
4. Finally, catalyst deactivations were studied to determine the stability of the catalysts.

Chapter one focuses on a brief introduction to porous and mesoporous silica materials. It also introduces supported nanoparticle catalysis and the issues at hand regarding the selective hydrogenation of acetylene.

Chapter two is the literature review, which goes into detail about aspects regarding both mesoporous silica and catalysis. This chapter focuses on why mesoporous silica, particularly MCM-41, is so useful with regards to catalysis. As well, it focuses on the issues at hand regarding acetylene hydrogenation with Pd, Au, and PdAu supported catalysts.

Chapter 3 is the experimental and instrumentation chapter that goes into detail about how mesoporous silica, MCM-41, is prepared as well as the preparation of the supported catalysts. It also goes into detail about the catalytic reaction as well as the characterization techniques.

Chapter 4 is the results and discussion section which explains the characterization of both the support for the catalysts, pore-expanded MCM-41, as well as the Pd, Au, and PdAu

supported catalysts. It also explains in detail the results of the selective hydrogenation of these catalysts.

Chapter 5 discusses the conclusions of this work and what can be addressed in the future to help solve the problem of acetylene hydrogenation. The first part, the conclusion states the findings of this work while the future work goes into detail about what can be done regarding the support for the catalysts, the reaction conditions, and finally the different metals which can be explored.

Chapter 2: Literature Review

2.1 General Overview

Worldwide ethylene demand and production have been increasing since the 1980's, reaching over 130 million tonnes annually. Ethylene is produced industrially via the steam cracking of small chain hydrocarbons.[1] However, during the process of steam cracking, impurities are introduced into the ethylene feed, particularly acetylene. The presence of acetylene in ethylene streams eventually leads to the poisoning of the polymerization catalyst since acetylene adsorbs at the active sites for ethylene and blocks the polymerization process.[2] The ethylene stream then needs to undergo a purification process and one step in this process is the selective hydrogenation of acetylene. In order to eliminate the deactivation of the polymerization catalysts, the acetylene content must be reduced to low parts per million (ppm), or even parts per billion (ppb), range.[3] Hydrogenation of acetylene requires high conversion and selectivity to ethylene in order to prevent the over hydrogenation of acetylene. However, in order to truly understand the hydrogenation of acetylene, all of the possible routes of hydrogenation must be understood and are shown in Figure 2.1.

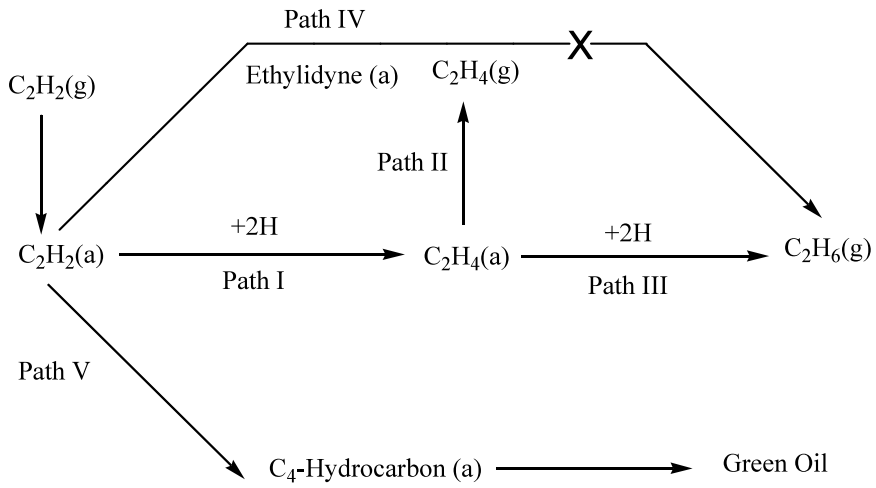

Figure 2.1: Possible Routes for acetylene hydrogenation.[3] Copyright Elsevier © 2012. Reproduced with permission.

Within the selective hydrogenation of acetylene, there are 5 understood paths which may occur.[3] They are as follows: path I is the partial hydrogenation pathway of acetylene to ethylene, which can be either desorbed as the ethylene product (path II) or further hydrogenated to ethane (path III). Ethylene selectivity can be improved by increasing path II and limiting path III. Path IV is the full hydrogenation of acetylene directly to ethane.[3] The adsorbed species, ethylidyne, had been suggested as an intermediate of path IV but later was found to just be a spectator of surface reactions. Path V lowers the ethylene selectivity and the catalyst lifetime due to the formation of oligomers of $(C_2H_3)_n$ where n is two to fifty. This is better known as green oil.[3] In order to address issues pertaining to the selective hydrogenation of acetylene, both the porous support as well as the metals must be explored.

2.2 Porous Solids Background

Porous materials have attracted a vast amount of attention, especially since the 1990's, due to their wide-range of applications. Ideally a porous solid should possess a narrow pore size distribution and there should be a readily tuneable pore size.[4] Additionally, it must show high hydrothermal stability and mechanical stability with high surface area and large pore volume.[5]

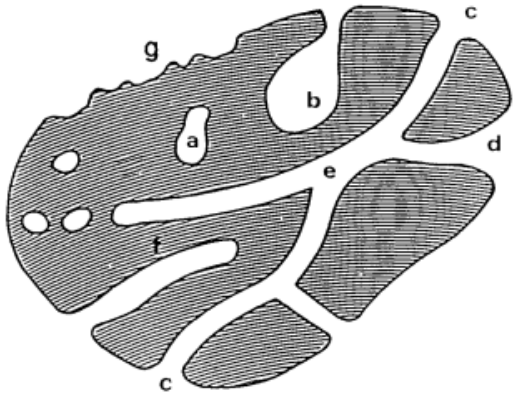

Figure 2.2: Illustration of a cross-section of a porous material.[6] Copyright IUPAC© 1994. Reproduced with Permission.

A solid material that contains cavities, channels, or interstices is known as porous, as shown in Figure 2.2. However, there are many different types of cavities within a porous material that needed to be understood.[6] Region a is known as closed pores in which the pore is completely enclosed and isolated from its surroundings. Regions b, c, d, e, and f are known as open pores and are in constant communication with their environment.[6] Some pores may only be open at one end (b and f) and are known as blind pores. Others are open at both ends and are called through-pores (e).[6]

An important characteristic of porous materials is the diameter of the pores. Solid materials with a pore diameter as low as 0.2 nm can be defined. Since the pore diameter is very important for the use of porous materials as a support, they are often separated into three different categories based on the size of their pore diameter. IUPAC[7] defined the following three classes of porous materials:

- Pore diameter < 2 nm → microporous material
- 2 nm ≤ Pore diameter ≤ 50 nm → mesoporous material
- Pore Diameter > 50 nm → macroporous material

In Figure 2.3, an example of the pore size and pore size distribution of a mesoporous material is depicted. However, it must be understood that the three classes are very important, but contain very different materials. Commonly in the micropore range, a material known as zeolites are crystalline and thus have very defined pore diameters. In the macropore range, silica gel is purely amorphous and its pores vary in size and in the distribution of these pores.[7] Mesoporous silicas are between microporous and macroporous material, both in pore diameter and pore size distribution. Well ordered silica materials are promising supports for catalysts since they possess pores that have a large enough diameter and are thus capable of immobilizing molecular catalysts and nanoparticles. They still have

the qualities in order to induce shape selectivity or hydrophobicity of the localized environment.[8]

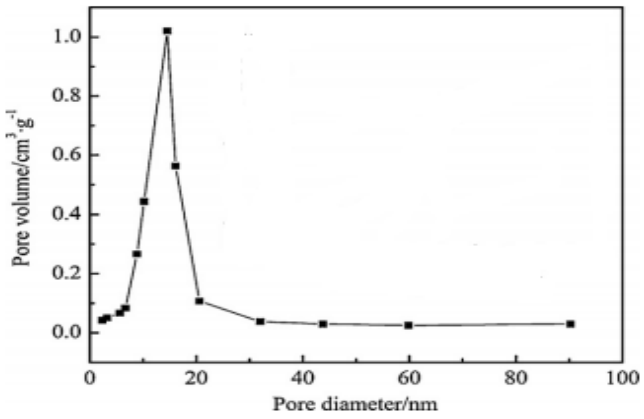

Figure 2.3: Example of Pore Size Distribution of a Mesoporous Material.[8] Copyright Elsevier © 2011. Reproduced with permission.

Ever since the discovery of highly ordered mesoporous materials in the early 1990's by the Mobil Company, there has been an enormous amount of interest in these materials.[9] Prior to the discovery of this family of mesoporous materials, porous materials possessed properties including broad pore size distribution and irregular pore size.[10] Therefore, there has been a vast undertaking in research due to the desirable properties of the M41S family of silicas.[11, 12] The ability to control such properties has allowed for numerous applications in catalysis[13-16], adsorption[17, 18], separation[19, 20], and host-guest chemistry[21, 22].

The most well known example of microporous materials are zeolites, which were discovered in the late 18th Century. Zeolites are crystalline aluminosilicates, which possess relatively small pore sizes (1.2 nm). This makes incorporation of larger guest species almost impossible.[23] Zeolites are tetravalently coordinated aluminosilicates that possess a high crystallinity due to their rigid framework, which enhances their thermal stability. It should also be noted that for every aluminium atom within the framework of the zeolites, a cation

such as sodium or potassium, must be introduced in order to balance the charges.[23] An example of one of the most common zeolites, Faujasite (FAU), is shown below in Figure 2.4. Since zeolites lack three-coordinate sites, there will also be a lack of surface hydroxyl groups, which could be attributed to the dehydrated nature of these materials.

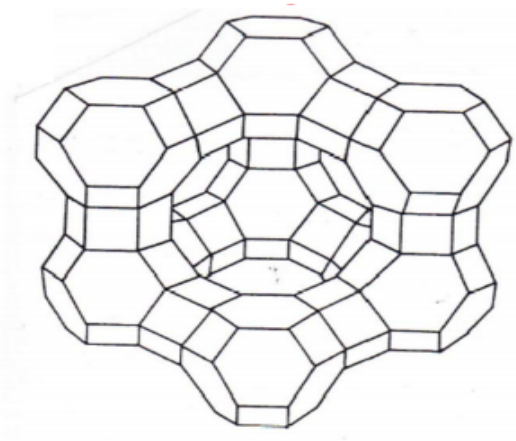

Figure 2.4: Structure of Faujasite (FAU). [24] Copyright Quimica Nova © 2002. Reproduced with permission

Due to the very small pore size distribution in zeolites, they are very useful for size specific applications, such as adsorption and shape selective catalysis. Even though the small pore size is beneficial for specific applications, it is also a drawback due to the fact that size specific processes often use molecules larger than 1.5 nm, particularly when dealing with heavy oil cracking and catalytic processes involving large molecules.[23-24]

2.2.1 Mesoporous Silica Materials

Perhaps of most importance within the family of M41S is the Mobil Composition of Matter 41, or MCM-41, which possesses a two dimensional hexagonal structure.[25] This hexagonal structure is formed by the self assembly of a cationic surfactant, typically cetyl-trimethylammonium bromide (CTAB) in the presence of a silicon source, usually silicon dioxide, under basic conditions.[9, 26] This results in MCM-41 possessing high surface areas,

pore volumes, and pore sizes, which are all desirable properties for this work. However, the pore size can be further altered by changing the length of the alkyl chain (C_8-C_{18}) in the surfactant. The pore sizes can also be expanded by the introduction of a swelling agent, such as mesitylene, which can vastly expand the pores.[27] The morphology can also be converted from hexagonal (MCM-41) to cubic (MCM-48) via hydrothermal treatment at 110 °C, as demonstrated below in the transmission electron microscopy (TEM) images.[28]

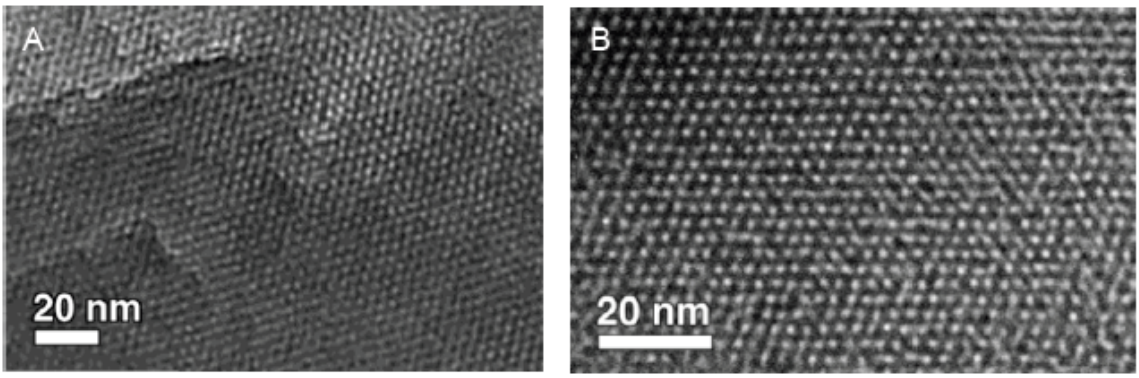

Figure 2.5: TEM images of MCM-41 (A) and MCM-48 (B). [28] Copyright American Chemical Society© 2003. Reproduced with permission

2.2.2 Surfactant Micelles

In terms of the surfactants used, there are three types: cationic, anionic, and neutral, or nonionic. The most commonly used surfactants have been cationic, and a variety of structures have been obtained due to the vast nature of the surfactants as well as by altering the alkyl chain lengths.[9, 29-31] However, there are problems associated with high cost and high toxicity. Anionic surfactants have not been studied as much as cationic surfactants. With that said, the future looks bright for the use of anionic surfactants as a template in mesoporous materials.[31-34] For example, it has been shown that anionic surfactants used in the templating

of alumina mesopores yield hexagonal mesophases whereas cationic surfactants do not.[33] Finally, the use of neutral surfactants has been extensively studied and many porous structures have been obtained.[35-37] In comparison to cationic surfactants, anionic surfactants have a much lower cost and toxicity associated with them.[35] Typical examples of surfactants, cationic, anionic, and neutral are displayed below in Table 2.1

Table 2.1: Examples of Surfactants: Cationic, Anionic, and Neutral

Surfactant Type	
Cationic	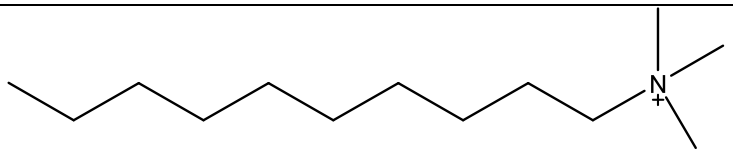
Anionic	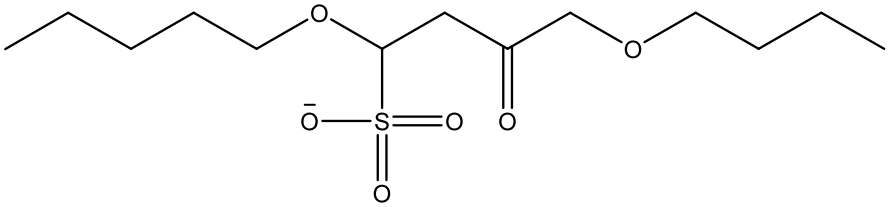
Neutral	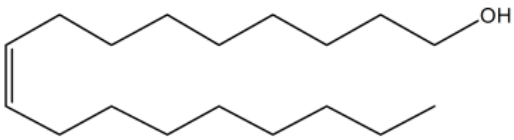

2.2.3 Mechanistic Pathways of MCM-41

In addition to understanding the way in which the surfactants work, one must understand the mechanism in which the M41S family is prepared. In Figures 2.6 and 2.7, two possible mechanisms for the formation of MCM-41 are suggested. The first mechanism says that there exists a liquid-crystal template due to the similarities between liquid crystalline surfactants phases and the mesostructured materials.[36, 37] In this proposed mechanism, the

structure is determined in the way in which the surfactant micelles pack into the liquid crystalline phase, which serves as a template for the synthesis of M41S family. In terms of micelles, the most energetically favorable form is spherical since the surface energy is minimized.[25, 39-40] The inorganic siliciate species occupies the space within the pre-formed pores of the hexagonal lysotropic crystal phase and are placed on the micellar rods (Figure 2.6). This is then followed by the polymerization of the silicate anions into the formation of the MCM-41 material.[25] By varying the surfactant concentration, the liquid crystalline phase firstly transforms into a cubic liquid crystalline phase and at the highest concentration, a lamellar liquid crystalline phase. However, in a large number of elucidation studies on the mechanism of MCM-41, the hexagonal liquid crystalline phase was not initially observed even though MCM-41 was still formed.[41-43]

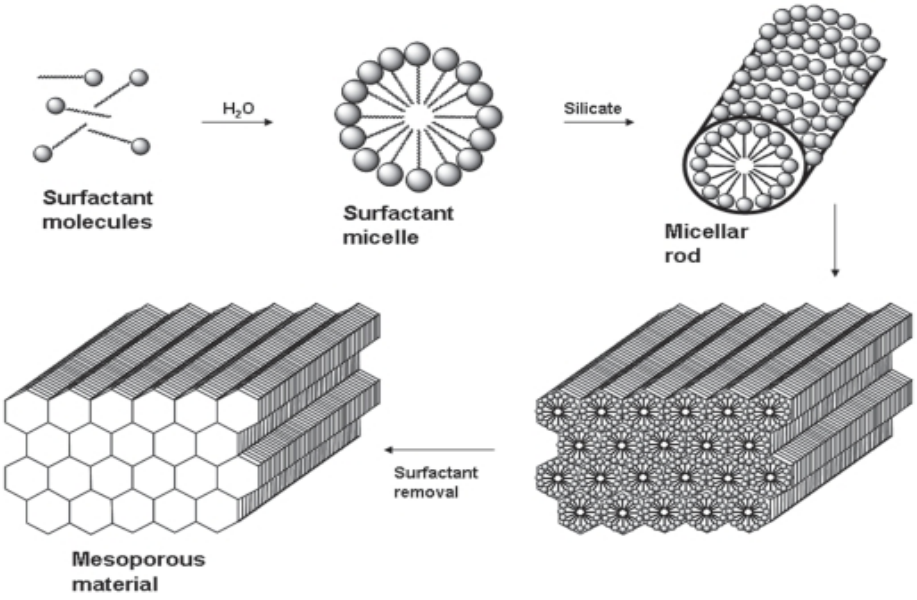

Figure 2.6: Mechanism for the Formation of MCM-41 via Liquid Crystal Template.[38]

Copyright Intech © 2011. Reproduced with permission.

In this alternative proposal, it is suggested that the inorganic silicate could dictate the way in which the surfactants order into specific mesophases (Figure 2.7). The reasoning for more than one possible mechanism lies in the fact that there are various surfactants used, but this mostly depends on the concentration of the surfactant in solution (charge density).[43] Both pathways involve various electrostatic interactions in which the silicate species interacts with the charged (positively or negatively) head group of the surfactant. During these interactions, the aggregation of the micelles is energetically unfavorable due to these electrostatic repulsions, which decrease through the formation of a monolayer of silica around the micelles, initiating the formation of the hexagonal structures.[44] In order to reduce the repulsions, the silicate ions start to condense, which results in the formation of a monolayer around the surfactant micelles. At this point, the surfactant micelles surrounded by silicate become "coated" and start to bunch together by condensing the silica layers.[44-46] The second pathway has additional evidence through the use of ^{14}N NMR which showed that liquid crystals are not present in the reaction medium in the preparation of MCM-41. Therefore, it is suggested that the mechanism starts by placing monolayers of the silicate species on the surfactant micellar rods, which pack into an ordered hexagonal structure.[47]

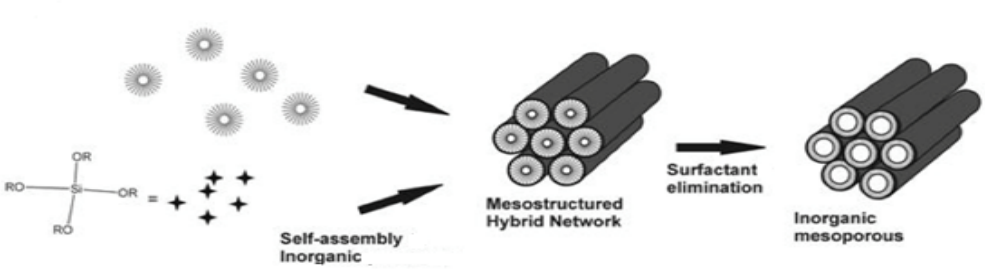

Figure 2.7: Self-templated formation of MCM-41.[38] Copyright Intech © 2011. Reproduced with permission.

Another plausible proposal for the synthesis of MCM-41 was proposed by Monnier et al. in 1993 where the interaction between the silicate and the surfactant generates the structures, which subsequently determines the nature of the mesophase.[48] In this proposal, there are three key steps as follows: 1) multidentate binding of the silicate anion to the positively charged surfactant through electrostatic interactions, 2) preferential polymerization of the silicate at the interface, and 3) charge density matching between the silicate and the surfactant.[47] This means that the silicate species counteract the charged surfactant micelles to form the mesophase, which is controlled by the multidentate binding of the silicate-surfactant interaction through packing density.[47-48]

2.2.4. Surfactant Packing

It is well known that the nature of the surfactant is very important in determining the mesophase of the silicate. This can be understood by looking at the packing parameter

$$g=Vla0 \quad (1)$$

where V is the volume of the hydrophobic surfactant chains, l is the surfactant chain length, and a_0 is the area of the hydrophilic headgroup of the surfactant molecule at the interface.[41] Simply by determining the packing parameter and knowing each corresponding value, the structural architecture of the mesophase can be determined. For example, in the preparation of MCM-41, which contains hexagonal pores, the packing parameter is less than one-third or one-half.[49-50]

Table 2.2: Packing Parameter of Different Mesophases[46].

g	Mesophase	Space Group	Example
<1/3	hexagonal	$P6_3/mmc$	SBA-15
1/3	Cubic	Pm3n	SBA-1
1/2	Hexagonal	p6m	MCM-41
1/2-2/3	Cubic	Ia3d	MCM-48
1	Lamellar	P2	MCM-50

It was found that two main factors influence the way the surfactant is packed; the first is the neutralization of the surfactant headgroup and the silanolate, or charged silanol, at the interface and the other is the organic chain packing.[25] Firstly, the lower the charge-density is at the interface, the higher the g values will be, which can give mesophases, such as hexagonal, cubic, and lamellar, as shown in Figure 2.8.

MCM-41 (Hexagonal) **MCM-48 (Cubic)** **MCM-50 (Lamellar)**

Figure 2.8: Different Mesophases of the M41S Family.[51] Copyright Elsevier © 2012. Reproduced with permission

As well, the longer the chain length in the surfactant, the higher the packing parameter will be. However, the charge-density has many key components to the neutralization at the interface as it depends on pH, co-surfactant, ionic strength of the solution, and counterion.[25] In terms of the packing density, it also depends on the temperature and the organic additives during the synthesis of the silicate.[46] This interaction of the silicate with surfactant is described as a self assembly process and forms the mesophase of material.

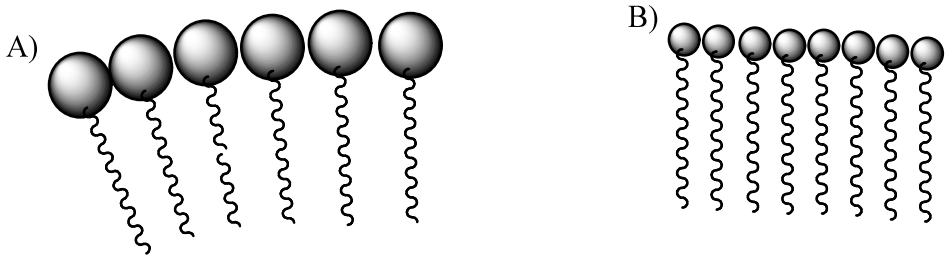

Figure 2.9: Micelles with Large Head Groups (A) and Small Head Groups (B)

2.2.5 Silicate-Surfactant Interactions

In order to truly understand how a material like MCM-41 is synthesized, it is critical to understand the interactions between the surfactant and the silicate. Currently there exist four main interactions between the silicate and the surfactant: S^+I^-, S^-I^+, $S^+X^-I^+$, and $S^-X^+I^-$ where S represents the surfactant, I represents the silicate species, and X represents the counterion.[43] The preparation of MCM-41 uses an anionic silicate species with a cationic surfactant, which forms hexagonal pores through strong Coloumb interactions (S^+I^-) in alkaline conditions. It was shown that the equilibrium between the silicate and surfactant can be adjusted by the presence of other ions in solution.[52] This shows that the addition of the

counterion may affect the morphology and the structure of the material. For example, it was demonstrated that the addition of sodium nitrate to cetyl-trimethylammonium bromide (CTAB) and silicate system resulted in the transformation from lamellar to a cubic or hexagonal phase.[53, 54]

Preparation of mesoporous silica occurs in acidic mediums in which the cationic silicate (S^+) cannot directly interact with the positively charged surfactant (I^+).[42, 54] In order to balance the charges a negative ion must be used, such as sodium nitrate, that will balance the charges of the silicate and surfactant species.[55] Due to the weaker interactions within the acidic media, surfactants are much easier to remove and can be removed through less harsh techniques, such as solvent extraction.[55]

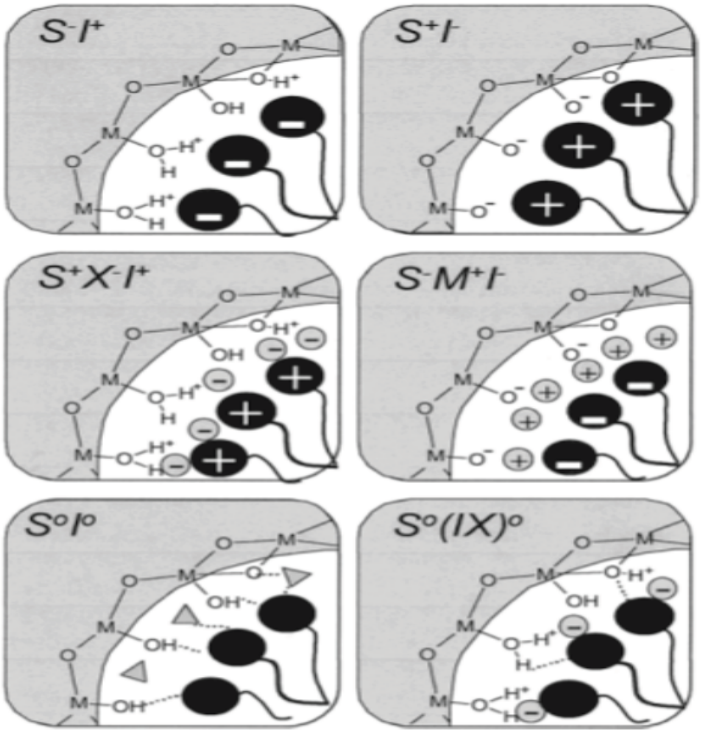

Figure 2.10: Six Different Types of Surfactant Interactions.[43] Copyright American Chemical Society © 2002. Reproduced with permission.

Even though both cationic and anionic surfactants have been used extensively in the past, the use of neutral or non-ionic surfactants must be examined. In the presence of neutral surfactants, the interaction $S^0H^+X^-I^+$, takes places directly (S^0I^0) or through hydrogen bonding followed by self-assembly between the neutral surfactants and the inorganic species. By forming mesoporous silicas using non-ionic surfactants, the ability to form silicate materials with more disordered frameworks that result in "wormhole motif" pore structures are obtained.[42, 54] The interaction S^0I^0 allows one to control the amphiphilic nature of the surfactant by altering the temperature. The understanding of these interactions is critical in producing such valuable materials since the choice of conditions, surfactant, and silicate source will control the morphology of these materials.[54]

2.2.6 Modifications of Mesoporous Silica Properties

Another modification that can be used to further improve the properties of MCM-41 is the ability to control the size of the pores. This is usually accomplished by varying the length of the alkyl chain of the surfactant.[25, 56] The surfactant most commonly used is a form of quaternary ammonium with the general formula: ($C_nH_{2n+1}(CH_3)_3N^+$), with n ranging from 8 to 18. This will result in the pores having a diameter of 2 to 5 nm. Although varying the alkyl chain length of the surfactant allows one to control the pore size to a certain extent, a much more useful technique for altering the pore size is called swelling.[57, 58] This is accomplished through the addition of auxillary organics, such as mesitylene, in which the organic molecules are absorbed in the core of the micelle and swell up, resulting in a much larger diameter.[59, 60] This will cause the pores to increase in size up to 100 nm.

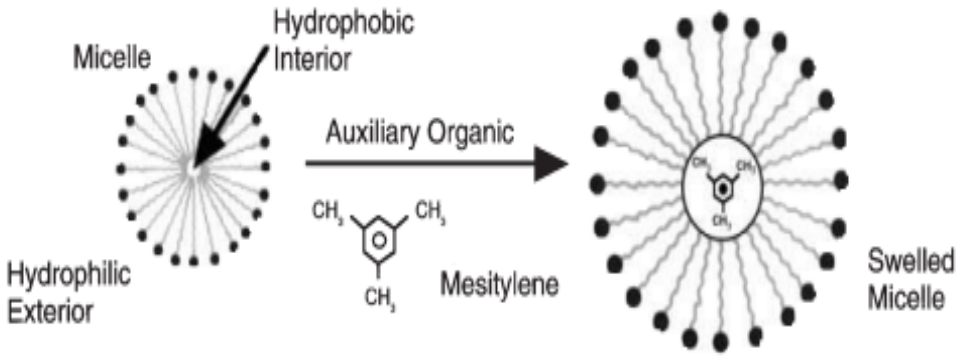

Figure 2.11: Formation of Swelling Micelle Surfactant.[60] Copyright Springer © 1998. Reproduced with permission.

2.2.7 Surfactant Removal

Once the mesoporous material has been synthesized, there needs to be a way to access the porous structure in order to use its valuable properties. The only way in which this is possible is by removing the surfactant from the framework.[61] Currently, the most commonly employed method is calcination. Calcination involves the heating of the silicate to about 550 °C in air, which will further oxidize the surface.[61, 62] However, it must be heated at a constant rate of no more than 2 °C per minute in order to avoid the decomposition of the framework and needs to be held for between four and eight hours.[63] As well, the calcination of these materials containing copious amounts of carbon-based species may be deposited as coke, which can result in some of the pores being blocked.[61] Issues arise when the material is functionalized with organic functional groups via surface silanol groups as they decompose at much lower temperatures than what is required for calcination.[62] Furthermore, this method has been found to affect the surface area, pore size, and pore volume of the material. For example, in the calcination of MCM-41, it was found that the pore size shrunk in size from 2.85 nm to 2.62 nm.[61]

Another viable alternative to calcination is solvent extraction. Solvent extraction involves placing the material in a solvent, such as ethanol, and stirring to remove certain surfactants, such as N, N-dimethyldecylamine.[64-65] Other common extractions include acid, oxygen plasma, and supercritical fluid extraction.[25] The most promising of the extractions is supercritical fluid due to its unique properties of low viscosity, tunability with regard to extraction, easy separation and recovery, and low toxicity and cost.[66] In terms of surfactant removal, it was shown that the surfactant could be easily recovered and the materials showed a much more uniform pore size distribution in comparison to calcined materials.[66] As well, it was shown that supercritical fluid extraction can effectively remove surfactant and successfully functionalize material without blocking the pores due to the enhanced diffusivity of the functionalized material in supercritical fluids.[67]

One of the more recent methods used to remove the template from MCM-41 is treatment with ultra-violet (UV) ozone.[68] Ozone is used to remove the organic surfactant at room temperature due to the weak interactions of the silicate with the surfactant. The material was treated with ozone by using a UV lamp with a wavelength known to produce ozone from atmospheric oxygen.[68] The pore size, obtained from Brunauer-Emmett-Teller (BET) analysis, was found to be larger with a much narrower pore size distribution as well as a much longer range order of the hexagonal pore system in comparison to calcination of MCM-41.[68] It was also found that the ozone treated material had a much higher Si-OH density, which will further lead to easier functionalization of the material. Overall, the main advantages of ozone treatments over thermal removal of surfactants via calcination are that there is no elimination of grafted organic molecules at room temperature and no organic solvents are needed.[69]

Another method to remove the template from the mesoporous material developed by Jabariyan et al in 2012 is through the use of sonication.[70] Ultra-sonication waves were applied to a solution of MCM-41 in ethanol while stirring at a specific temperature.[70] The material was recovered and dried. Through this method, it was found that ultra-sonication led to the disruption of the micelles in the pores, causing them to be released into solution, which can be further recovered and reused.[70] As well, it was found that surface area, pore volume, and long range order of the hexagonal pores did not suffer in comparison to the calcined material.[70]

2.3 Catalysis

Once the material has been synthesized, it can be used in many different applications. One such application is as a support in heterogeneous catalysis. In general, catalysis is the acceleration of a chemical reaction due to the presence of a catalyst. A catalyst works by forming bonds with the reactant, which eventually forms a product while the catalyst detaches from the product and can be recovered.[71, 72]

In order to truly understand the catalytic cycle, the potential energy diagram, shown in Figure 2.12 must be understood. In the non-catalyzed reaction, the reaction proceeds due to the interactions, which must possess a very high kinetic energy in order for the reaction to occur, between the reactants and when there is enough energy to surpass the activation barrier, products will be formed.[73] In terms of the catalyzed reaction, the kinetic energy of the molecules can be lower since the activation energy barrier required for the reaction to proceed, is much lower. Even though the activation energy barrier is lowered, the overall energy between the reactants and the products remains the same. After the lowering of the

energy barrier, there is also an endothermic step in which the product is separated from the catalyst and the catalyst can then be recovered and reused.[71]

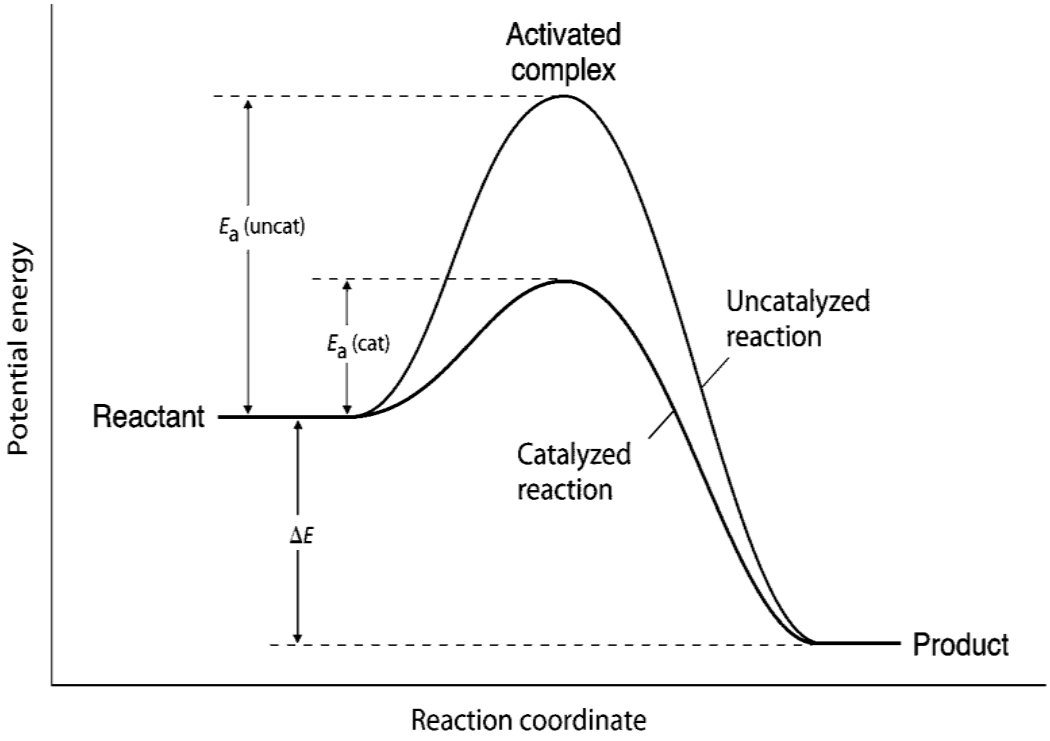

Figure 2.12: Potential Energy Diagram for a Reaction with and without a Catalyst.[74]

Copyright Pearson Benjamin Cummings © 2007. Reproduced with permission.

Even though catalysts come in many different shapes and sizes, they all possess the same ability to accelerate the reaction. With that being said, there are three main branches of catalysis: bio-catalysis, homogenous catalysis, and heterogeneous catalysis. However, only heterogenous catalysis with an emphasis on nanoparticle catalysis will be explored.[75]

2.3.1 Heterogeneous Catalysis

The most commonly used form of catalysis is what is known as heterogeneous catalysis in which the catalysts are in a different phase than that of the substrate. Typically,

the catalyst is in the solid phase while the substrate is in the liquid or gas phase.[76-78] Most heterogeneous catalysts used are typically supported on a porous material, such as MCM-41, which helps both environmentally as well as financially as not as much of the metal catalyst is needed.[79]

Generally speaking, heterogeneous catalysts work by one or more substrates being adsorbed on to the surface of the active sites. At this point, different interactions are happening between the catalyst and the substrate, which makes them much more reactive.[71] Once the reaction has been completed, the products are desorbed from the catalyst's surface, which leaves an open active site to which another substrate can come in and attach.

One well known group of heterogeneous catalysts uses various metals, such as platinum, palladium, and rhodium, supported on solids, such as alumina or SBA-15, which converts poisonous gases, such as carbon monoxide, to non-poisonous gases, such as carbon dioxide.[71] The catalytic cycle begins by adsorbing carbon monoxide and oxygen onto the surface of the catalyst. The oxygen molecule is then dissociated into two oxygen atoms that are adsorbed onto the surface of the catalyst.[71] The adsorbed oxygen atoms and carbon monoxide molecule then react on the surface to produce carbon dioxide, which is then desorbed in a matter of seconds.[71]

Another example of the use of heterogeneous catalysts involves the production of ammonia through the Haber-Bosch process. The Haber-Bosch process involves the use of heterogeneous catalysts, such as an iron catalyst over alumina, to produce ammonia.[78-79] The process begins with nitrogen gas being adsorbed onto the surface of the catalyst. The adsorbed nitrogen is then broken down into two nitrogen atoms.[80] The same process then

occurs with hydrogen gas and one adsorbed nitrogen atoms reacts with three atoms of hydrogen to form adsorbed ammonia. The adsorbed ammonia then desorbs from the catalyst, resulting in the production of ammonia.[81]

2.3.2 Nanoparticle Catalysis

A type of heterogeneous catalysts called metallic nanoparticle catalysts have been studied extensively due to the difference between bulk and nanoparticle properties. These are very attractive as potential candidates for catalysts due to their high activity and chemoselectivity.[81] However, nanoparticles are known to aggregate and form larger particles due to their large surface areas, which need to be stabilized in order to be deemed a suitable catalyst.[81]

Nanoparticles are clusters that contain tens of atoms to tens of thousands of metallic atoms, which are stabilized by ligands or surfactants on the surface.[82] They vary in size from less than one nanometer to greater than one-hundred nanometers, but the most active are only a few nanometers in diameter.[82] Nanoparticle catalysts are quite complex in nature due to their unique mechanistic features. The nanoparticles themselves can be used as catalysts in homogenous systems or they can be further anchored onto a support and used in heterogeneous catalysis.[82]

Nanoparticles were first seen two thousand years ago as gold particles, which were used as pigments for esthetics.[82] Pioneering work into nanoparticles was looked at by Faraday who showed that a red solution of gold nanoparticles formed through the reduction of tetrachloroaurate with phosphorous as a reducing agent.[83-84] Improvements upon this method were achieved in 1993 by using sodium borohydride as a reducing agent in a

biphasic organic-water solvent system with a phase transfer reagent, such as $[N(C_8H_{17})_4Br]$. This reagent displaces the material into the desired phase.[85]

Catalysts with metallic nanoparticles became popular in the 1950's with catalytic uses in hydrogenation, hydrosilylation, and hydration of unsaturated organic functional groups.[83-86] Many different examples of metallic nanoparticles exist since their discovery in the mid 20th century; Nord discovered the reduction of nitrobenzene in 1940[87], Haruta found that small gold nanoparticles supported on oxide catalyzed carbon monoxide oxidation by O_2 at ambient temperature were active due to their small diameter[88-89], and in the 1980's Hirai and Toshima used surfactants (cationic and anionic) to stabilize active platinum nanoparticles through reduction of H_2PtCl_6 either through a photochemical reduction or through reduction with hydrogen gas[90]. These are three examples of catalytic nanoparticles that helped lead to the explosion of research done at the turn of the 21st century in the field of nanoparticle catalysis.

Within this expansion of research, there were two main goals to be achieved: improving the activity, selectivity, and lifetime of the catalyst and understanding the catalytic mechanisms of these catalysts. Even though the end goals are the same, the methods for preparing the catalysts are not. The methods include: impregnation[91], sol-gel[92], gas-phase organometallic deposition[93], microemulsion[94], and cross-linking[95].

Not only have various methods been employed to develop these catalysts, but the use of different metals within these catalysts has also been used. The most commonly explored metals are Au, Ag, Pt, and Pd.[96] The metal, palladium, will be reviewed for its use in nanoparticle catalysis in the selective hydrogenation of acetylene.

2.3.3 Palladium-Based Supported Catalysts

Palladium based catalysts have been known to be the best catalysts for the selective hydrogenation of acetylene due to their much higher catalytic performance than that of other catalysts, such as platinum supported on alumina.[97] Even though palladium catalysts are superior to other catalysts, they also have their limitations; they have low selectivities at high conversions and tend to form oligomers, which leads to the formation of green oil.[98] The formation of green oil results in a shortened recycle time and lifetime of the catalyst.[99] Many efforts have been made to increase the selectivity at high conversions, such as pre-treatment with oxygen based compounds[100], altering supports to contain transition metal oxides[100], poisoning active palladium sites[101], functionalization of support with amine groups[102], and introduction of a second metal to the catalyst[103]. The last two will be explored in detail.

Metal nanoparticles, particularly palladium, have been attractive for modern technological applications due to their physicochemical properties in a certain nanometer range of the particles.[103] However, some of these applications can be limited due to the aggregation processes that typically occur in the activation stage, and particularly during calcination. The use of porous supports has been shown to decrease the growth of metal nanoclusters.[104] By applying common reducing agents, such as sodium borohydride, it can lead to the aggregation of metal nanoclusters in the synthesis conditions.

The ability to functionalize mesoporous silica has attracted much attention due to its ability to graft metals upon the surface, or stabilize the metals' surface. Due to this, the metal precursors can be highly dispersed on the support through strong interactions with the organic functionalities.[103]

2.3.4 Functionalization of Silica with Amines

A paper written by Wang et al in 2009 demonstrates that palladium nanoparticles supported on modified silica with grafted 3-aminopropyltriethoxysilane showed unusual catalytic activity in terms of acetylene hydrogenation.[104] The ethylene selectivity was found to rise with increasing acetylene conversion at higher temperature and higher hydrogen pressure. They proposed that the organic groups play a key role in determining the catalytic activity of this catalyst through altering the electronic properties.[105] Another example showed that quaternary ammonium surfactants can be used as scavengers for palladium supported nanoparticles.[106] These catalysts showed very good results, both in terms of high activity and selectivity at high temperatures.[106]

2.3.5 Gold-Based Catalysts

Ever since the pioneering work of Hutchings and Haruta on gold catalysis, particularly on carbon monoxide oxidation at low temperatures, gold nanoparticles have been looked at for many applications in catalysis.[107] These include acetylene hydrochlorination, synthesis of hydrogen peroxide, and reduction of NO to N_2.

Even though many examples exist with regard to gold catalysis, the origin of the active sites associated with the supported gold nanoparticle catalysts is still highly under debate due to their complex nature.[108] The challenge with gold catalysts, even today, remains at controlling the particle size distribution and aggregation of these nanoparticles.[109] Nevertheless, it is agreed upon that the catalytic activity of gold catalysts is influenced by five factors: (i) the morphology of gold nanoparticles, (ii) the catalyst synthesis techniques, (iii) the nature of the support, (iv) the interactions between the gold and the support, and (v)

the oxidation state of gold.[108-111] The preparation of gold supported nanoparticle catalysts typically occur through the use of a metal complexation and reduction method, as demonstrated below in Figure 2.13.

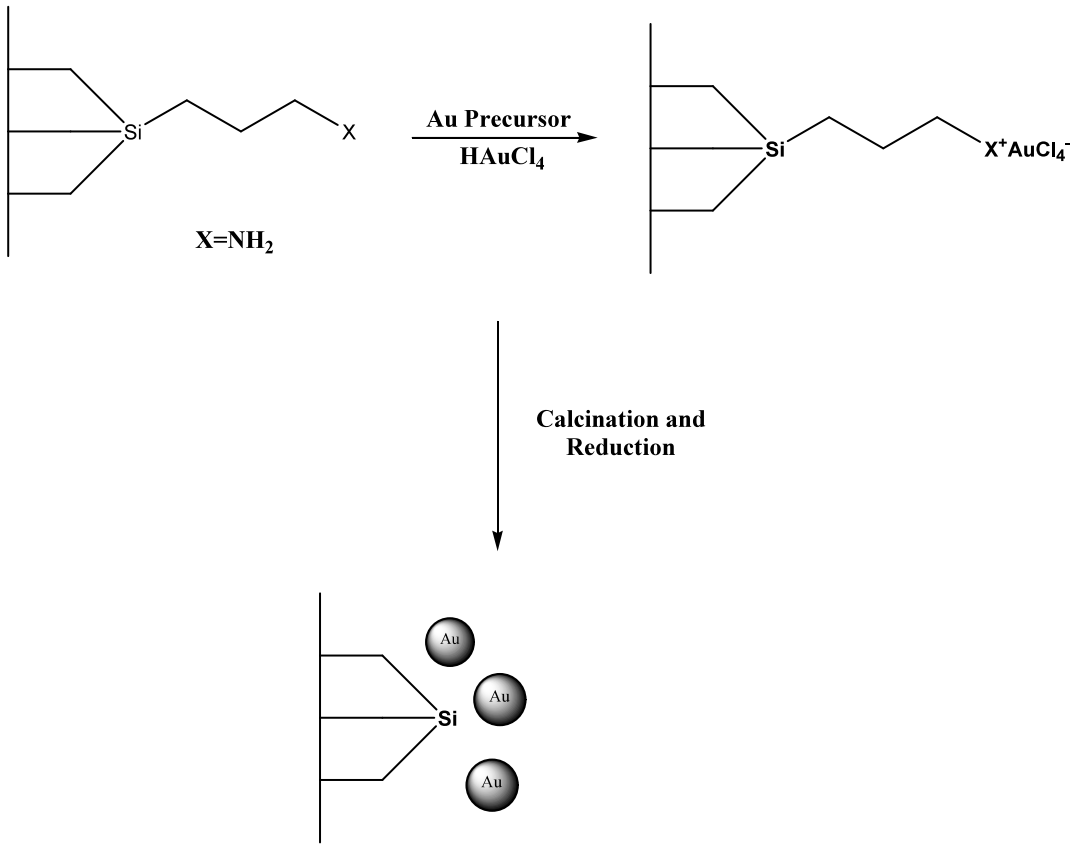

Figure 2.13: Preparation of Supported Gold Nanoparticles.[111] Copyright MDPI AG ©2011. Reproduced with permission.

Two of the most important aspects when dealing with gold supported catalysts, are both the particle size and the support. The size dependence of activity for gold can be illustrated by the fact that bulk gold is inert.[110] The relationship between particle size and activity has been investigated, but there has not been a consensus reached. It is argued that increased numbers of low coordinated gold atoms are needed, while others may argue that it is based on the electronic effects due to the particle size.[108]

Relating the catalytic activity of gold to the particle size was completed for carbon monoxide oxidation and it is seen that the complete particle size distribution must be considered.[111] However, it was argued that catalysts with a broad particle size distribution showed that the smaller particle sizes contributed most to the activity.[111] It was also demonstrated that particle size and nature of the support affect both reactivity and selectivity of the hydrogenation of dinitrobenzene.[111]

In order to address the effects of low selectivity of palladium supported catalysts, gold was used as it is unique and able to produce alkenes with almost total selectivity due to the stronger adsorption of the alkyne.[109] The stronger adsorption inhibits the re-adsorption from occurring, and therefore, will disallow the further hydrogenation to the alkane.[109]

It was first reported by Jia et al. that monometallic gold could be used as an alternative for the partial hydrogenation of acetylene. The catalysts were found to be 100% selective between 313-523 K, with only total hydrogenation above 573 K.[112] Furthermore, it was shown that the activity was dependent on particle size, with maximum activity achieved at 3 nm.[112] Choudhary and co-workers' results confirmed the particle size dependency of the hydrogenation of acetylene that Jia first reported.[109] However, the activity of the supported gold was found to be low and a deactivation was observed, due to coke deposition.[109] It was also shown that 100% selectivity on 1.95% Au supported on cerium oxide below 573 K was able to be achieved.[109]

Due to the high selectivity of gold nanoparticles, Segura et al. investigated why gold had a much superior selectivity in alkyne partial hydrogenation. Density functional theory simulations showed that the high selectivity was due to the preferential adsorption to alkynes

at the edges of gold nanoparticles. In order to confirm these findings, gold supported on cerium dioxide found that selectivities of 80-95% were observed at 473-573 K.[108]

2.3.6 Bimetallic Palladium-Gold Catalysts

Even though the selectivities are unusually high, the activities have been found to be quite low, particularly at low temperatures. One of the best methods to address this issue is to introduce gold as a metal alloy to palladium. The catalytic activity of bimetallic nanoparticles has been shown to change with their composition.[106] There are three types of changes that can occur through the addition of another metal, as demonstrated in Figure 2.14.

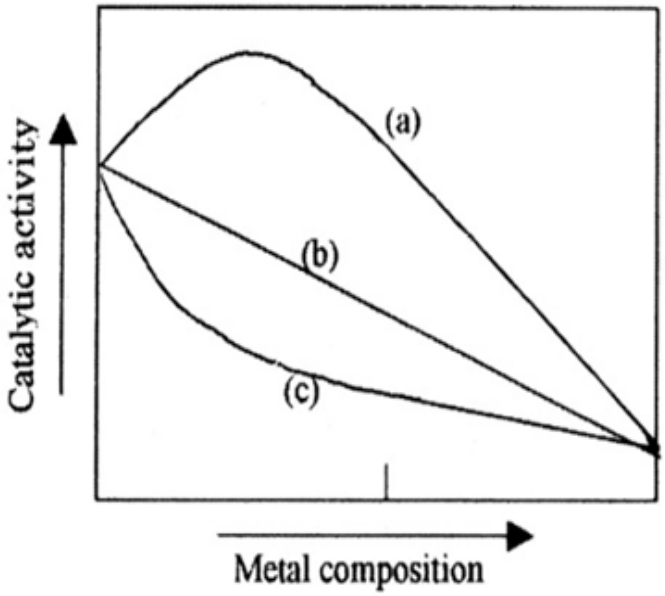

Figure 2.14: Three Possible Scenarios upon Addition of Another Metal.[106] Copyright Springer © 2004. Reproduced with permission.

Curve A shows that the addition of a another metal, B, increases the catalytic activity of metal A, even though there is little to no catalytic activity of B.[106] Curve B demonstrates

that there are no interactions between the two metals and the catalytic activity is not affected. Curve C proves that the addition of B decreases the catalytic activity of A.[106]

Typically, there are two main effects that are due to the addition of a second metal; the ligand effect and the ensemble effect. The ligand effect is an electronic effect in which the structure, reactivity, and properties of the catalyst are affected.[106] In terms of the effects of the addition of B, the electron density and the electronic structure of metal A can be altered. However, metal B must be located near metal A and is most effective next to the catalytic site.[106] The ensemble effect, however, is a steric effect in which each atom occupies a certain space and this may affect the molecules shape and activity.[106] In contrast to the ligand effect, both metals are on the surface of the metal particles due to the fact that both metal A and B attack the substrate together. In terms of the location of metal B, it is not necessary to be directly next to A, but it would be much easier to attack the substrate in this position.[106] These two effects are demonstrated below in Figure 2.15.

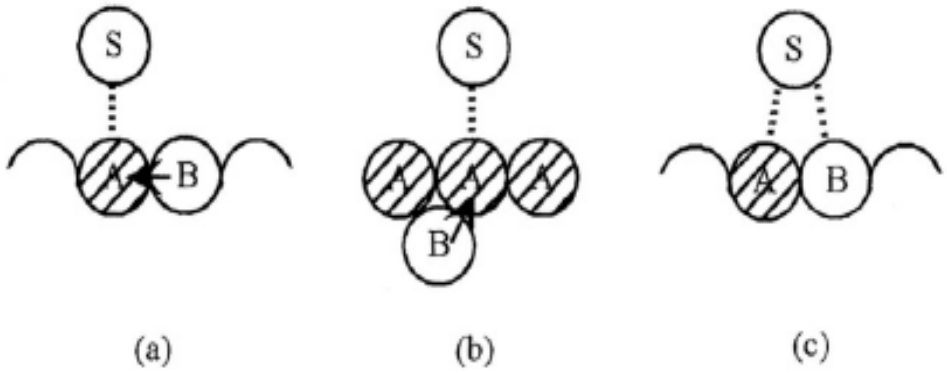

Figure 2.15: Schematic Representation of the Ligand Effect (a and b) & the Ensemble Effect (C). [106] Copyright Springer © 2004. Reproduced with permission.

Many examples of bimetallic catalysts exist, especially in terms of both palladium and platinum alloyed with a group IB metal, such as gold or silver.[113] The early work on this demonstrated the rigid band theory in which palladium, a group VIII metal, possessed a partially unoccupied d-band with a group IB metal occupying a completely filled d-band. However, it was shown that catalytic activities were not related to occupancy of d-bands.[113]

Not only has the use of gold in monometallic catalysis expanded, but so has its use in bimetallic catalysts. One catalyst in particular, the palladium-gold bimetallic species, has been explored due to the promoting effect of gold on catalytic activity and selectivity.[114] Furthermore, they have also shown that they are resistant to poisoning.[107] They have been used in the oxidation of alcohols to aldehydes or ketones, production of hydrogen peroxide, production of vinyl acetate, and in the hydrogenation of unsaturated hydrocarbons.[115] The bimetallic catalyst of palladium-gold will be explored with regard to selective hydrogenation of acetylene.

In terms of gold-palladium catalysts, there have been many over the years, especially since the 1990's. For example, the dechlorination of trichloroethene has been subjected to both palladium and palladium-gold supported on alumina.[116] It was found that the PdAu catalysts supported on alumina were much more active compared to the palladium supported on alumina.[116] Another important example involves the oxidation of ethanol in which PdAu catalysts were shown to be highly active in a basic medium.[107]

Even though both of these reactions are highly important, they do not address the issues at hand regarding hydrogenation of unsaturated hydrocarbons, particularly acetylene. The first palladium-gold catalyst for the hydrogenation of acetylene was developed by the

Dow Chemical Company and patented in 1957.[117] However, issues arose regarding catalyst lifetime, activity, and selectivity.[110] Other attempts to use PdAu supported catalysts for hydrogenation of unsaturated hydrocarbons have been attempted with varying amounts of success. Attempts to catalyze the hydrogenation of butadiene using PdAu catalysts have also been shown to enhance the selectivity. Work completed by Choudhary et al in 2002 used both monometallic palladium and gold catalysts as well bimetallic PdAu catalysts supported on titanium oxide.[118] The monometallic gold catalyst showed extremely high selectivity and the palladium catalyst showed high very high activity. Therefore, PdAu bimetallic catalysts were found to drastically increase the selectivity of the palladium catalysts towards acetylene hydrogenation.[118]

However, even though both of these examples were shown to use palladium as an enhancer, it is typically known that the addition of gold tends to increase the selectivity of catalyst towards the hydrogenation of the reaction of interest.[118-119] This is because the introduction of a second metal into the palladium matrix decreases the number of multi-coordination sites of Pd for the dissociative adsorption of acetylene and reduces the formation of β-Pd hydride, which both decrease ethylene selectivity.[104] However, another possibility exists suggesting that the addition of Au will cause an increase in the Pd d-band electron density, which should further help to improve selectivity of ethylene.[104]

Chapter 3: Experimental & Instrumentation

3.1 Materials

Cab-O-Sil M5 fumed silica was purchased from Cabot Corporation and used as received. Cetyltrimethylammonium bromide, tetramethylammonium hydroxide, dimethyldecylamine, potassium tetrachloropalladate(II), silver (I) nitrate, and sodium borohydride were purchased from Aldrich and used as received. Ethanol (99%) was purchased from Fischer and used without further purification. Gold (III) chloride hydrate was purchased from Strem Chemicals and used as received. Hydrogen, nitrogen, 10% H_2 in N_2, 10% H_2 in argon, acetylene, argon, and helium cylinders were purchased from Linde Canada and used as received.

3.2 Preparation of Pore-Expanded MCM-41 Silica

MCM-41 was synthesized through the use of Cab-O-Sil M5 fumed silica, cetyltrimethylammonium bromide (CTAB), and tetramethyl ammonium hydroxide (TMAOH). The resulting molecular composition of the mixture was 1.0 SiO_2: 0.32 TMAOH: 0.45 CTAB: 67 H_2O. The resulting material was then heated in a Teflon-lined autoclave at 100 °C under autogenous pressure for 40 hours. The material was then filtered, washed with a copious amount of deionized water, and dried at room temperature. Pore-expanded MCM-41 (PE-MCM-41) was prepared through the enlargement of the pores of MCM-41 through a hydrothermal treatment involving N, N-dimethyldecylamine (DMDA) as a swelling agent. This is completed by adding DMDA to water creating an emulsion and stirred rapidly. The MCM-41 silica was then added to the emulsion and stirred for 15 minutes. The DMDA to MCM-41 ratio was 1.25 by weight. The solution was then heated at 120 °C for 72 hours while stirring. The solution was then filtered, washed with copious amounts of deionized

water, and dried. This material was labelled as PE-MCM-41-W. The DMDA was then selectively removed by a common organic solvent, such as ethanol, to give PE-MCM-41-E, where E stands for ethanol extracted. As well, calcination of either PE-MCM-41 or PE-MCM-41-E generated PE-MCM-41-C, where C stands for calcined.

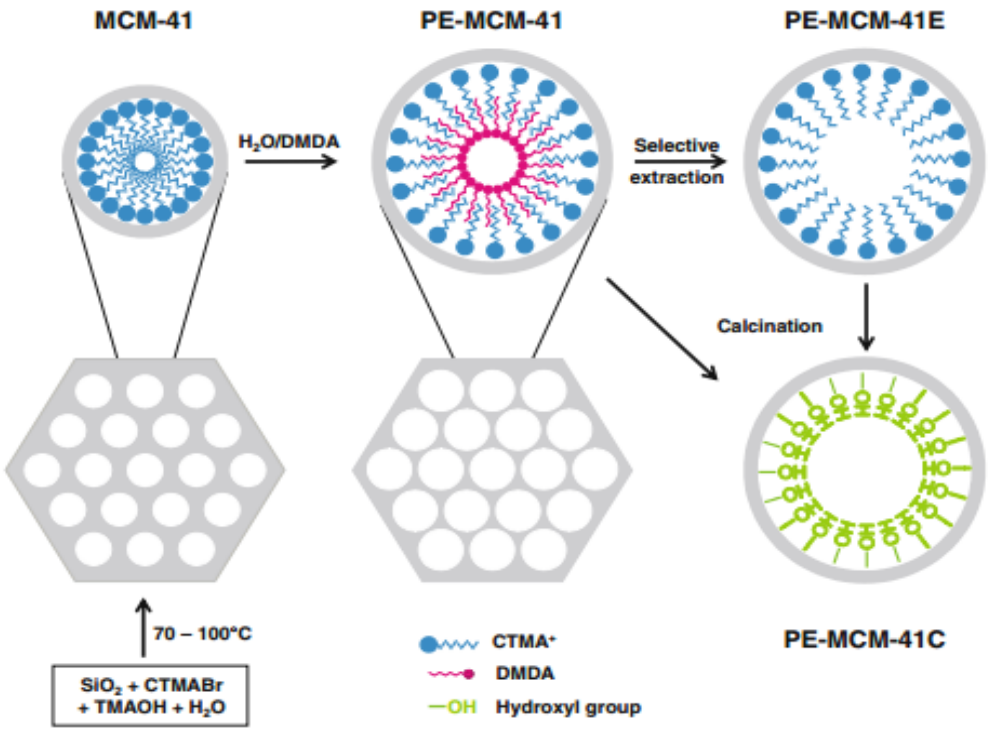

Figure 3.1: Preparation of PE-MCM-41 Silicas.[120] Copyright Springer © 2010. Reproduced with Permission.

3.3 Preparation of Palladium Supported Catalysts

3 grams of PE-MCM-41-W was placed in 50 mL of deionized water and stirred for 30 minutes. K_2PdCl_4 (46 mg, 0.14 mmol) was then placed in an additional 25 mL of deionized water, added to the solution, and stirred for one hour under a nitrogen atmosphere. The material was then filtered, washed with excess deionized water, and dried at 50 °C. The resulting material was yellow in color. The material was then placed in 75 mL of deionized

water and was reduced with sodium borohydride. $NaBH_4$ (54 mg, 1.4 mmol) was dissolved in 15 mL of deionized water and was added to the solution. After adding the sodium borohydride, the color shifted from yellow to dark grey. The material was then filtered, washed with deionized water, and dried. Cl^- impurities were removed from the products via multiple water washes until no AgCl precipitates formed upon addition of $AgNO_3$. This first material was labelled as Pd-MCM-41-W. Some of the first material was then taken, washed with excess ethanol, and dried at 40 °C under a nitrogen atmosphere. This second material was labelled as Pd-MCM-41-Et. The first material was then taken and calcined in air at 550 °C, followed by reduction of the material under hydrogen at 300 °C. This catalyst was labelled as Pd-PE-MCM-41-CR.

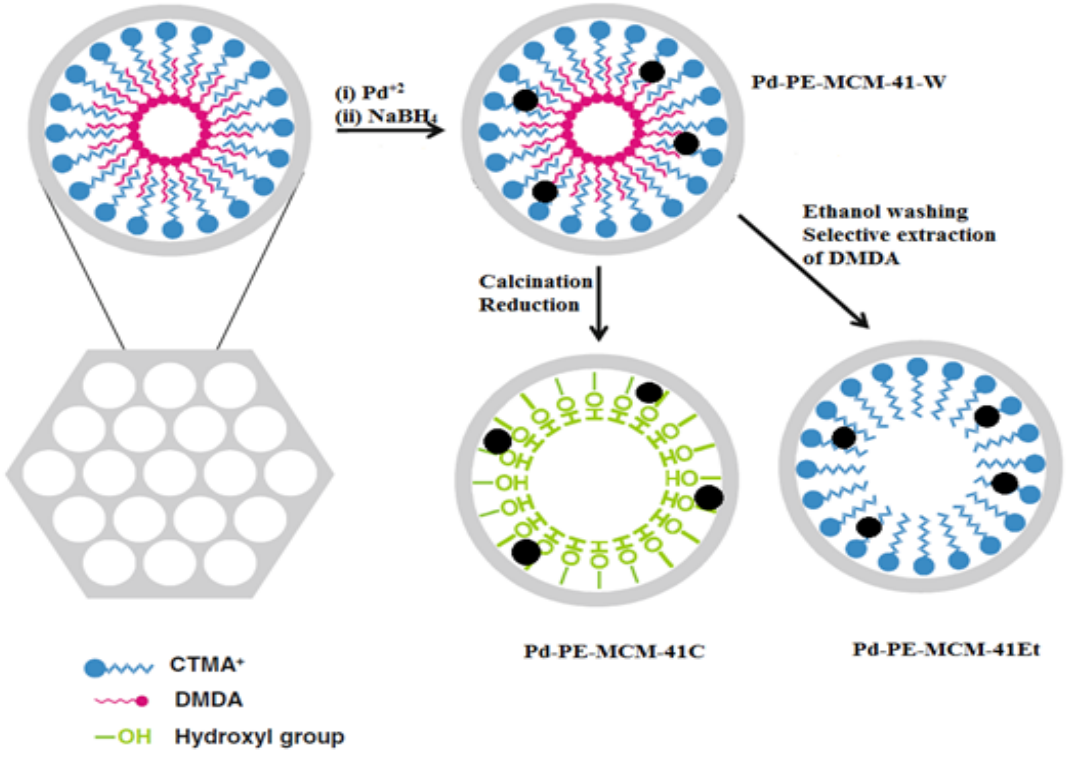

Figure 3.2: Preparation of Supported Palladium Nanoparticles.[120]

Copyright Springer © 2010. Reproduced with Permission.

3.4 Preparation of Gold Supported Catalysts

Seven grams of PE-MCM-41 was placed in 125 mL of deionized water and stirred for 30 minutes. $HAuCl_4$ (37 mg, 0.11 mmol) was then placed in an additional 25 mL of deionized water and added to the solution and stirred under nitrogen for 30 minutes. Once added, a yellow color was initially observed. However, upon stirring for thirty minutes, a dark purple color was observed, indicating an in situ complexation of DMDA and Au^{3+} took place. The mixture was then filtered, washed with copious amounts of deionized water, and dried at ambient conditions. The filtrate was red in color, indicating that during filtration some of the gold content was lost. A solution of $NaBH_4$ (42 mg, 1.1 mmol) in 50 mL of deionized water was added to the material and stirred for 30 minutes. The solution was then filtered, washed with deionized water, and dried. In order to ensure no Cl^- ions were present, the filtrate was tested with $AgNO_3$ and washed until no AgCl precipitates form. This first material is labelled as Au-PE-MCM-41-W. Some of the first material was then washed with excess ethanol, and dried. This material is labelled as Au-PE-MCM-41-Et. Some more of the first material was then calcined in air at 550 °C, followed by a reduction at 300 °C in excess hydrogen. This material was labelled at Au-PE-MCM-41-CR.

3.5 Preparation of Bimetallic Palladium-Gold Catalysts

Seven grams of PE-MCM-41 was in placed 125 mL of deionized water and stirred for 30 minutes. K_2PdCl_4 (36 mg, 0.11 mmol) was then placed in an additional 25 mL of deionized water and added to the solution. $HAuCl_4$ (38 mg, 0.11 mmol) was then placed in another 25 mL of deionized water, added to the mixture, and stirred for one hour under nitrogen. Once added, a yellow color was initially observed. However, upon stirring for one

hour, a dark purple color was observed, indicating a complexation with amines took place. The mixture was then filtered, washed with copious amounts of deionized water, and dried at ambient conditions. The filtrate was red in color, indicating that during filtration some of the gold content was lost. A solution of $NaBH_4$ (42 mg, 1.1 mmol) in 100 mL of deionized water was added to the material and stirred for 30 minutes. The solution was then filtered, washed with deionized water, and dried. The filtrate was tested with $AgNO_3$ and washed with water until no AgCl precipitates formed. This first material is labelled as PdAu-PE-MCM-41-W. Some of the first material was then washed with excess ethanol, and dried. This material is labelled as PdAu-PE-MCM-41-Et. Some more of the first material was then calcined in air at 550 °C, followed by a reduction at 300 °C in excess hydrogen. This material was labelled at PdAu-PE-MCM-41-CR.

3.6 Selective Hydrogenation of Acetylene and Product Analysis

A total flow of 80 mL/min consisting of C_2H_2, N_2, and 10% H_2/N_2 were passed over a known amount of catalyst (1.16×10^{-4} mmol Pd). The acetylene content was 2%, and the ratios of hydrogen to acetylene were one to one, two to one, and four to one, with nitrogen making up the rest of the 80 mL. The palladium content was kept constant in the Palladium and the Palladium-Gold catalysts. The catalytic experiments were run at 25-100 °C, with intervals of 15 °C for the palladium catalysts while the palladium-gold and gold catalysts were run to 115 °C. Once the highest temperature was reached, the experiments were also run from 115-25 °C (or 100 °C) to ensure no coke deposition occurred. The product was analyzed using an Agilent 6890N gas chromatography (GC) instrument. The GC is equipped with a 50 m long Chrompack capillary column and a flame ionization detector (FID). The carrier gas used within the gas chromatography was industrial grade argon as well as hydrogen. Connected to

the GC is an isolated thermally insulated fixed bed-U-shaped quartz reactor mounted in a tubular furnace. Quartz wool was used as plugs to keep the catalyst within the reactor. A K-type thermocouple was placed in the quartz reactor and was in contact with the catalyst bed in order to control the temperature of the catalyst using a PID controller. The flow rates were controlled via mass flow controllers and a manual mass flow meter was placed at the exit of the GC to ensure no gas was lost during the injection. The results were analyzed through online gas chromatography software.

3.7 Thermogravimetric Analysis

Thermal decomposition measurements were performed with the use of a TA Instruments TGA Q500. All samples were loaded into platinum TGA pans and analyzed under an inert nitrogen atmosphere. Chamber purging at a rate of 100 mL per minute was allowed to occur for 5 minutes before the start of each run. All samples run used the TGA isothermal method followed by the high-resolution ramp method. The isothermal method involves heating the material up 120 °C and holding it 90 minutes in order to remove traces of water from the sample. The ramp method involves linearly heating the material at a constant rate until the desired temperature was reached. Samples were heated at a rate of 2 °C per minute to 400 °C.

3.8 Inductively Coupled Plasma Optical Emission Spectrometry

Inductively coupled plasma (ICP) optical emission spectrometry involved the use of a Varian Vista Pro instrument equipped with a CCD array. Each sample (0.020g) is first digested through the use of a 3:1 ratio of hydrochloric acid to nitric acid and allowed to sit

for 2 hours. The samples were then heated at 120 °C for 5 hours and cooled. Finally the samples were diluted with 2% nitric acid to a range of 10-20 ppm.

3.9 Scanning Transmission Electron Microscopy

Scanning transmission electron microscopy (STEM) and energy dispersive X-ray spectroscopy (EDX) were performed on a JEOL 2010F microscope operating at 200 kV. Both the ethanol washed and calcined samples (Pd-PE-MCM-41-Et and Pd-PE-MCM-41CR) were dispersed in ethanol and sonicated. The solution was then placed on carbon coated copper grids (200 mesh) and allowed to dry. The sample Pd-MCM-41-W followed the same procedure except it was dispersed in water rather than ethanol.

3.10 Temperature Programmed Reduction and Pulse Chemisorption

Temperature programmed reduction (TPR) operates through the use of Zeton Altamira AMI-200 instrument. This instrument uses mass flow controllers (MKS), thermal conductivity detector (TCD), and a mass spectrometer. The control and data acquisition is operated by LABVIEW application software. The samples are placed into a quartz reactor in which quartz wool is placed. The catalyst is inserted on top of this and plugged with additional quartz wool. A K-type thermocouple is then placed in the catalyst bed in order to monitor the temperature. The catalyst bed is then heated up to 200 °C at a rate of 10 °C per minute and held for 60 minutes at 30 mL/min of 10% H_2 in argon. The TCD current and gain are 75 mA and 10, respectively. Once reduced, argon is flown over the sample to ensure no excess hydrogen molecules are on the surface.

Once reduced, the sample was cooled to 40 °C, hydrogen pulse chemisorption was applied by flowing known pulses over the catalyst. Twenty pulses were applied to the sample

until the sample became saturated with hydrogen. In order to accurately determine the amount of hydrogen adsorbed, pulse calibration was completed. Five pulses were completed and this would allow, the amount of hydrogen adsorbed to be calculated.

3.11 Nitrogen Porosimetry

Nitrogen porosimetry samples were run on a Micromeritics ASAP 2020 instrument. Prior to the measurement, the calcined samples underwent a pre-treatment at 100 °C under vacuum for 2 hours while the water washed and the ethanol washed samples underwent a treatment at 50 °C. The measurements were performed at 77 K using a static-volumetric method. The empty volume was measured with helium gas. The software used was ASAP 2020 V. 3.00 and the method used for the calculations of the surface area and the pore volume was the BJH method while pore size and pore size distribution was the Kruk-Jaroniec-Sayari (KJS) method.

3.12 Fourier Transform Infrared Spectroscopy

All IR spectra were collected with a Nicolet 6700 Fourier Transform Infrared spectroscopy (FTIR) instrument with a resolution of 4 cm^{-1}. Each spectrum went through 64 background and sample scans. Samples were prepared by placing samples on a Zinc-Selenium plate and directly taking the FTIR of it. The software used to obtain FTIR samples was OMNIC.

Chapter 4: Results and Discussion

4.1 Characterization of Pore Expanded MCM-41 Silicas

The first and typically most important step in any heterogeneous catalysis project involves the preparation and the synthesis of the support being used. The material of interest in this case was PE-MCM-41, which was proposed in two steps. MCM-41 was first synthesized in the presence of CTAB followed by pore enlargement using a post-synthesis treatment in the presence of DMDA. The DMDA is used as a swelling agent following the completion of MCM-41 in order to undergo a pore expansion. The resulting material (PE-MCM-41) contained both $CTMA^+$ and DMDA surfactants. Due to the favourable hydrophobic interactions, it is believed that they self-organize inside the pore channels into concentric cylinders comprised of an inverted DMDA micelle with a regular $CTMA^+$ micelle[120], as demonstrated in Figure 3.1. The amine head groups from the DMDA are pointing towards the pore center that creates a hydrophilic channel within the pores of PE-MCM-41.

Once the material has been synthesized, it is very important to characterize the properties of this material. One of key characteristics is the adsorption of probe molecules to determine the surface area and the pore size distribution. The process of adsorption takes place between the adsorbent (solid) and the adsorbate (gas), which can be quantitatively described by an adsorption isotherm.[121] According to IUPAC, there are six types of isotherms used for classifying porous materials into microporous (type I), non-porous or macroporous (type II and III), or mesoporous (type IV and V) materials. Type VI corresponds to the stepwise multilayer adsorption.[121] The step-height represents the

monolayer capacity for each adsorbed layer and may remain constant for several steps. The shape of the isotherm can be very useful as it gives insight into the interactions between the adsorbent and the adsorbate, monolayer or multilayer adsorption, filling and emptying of the pores, and the pore size.

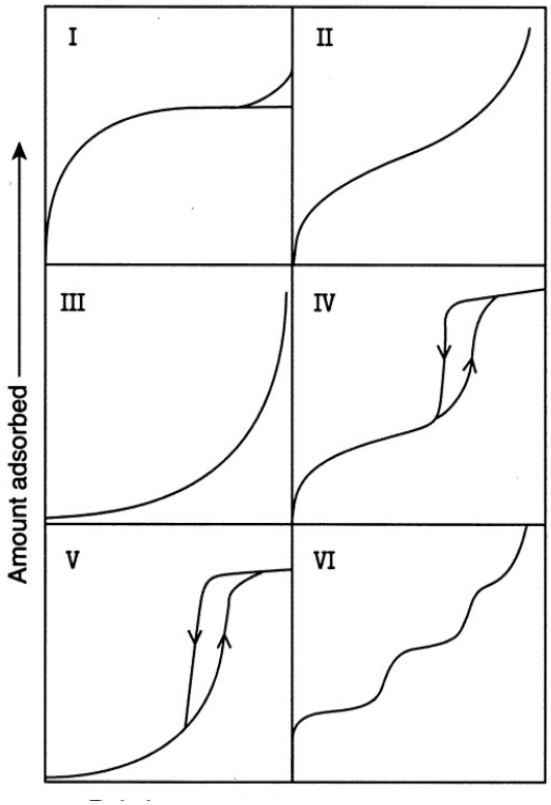

Figure 4.1: IUPAC Classification of Adsorption Isotherms.[121] Copyright IUPAC © 1982. Reproduced with permission

The idea that adsorption was related to an exposed surface was originally developed by Langmuir in which he proposed that the adsorption was due to an equilibrium between the gas and the adsorbed phase.[121] This resulted in a surface layer that was only one molecule in thickness. Brunauer, Emmett, and Teller looked into this and found that for physical adsorption multilayer formation is possible if the first layer adsorbed acts as a substrate for

further adsorption.[122] From this, it is possible to calculate the amount of gas required for complete monolayer coverage, as shown below

$$\text{[illegible]} = \text{[illegible]}(\text{[illegible]}/\text{[illegible]}0)(1-\text{[illegible]}/\text{[illegible]}0)(1-\text{[illegible]}/\text{[illegible]}0+\text{[illegible]}(\text{[illegible]}/\text{[illegible]}0) \quad (1)$$

Type IV isotherms are the most common for mesoporous materials and the most common characteristic of this isotherm is its hysteresis loop, which is due to capillary condensation and evaporation in mesopores. Within the type IV isotherm, there exist three main distinct areas.[121] The first curve in the isotherm, shown as region A in Figure 4.2, indicates that the point at which the first monolayer of nitrogen molecules have adsorbed to the surface. Using the BET equation, the surface can be calculated, as shown below

$$1\text{[illegible]}[(/\text{[illegible]}-1) = 1\text{[illegible]} + \text{[illegible]}-1\text{[illegible]} \quad (2)$$

where V is the amount of nitrogen adsorbed at equilibrium, c is the BET constant, V_m is the monolayer capacity, and P and P_0 are the equilibrium and saturation pressure of the adsorbates at the temperature of adsorption.[122] The BET equation is expressed in the linear form in the range of $0.05 < P/P_0 < 0.35$, which forms a straight line, known as the BET plot. The slope and y-intercept are equal to $(c-1)/V_m c$ and $1/V_m c$. the slope and the intercept of the plot, V_m and c can be determined.[122] Finally, the surface area is related to the cross-sectional area of the adsorbate gas (1.62 nm^2 for N_2):

$$S_{BET} = V_m \, A_{CS} \text{[illegible]} \quad (3)$$

where S_{BET} is the surface area, N is Avogadro's number, A_{CS} is the cross sectional area of the adsorbate gas, V_m is the monolayer capacity, V is the molar volume of the adsorbate, and a is the mass of the adsorbent.

The second region that should be noted is section B in Figure 4.2, where capillary condensation starts. N_2 gas is adsorbed as liquid to fill in the remaining volume in the mesopores. This area is used to determine the pore size distribution due to the fact that the volume of pores with a certain diameter is related to the pressure and the amount of nitrogen condensed at that pressure.[123] This means that the slope at the capillary condensation is related to the width of the pore size distribution. The Barret-Joyner-Halenda (BJH) method is the most used to determine the pore size distribution.[123-124] It is based on the Kelvin equation that relates pore diameter to pressure:

$$\square\square\square 0=2\gamma\square\square \mathrm{RTln}\square\square 0 \quad (4)$$

where r is the radius of the droplet of nitrogen, γ is the surface tension of the nitrogen droplet, R is the universal gas constant, and T is the absolute temperature in kelvin. The pore size distribution can then be calculated by taking the derivative of pore volume as a function of the pore radius. However, this method has been known to underestimate the pore size significantly since it does not take into account the thickness of the film at a particular gas pressure.[124] A more recent method, Kruk-Jaroniec-Sayari (KJS) applies a correction factor in order to account for this thickness, as shown below:

$$\square(\square\square 0)=2\square\square\square\square\square\square\square\square(\square\square 0)+\square+\square\square \quad (5)$$

where r is the pore size as a function of relative pressure, γ is the surface tension, V_m is the molar volume of the adsorbate, R is the universal gas constant, T is the absolute temperature in Kelvin, τ is the film thickness, and C_F is a correction factor of 3 Å.[124]

The third region in the isotherm, indicated as region C in Figure 4.2, is where pore saturation occurs. From this, textural properties can be gathered, including the calculation of

pore volume.[123-124] Pore volume is calculated by applying the following equation:

$$V_p = V_T * c \quad (6)$$

where V_p is the pore volume, V_T is the total volume adsorbed at partial pressure close to $P/P_0 = 0.995$, and c is a constant.

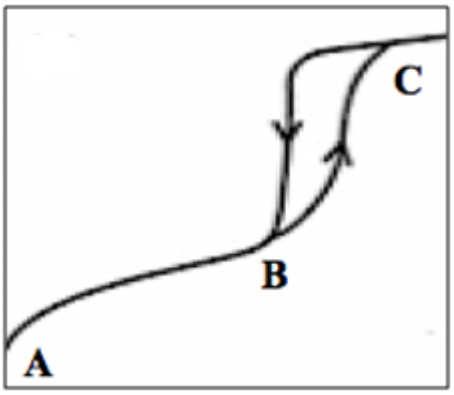

Figure 4.2: Type IV Isotherm Showing Three Distinct Regions of Different Adsorption.[121] Copyright IUPAC © 1982. Reproduced with permission

After the adsorption isotherm is completed, the adsorbed nitrogen gas is desorbed gradually by decreasing the pressure. In many cases, there is a range of pressure where the adsorption and desorption isotherms are not superimposed, thus forming a hysteresis loop. Such a loop appears when the capillary condensation and evaporation in and from mesopores take place at different pressures. The two most noticeable types are H1 and H4 in which H1 is almost vertical with the isotherm whereas H4 is horizontal with the isotherm over a large range of P/P_0. However, H2 and H3 are intermediates between H1 and H4 and may be seen as intermediates of them.[121] The most common hysteresis loop, H1, is associated with

mesoporous materials and consists of uniform pore sizes with regular shape. Finally, low-pressure hysteresis, shown by the dash lines in Figure 4.3, can only be removed via de-gassing at higher temperatures.[121] This is based on the swelling of a porous material with the molecule being the same width of the adsorbate molecule.

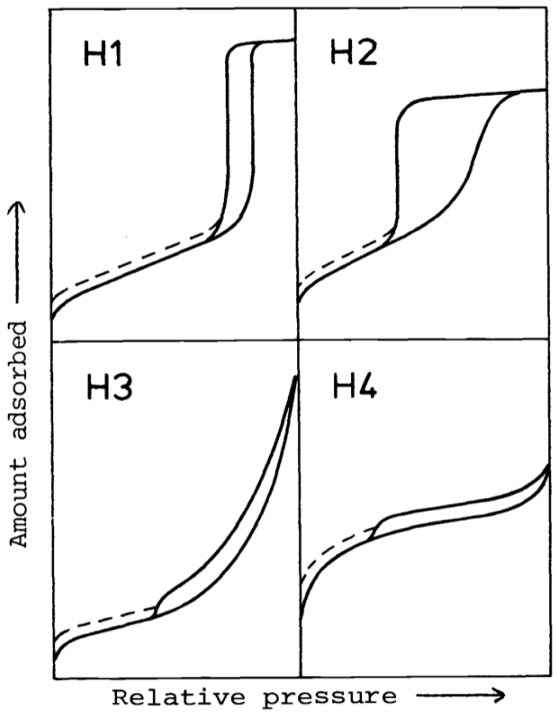

Figure 4.3: IUPAC Classification of Hysteresis Loops in Adsorption Isotherms.[121]

Copyright IUPAC © 1982. Reproduced with permission

Table 4.1: Structural Properties of PE-MCM-41

Material	**S_A (m^2/g)**	**V_p (cm^3/g)**	**d_p (nm)**
PE-MCM-41-W	59.8	0.11	7.3

PE-MCM-41-Et	390.0	0.98	8.4
PE-MCM-41-C	929.7	1.96	9.1

*S_A denotes surface area, V_p denotes pore volume, and d_p denotes average pore size

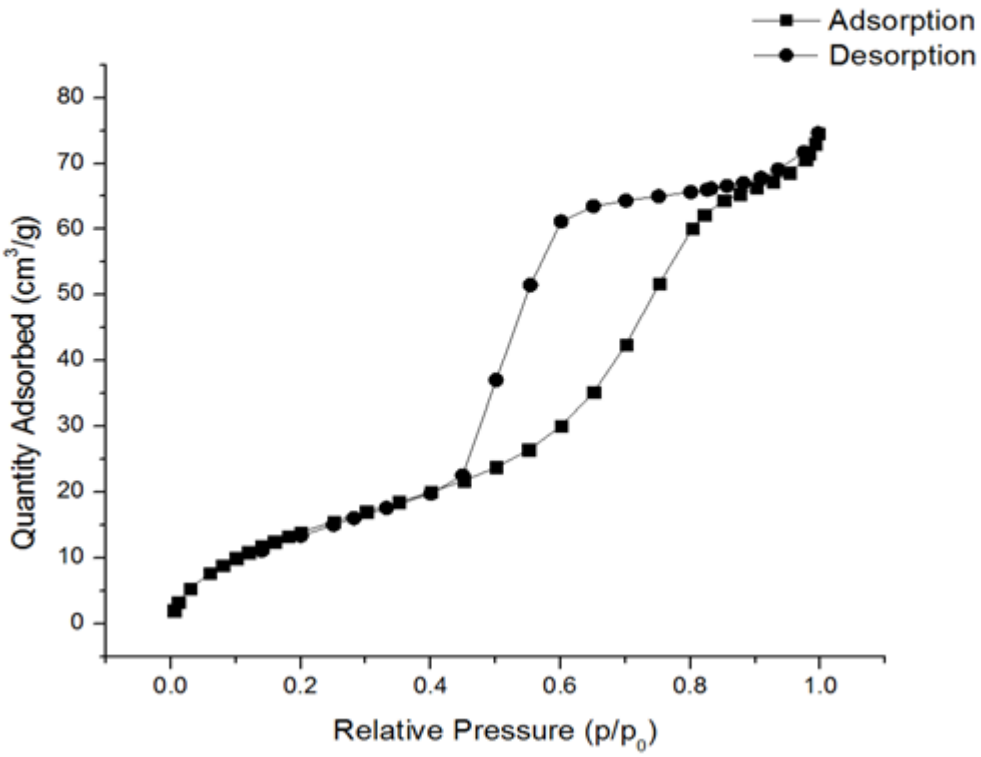

Figure 4.4: N_2 Adsorption-Desorption Isotherm of PE-MCM-41-W.

The as-synthesized PE-MCM-41-W material shows a relatively low BET surface area and pore volume, as displayed in Figure 4.4 and 4.5. Selective extraction of DMDA through the washing of PE-MCM-41-W with ethanol displays increases of both surface area and porosity. It should be noted that the PE-MCM-41-CR material displays the highest surface area and porosity since there is no remaining surfactant that can block the pores, which will

in turn cause a decrease in the surface area and porosity of the material. It should also be noted that PE-MCM-41 silicas display a type IV isotherm with a H1 hysteresis loop, showing that it is a mesoporous material.

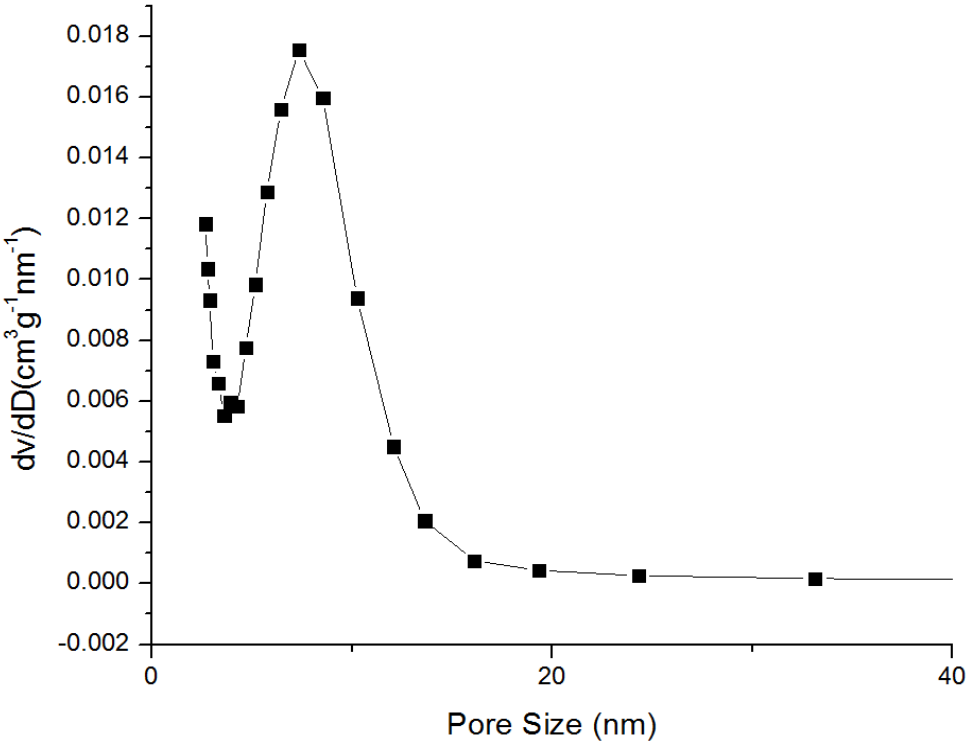

Figure 4.5: Calculated Pore Size of PE-MCM-41-W

The amount of surfactant in all three materials can be measured through the use of thermogravimetric analysis. Within the TGA of PE-MCM-41-W, as shown in Figure 4.6, there exists one overlapping peak, which represents the loss of both DMDA and $CTMA^+$. This is composed of roughly 43% of the material with the remaining material being SiO_2 with surface hydroxyl groups. During the selective removal of DMDA through washing with ethanol, all of the DMDA is removed, as evident in the TGA. The TGA shows loss of 33% mass and the remaining material is SiO_2. It should be noted that due to the overlapping of the $CTMA^+$ and the DMDA, some DMDA might remain in the PE-MCM-41-Et. However, it

was confirmed by FTIR that no DMDA was present in PE-MCM-41-Et. For the calculations, it is assumed that all of the DMDA has been selectively extracted. The calcined material shows no loss due to both DMDA and $CTMA^+$ decomposing before 550 °C.

Table 4.2: Thermal Properties of PE-MCM-41

Material	*DMDA	*$CTMA^+$
PE-MCM-41	0.188	0.554
PE-MCM-41-Et	0	0.554
PE-MCM-41-C	------	------

*Reported as amount surfactant in grams per gram of silica

The amount of surfactant per gram of silica can be calculated knowing both the percent remaining after decomposition and the amount of material used. This number, using the PE-MCM-41-W will consist of both DMDA and $CTMA^+$. In order to determine the amount of only $CTMA^+$ present, the PE-MCM-41-Et silica was used. The amount of surfactant in the PE-MCM-41-W sample was subtracted from the PE-MCM-41-Et sample, which gives the amount of DMDA in the sample with the rest being $CTMA^+$. An inverse division was then performed on the amount of silica in the sample, and both DMDA and $CTMA^+$ were multiplied by this constant in order to determine the amount of surfactant per gram of silica.

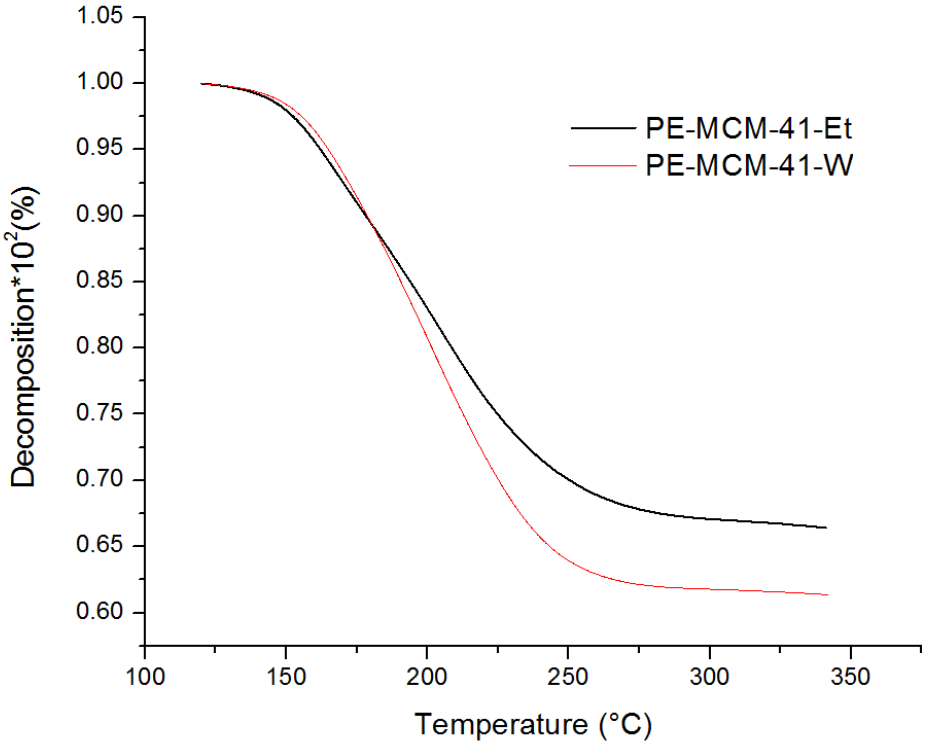

Figure 4.6: TGA of PE-MCM-41-W and PE-MCM-41-Et under N_2

In order to show that the structure of PE-MCM-41 was correct, FTIR was performed. This instrument works by passing IR radiation through a sample. The sample then absorbs some of the infrared radiation and some of it is transmitted. The resulting spectrum shows a "molecular fingerprint" of the sample, which allows one to identify chemical bonds and functional groups.

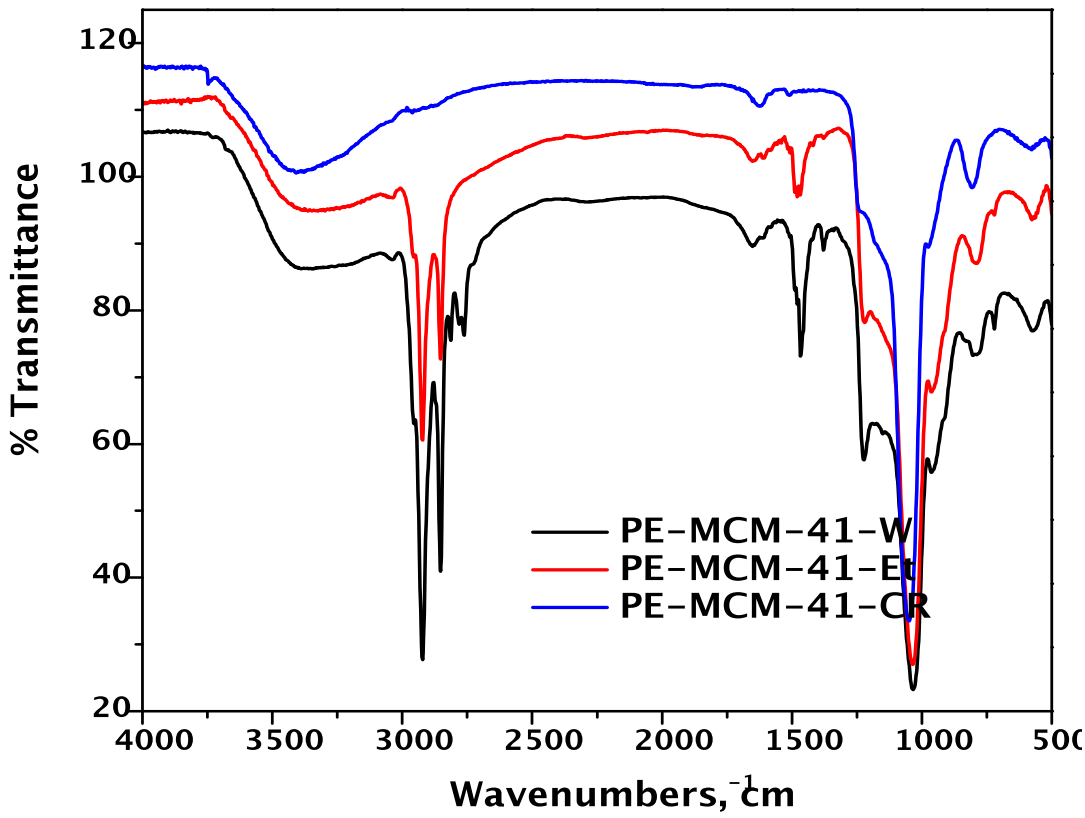

Figure 4.7: FTIR Comparison of the Three Pore Expanded Silicas. PE-MCM-41-CR (Top), PE-MCM-41-Et (Middle), and PE-MCM-41-W (Bottom).

By analyzing the fingerprints of PE-MCM-41-W, PE-MCM-41-Et, and PE-MCM-41-CR, slight differences could be seen. The assignments of PE-MCM-41-W are seen in Table 4.3, which will be further compared to both PE-MCM-41-Et and PE-MCM-41-CR. By comparing the water washed sample with the ethanol washed sample, there were two peaks different from PE-MCM-41-W, shown at 2700 cm^{-1}, which are due to the vibrations within DMDA, specifically the C-H sp^3 stretch of the N-CH_3 functionality. In order to prove the stretch was due to the C-H group, both (N, N-dimethyl-3-aminopropyl) trimethoxysilane (DMAP) and 3-aminopropyltriethoxysilane (APTES) were run on the FTIR. The main difference between DMAP and APTES occurred at 2807 and 2751 cm^{-1}, which was

attributed to the stretching of C-H bond on the nitrogen. As this group is not present on APTES, these peaks did not occur.

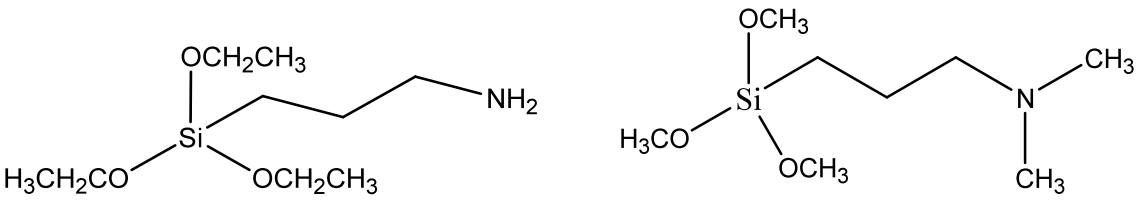

Figure 4.8: Structure of APTES (Left) and DMAP (Right).

When looking at DMDA and $CTMA^+$, it is apparent that they both contain N-CH_3 functional groups, however, when the FTIR of DMDA and $CTMA^+$ are run, only the peaks corresponding to the N-CH_3 with C-H sp^3 stretching are present in DMDA. Even though they were not observed in the $CTMA^+$ FTIR, they are still present in the structure of the DMDA. One possibility for this explanation is due to the positively charged ammonium, the CH_3 stretches are shifted to a higher wavenumber, thus no peaks in the range of 2700 cm^{-1} are observable. Upon the calcination of PE-MCM-41 to remove both DMDA and $CTMA^+$, only two peaks were seen at 3300 cm^{-1} and 1050 cm^{-1}, which correspond to O-H stretch and the Si-O stretch, respectively. This indicates that no surfactants are present in the PE-MCM-41-CR silica.

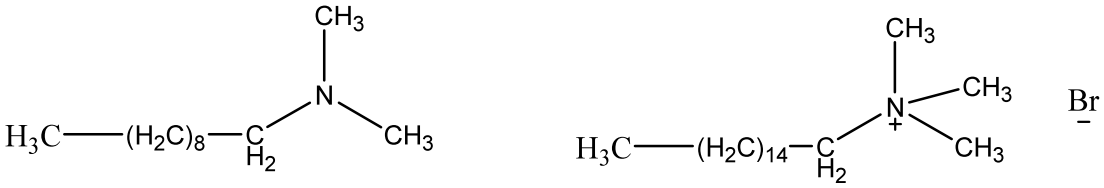

Figure 4.9 Structures of DMDA (Left) and $CTMA^+$ (Right).

Table 4.3: Assignment of Bands in the FTIR of PE-MCM-41-W.

Frequency (cm^{-1})	Assignment	Molecular Motion
3360	O-H	Stretching
2924	C-H	Stretching
2853	C-H	Stretching
2762	C-H	Stretching
1466	C-H	Bend
1223	C-N	Bend
1085	Si-O	Stretching

4.2 Characterization of Pore Expanded MCM-41 Palladium Supported Catalysts

The palladium containing PE-MCM-41 catalysts were prepared through an impregnation technique, which aimed for a palladium content of 0.5% by weight. However, leaching of palladium was observed in the filtrate of the material. This was confirmed by both the color of the filtrate and through ICP measurements of the sample and filtrate. The ICP reading of the filtrate gave indication that leaching did occur. The solid catalysts ICP measurement was also completed and it resulted in a 0.35% palladium by mass. Selective extraction of DMDA led to an ICP reading of 0.65% palladium by mass. No leaching was observed during DMDA extraction, as confirmed through ICP. Finally, the material was calcined at 550°C, which resulted in a palladium content of 1.11% by mass.

PE-MCM-41 consists of a hydrophobic channel, as shown in Figure 3.1, that is able to facilitate the penetration of water-soluble species, including cations within the pore

channels. These cations interact strongly with the amine functional groups, creating a driving force to place the palladium ions inside the pores.[120] The Pd^{2+} ions are complexed to the amine groups of the DMDA. Reduction via $NaBH_4$ provides a highly dispersed catalyst (Pd^0). To further prove this, the ICP analysis of the filtrates showed a much higher concentration of palladium in PE-MCM-41-Et and PE-MCM-41-CR.

Typically, the size of palladium nanoparticles is found to play an important role in determining how effective these catalysts are. For example, in the hydrogenation of carbon dioxide to methanol, it was seen that as the particle size increased from 2.1 nm to 10.1 nm and the increase in particle size caused the selectivity to be decreased.[125] This shows that particle size may have a prominent effect on the catalytic performance.

The best way to determine the average particle size and the particle size distribution is through a technique known as scanning transmission electron microscopy (STEM). [120] This produces an image in which the particle size and particle size distribution can be determined, as shown in Figure 4.10. For each image, 50 particles were measured and from this the average particle size and particle size distribution were determined. The STEM images and particle size distribution of the three catalysts are seen in Figure 4.10 while the results are further described in Table 4.4.

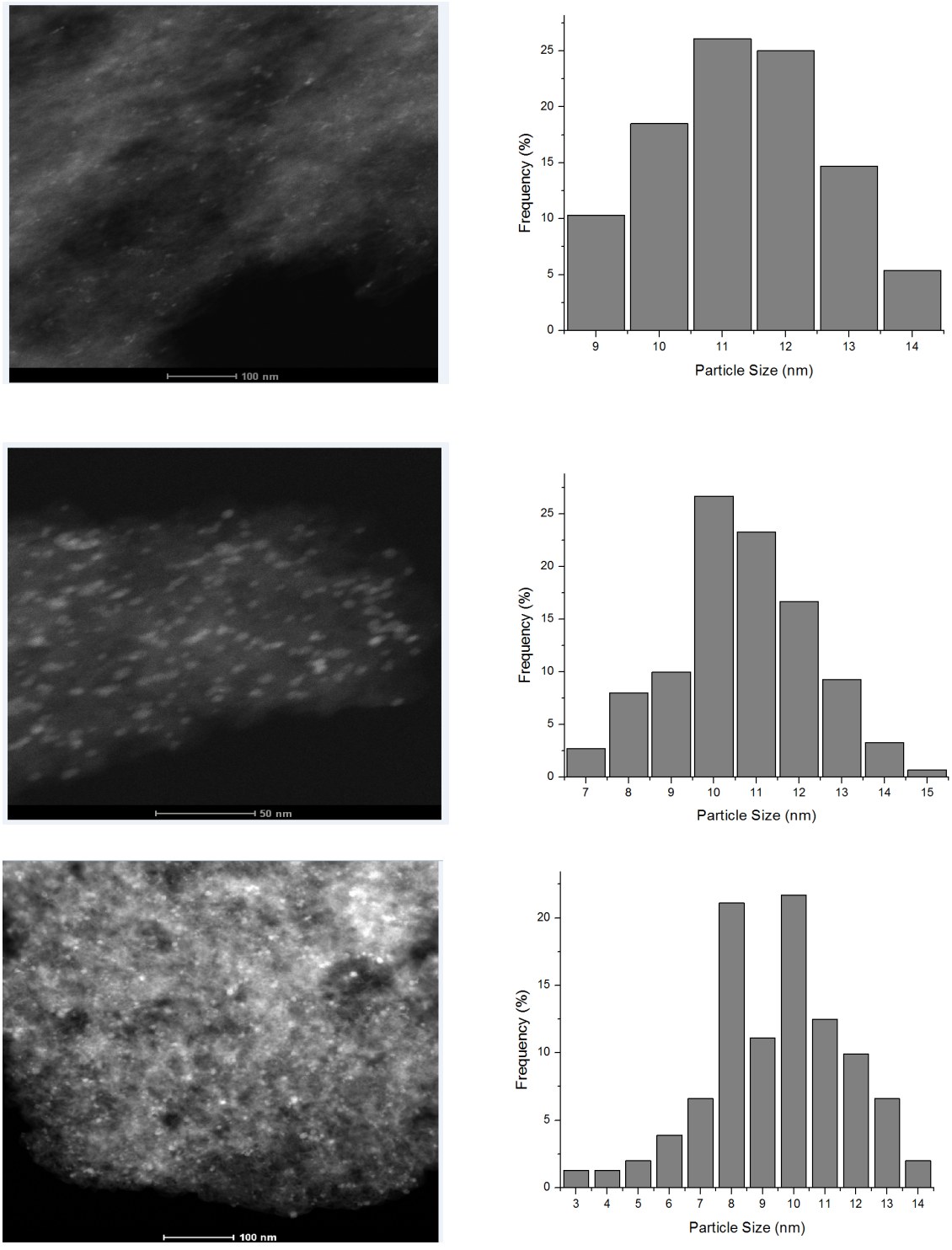

Figure 4.10: STEM and Pore Size Distribution of Pd-PE-MCM-41-W (top), Pd-PE-MCM-41-Et (middle), and Pd-PE-MCM-41-CR (bottom).

The Pd particle size distributions for the resulting catalysts were determined through STEM observation by measuring about 50 particles in each image for four images per sample. It can be seen that the mean diameter as well as the particle distributions shift to lower value upon calcination. For the sample, Pd-PE-MCM-41-W, the particles ranged from 9-14 nm in size, with a mean diameter of 11.8 nm. For the Pd-PE-MCM-41-Et, the particles ranged from 7 to 15 nm, with a mean particle size of 11.4 nm. As one can see, this decreased upon washing with ethanol. This could be from the washing of ethanol, in which some of the aggregation achieved with washing with water could disappear, resulting in a smaller mean particle size and wider pore size distribution. The third catalyst, Pd-PE-MCM-41-CR, ranged in size from 3 to 14 nm with a mean diameter of 10.2 nm, as seen in Figure 4.10. It is possible that both Pd-PE-MCM-41-W and Pd-PE-MCM-41-Et surfaces were oxidized, thus showing a larger particle size. This hypothesis is supported since the TPR profile of Pd-PE-MCM-41-CR showed no reduction peak while both Pd-PE-MCM-41-Et and Pd-PE-MCM-41-W did. This indicates that the palladium species was already reduced to the Pd^0 oxidation state for Pd-PE-MCM-41-CR catalyst.[126]

Table 4.4: Statistical Data for STEM Results of the Palladium Supported Catalysts

Sample	Mean (nm)	Std. Dev.	Min.	Max
PE-MCM-41-W	11.77	1.70	9.04	14.77
PE-MCM-41-Et	11.36	1.77	7.06	15.64
PE-MCM-41-CR	10.17	2.12	3.52	14.98

Hydrogen temperature programmed reduction was then run at different temperatures in order to achieve the best reduction temperature. The TPR reactions were run from 200-500 °C in 100 °C intervals and it was found the maximum thermal conductivity (TCD) signal for the catalyst Pd-PE-MCM-41-W occurred at 186 °C.[127] This shows that the maximum number of Pd^{2+} sites, typically in the form of palladium (II) oxide are reduced under 200°C to Pd^0 oxidation state. As the temperature is increased the TCD signal shows a weaker signal due to the interaction of hydrogen with Pd at higher temperatures. When washed with ethanol, the catalyst Pd-PE-MCM-41-Et showed maximum TCD signal at 187°C, indicating the DMDA does not play a significant role in the reduction of Pd^{2+} to Pd^0, but rather just the uptake of Pd^{2+} ions. The catalyst Pd-PE-MCM-41-CR was also run, but no evidence of reduction occurred due to palladium already being reduced to Pd^0 oxidation state.

Hydrogen pulse chemisorption consists of the adsorption of hydrogen on the palladium active sites until they become saturated with hydrogen and no more can be retained.[128] It is commonly used in order to measure the metal area of the catalyst. This technique allows the metal surface to be evaluated by measuring the number of surface metal atoms.[129] The metal area can be further calculated, as shown below:

$$\square\square=\square\square\square\square\square\square\square*\square\square\ \square\square\square \qquad (7)$$

where M_A is the metal area, M_{CSA} is the cross-sectional area of one palladium atom (7.862 nm^2), N_A is Avogadro's constant, M_D is the percent dispersion of the sample, wt is the percent metal loading of the sample, and M is the atomic weight of the sample.[129]

The metal dispersion, M_D, is another important piece of information regarding catalysts. Metal dispersion is the number of free metal atoms divided by the total number of metal atoms in the catalyst, expressed as a percentage. It is further defined as:

$$\text{D} = \frac{V_m \cdot N_A}{22414} * \frac{M}{wt} * 100$$

(8)

where V_m is the adsorbed volume of the monolayer, N_A is Avogadro's number, M is the atomic weight of the sample, and wt is the percent metal loading of the sample. [129]

The particle size can then be further calculated by applying the following equation:

$$p = \frac{6000}{\text{metal area}} *$$

(9)

where ρ is the density of palladium (ρ = 11.4 g/cm^3). The results are shown below in Table 4.5. However, an error up to 25% has been observed in many cases when calculating the metallic particle size.[129]

Table 4.5: Textural Properties of the Supported Palladium Catalysts

Catalyst	Uptake of H_2	Dispersion (%)	Metal Area	Particle Size
Pd-PE-MCM-41-W	3.3	9.5%	0.52	10.1
Pd-PE-MCM-41-Et	3.4	10.2%	0.56	9.4
Pd-PE-MCM-41-CR	3.6	11.1%	0.61	8.6

*** Units of Uptake of H_2 are μmol/g and metal area is m^2/g**

From Table 4.5, the textural properties of the metallic surface of palladium can be seen. The metal dispersion, which is based on particle size, shows a higher percent dispersion for smaller particle size. Pd-PE-MCM-41-W displays a larger particle size than that of Pd-PE-MCM-41-CR, while the dispersion is higher for the calcined sample. This in agreement not only in this work, but many examples of higher dispersion for a smaller particle size is shown in literature due to the higher percentage of surface atoms.[128]

Finally, the nitrogen adsorption results, shown in Table 4.6, do not show much of a change indicating that that there is no real change to the textural properties of the support upon deposition of palladium nanoparticles in the pores. It should also be noted that when comparing the catalysts to the PE-MCM-41 silicas, there was no change in the overall shape of the isotherm, indicating that the structural integrity of the PE-MCM-41 silica was maintained.

Table 4.6: N_2 Adsorption Results for Palladium Catalysts

Catalyst	S_A (m^2/g)	V_p (cm^3/g)	d_p (nm)
Pd PE-MCM-41-W	59.5	0.10	6.50
Pd-PE-MCM-41-Et	390.0	0.98	8.44
Pd-PE-MCM-41-CR	860.3	1.90	9.08

4.3 Selective Hydrogenation of Acetylene over Palladium Nanoparticles

Once the characterization of both the support and catalysts was complete, the catalytic activity of the catalysts was examined. The goal of this was to achieve high

selectivity and high conversion with good catalyst lifetimes in terms of the selective hydrogenation of acetylene.

First and foremost, the understanding of the reaction at hand is critical. As explained in section 2.1, there are five possible pathways (Figure 2.1) that may occur through the hydrogenation of acetylene. The three main reactions that must be closely examined are the partial hydrogenation to ethylene, partial hydrogenation to ethylene followed by hydrogenation to ethane, and finally the direct hydrogenation of acetylene to ethane, as shown below by the three reaction schemes.

$$C_2H_2 + H_2 \rightarrow C_2H_4 \quad (10)$$

$$C_2H_4 + H_2 \rightarrow C_2H_6 \quad (11)$$

$$C_2H_2 + 2H_2 \rightarrow C_2H_6 \quad (12)$$

Even though these are the three main reactions that need to be looked at, the over hydrogenation of acetylene must be eliminated as it tends to deactivate the catalysts in the purification process of the ethylene stream. Furthermore, one side reaction that can occur is the polymerization of ethylene to form green oil, which results in significantly decreasing the recyclability and lifetime of these catalysts.

In order to understand the mechanism of acetylene hydrogenation, the kinetics of it must first be understood. It was proposed in 1962 that since the enthalpy of adsorption of acetylene is higher than ethylene the surface coverage ratio of acetylene to ethylene would always be high.[130] A further proposal suggests that there are two types of active sites, which

are created via carbonaceous deposits in which only some of these sites only take part in acetylene hydrogenation whereas the other site is open to all other types. The site, which adsorbs acetylene and hydrogen, may be too small for other species.[130] However, the source of the carbonaceous deposits is still being questioned in terms of its origin and is still unknown to this date. In 2000, it was found that there are various types of surface carbon and that only the type of carbon, not the amount that will contribute to the selectivity of ethylene.[130]

From this information, two plausible mechanisms are possible, as shown in Figure 4.11; in the first mechanism, the acetylene, in the form of vinylidene, is absorbed simultaneously along with hydrogen molecules on the catalyst surface. This is known as the Langmuir-Hinshelwood mechanism and is most commonly accepted.[130] The second mechanism, more commonly known as the Al-Ammir mechanism, involves a hydrogen transfer from the carbonaceous deposits to the vinylic intermediate.[130]

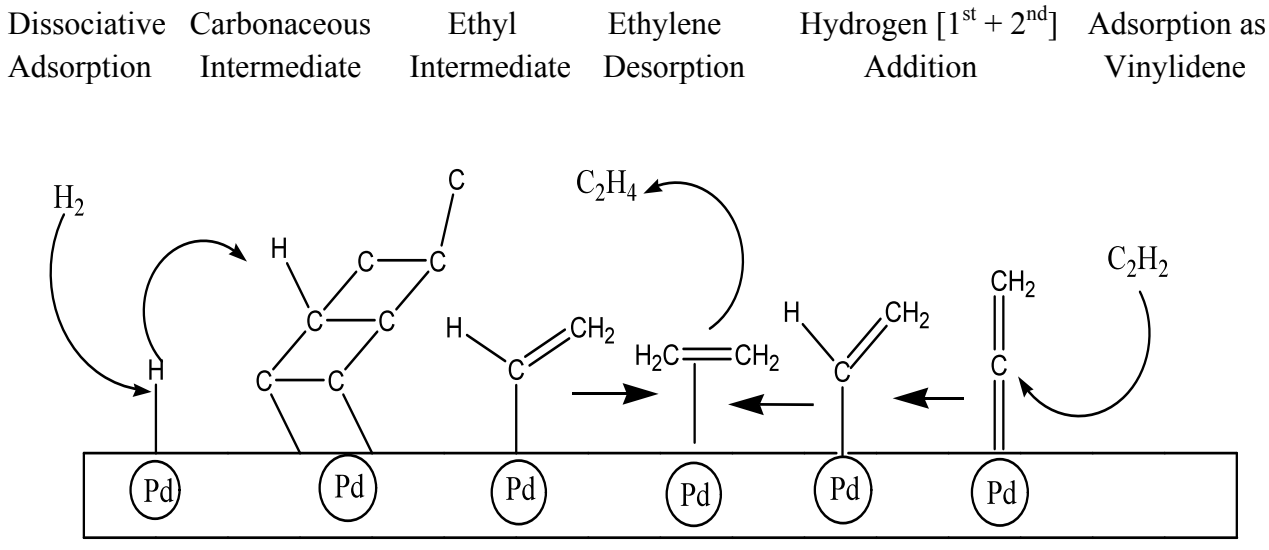

Figure 4.11: Two Possible Mechanisms for Selective Hydrogenation of Acetylene.

Now that the general acetylene hydrogenation mechanism is understood, the terms conversion and selectivity must also be understood. Conversion is defined as the fraction of starting material consumed in the reaction.[104] For example, the conversion of acetylene is defined as:

$$C = \frac{(\text{reactant}) - (\text{product})}{(\text{reactant})} \times 100$$

(13)

The selectivity is defined as the amount of desired product achieved from the conversion of the starting material[104]. The selectivity towards ethylene is defined as:

$$S = \frac{C_2H_4\ (\text{product})}{C_2H_2\ \text{reactant} - C_2H_2\ (\text{product})}$$

(14)

Now that both the conversion and selectivity are understood, the main goals of this project can be discussed. For the PE-MCM-41-W catalyst, 35 mg ($1.16 * 10^{-4}$ mmol Pd) was placed in the reactor. The catalyst was then pre-treated with hydrogen as well as increased temperatures (75 °C for Pd-PE-MCM-41-W and Pd-PE-MCM-41-Et, 300 °C for Pd-PE-MCM-41-CR, 50 mL/min H_2). Once cooled, the reactions were run at 25 °C to 100 °C at 15 °C intervals and then from 100 °C to 25 °C in order to ensure coke deposition did not occur. The samples were injected with 80 mL/minute, which is composed of 2% acetylene with increasing amounts of hydrogen (12.5, 28, and 56 mL/minute) of H_2 with the remaining made of up nitrogen (56, 44, and 15 mL/minute). The conversion and selectivity results for Pd-PE-MCM-41-W are displayed in Figures 4.12 and 4.13.

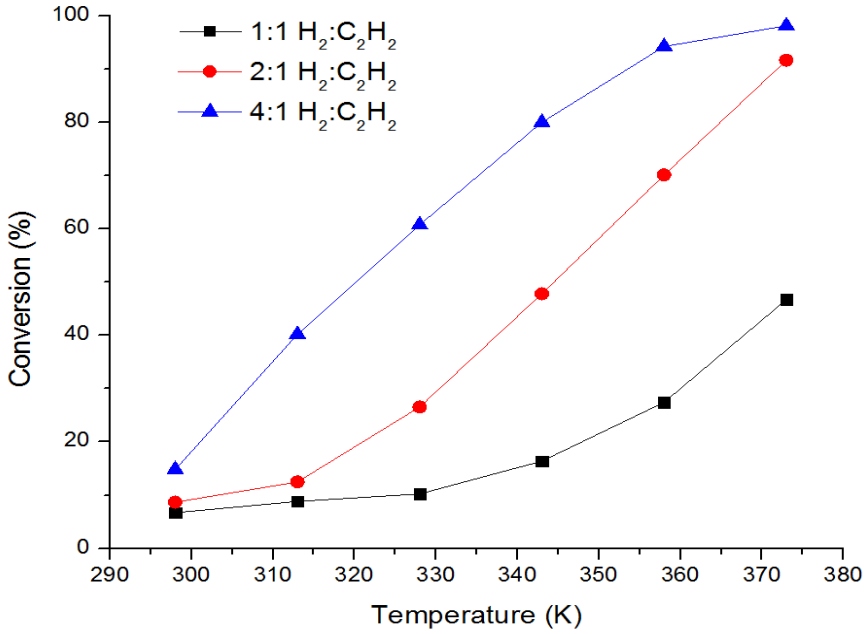

Figure 4.12: Conversion of Acetylene using the Pd-PE-MCM-41-W Catalyst

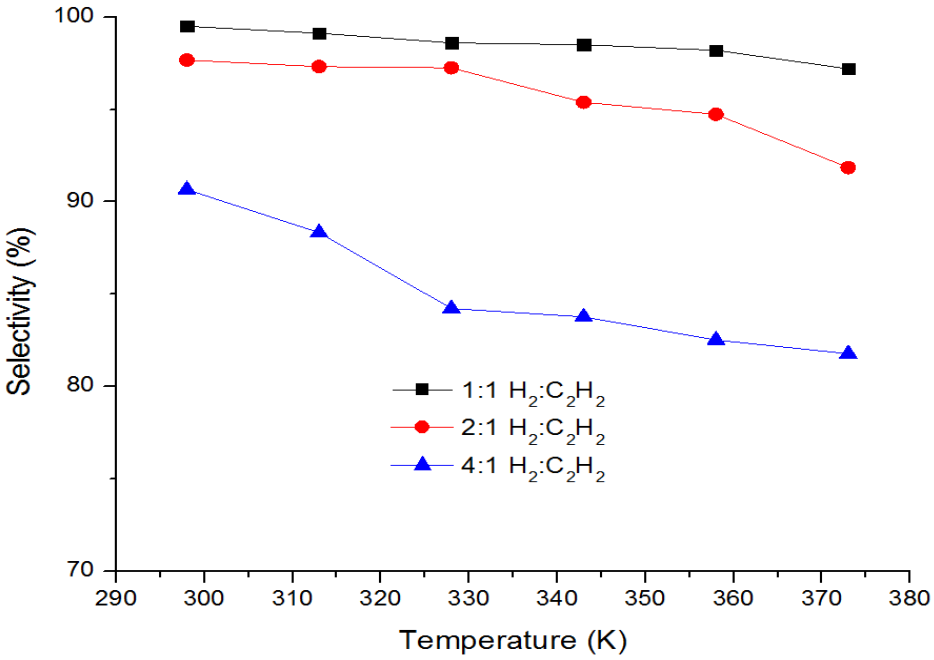

Figure 4.13: Selectivity of Ethylene using the Pd-PE-MCM-41-W Catalyst

For the 1:1 ratio of hydrogen to acetylene, there was little change to the selectivity up to 373 K, while the conversion rose to 47%. However, there was still over 50% acetylene remaining and therefore, the ratio of hydrogen to acetylene was increased to 2:1. By increasing the number of hydrogen molecules available for adsorption to the palladium active sites, the conversion increased to 99% at 373 K. The selectivity was found to drop as the hydrogen concentration increased, thus becoming less selective of hydrogenating acetylene to ethylene or ethane. It should also be noted that the selectivity decreases with increased temperature. The last ratio that was tested was four to one of hydrogen to acetylene and what was observed was that the conversion reached approximately 100% at 358 K. This essentially means that continuing past 358 K is pointless, as it will only lead to a faster deactivation of the catalyst.

The amount of catalyst (35 mg) was then increased to 60 mg in order to understand the effect it has on both the conversion and selectivity. As shown in Figure 4.14, the conversion increased significantly but at much lower temperatures. For example, the conversion at 328 K in Figure 4.12 in a 2:1 ratio of hydrogen to acetylene was 47%, while in Figure 4.14 it is 93%. This wouldn't be a problem as a higher conversion is better at a lower temperature; however, the selectivity also significantly drops from 91% to 60%, thus causing significant problems if continued.

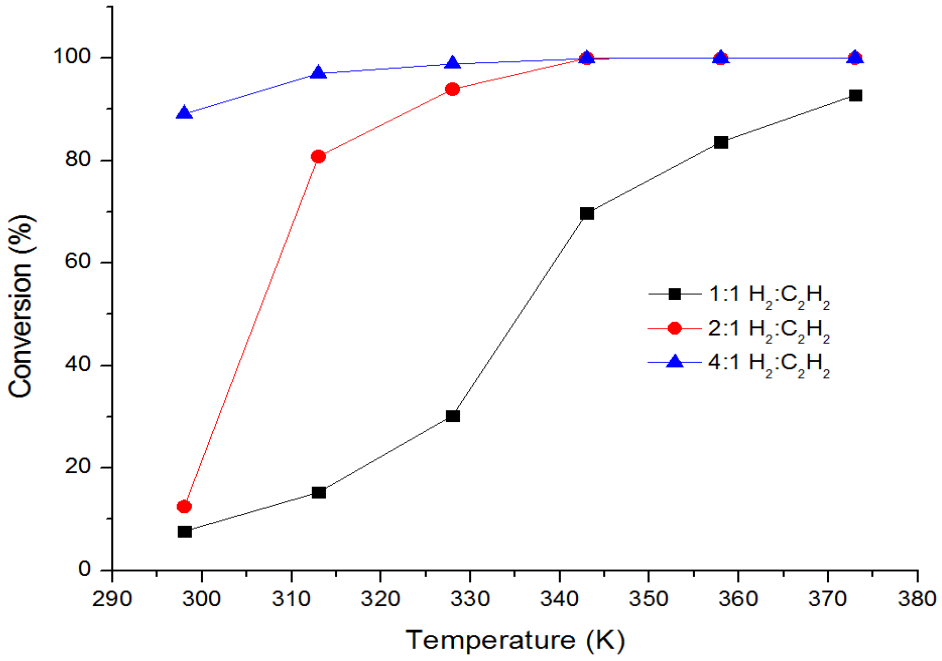

Figure 4.14: Conversion of Acetylene using Pd-PE-MCM-41 with 60 mg of Catalyst.

The next catalyst that was looked at was Pd-PE-MCM-41-Et, in which the Pd-PE-MCM-41-W was further washed with copious amounts of ethanol in order to remove the DMDA. The removal of DMDA was confirmed by nitrogen adsorption, TGA, and FTIR, shown in Figures 4.4, 4.6, and 4.7. By comparing the results between Pd-PE-MCM-41-W and PE-MCM-41-Et it is evident that both the conversion and selectivity were significantly lowered. At ~99% conversion for the PE-MCM-41-Et the selectivity was 62% while for PE-MCM-41-W the selectivity is 84%. This shows that not only does DMDA play a key role in controlling the conversion but, it also drastically increases the selectivity, as seen in Figures 4.15 and 4.16.

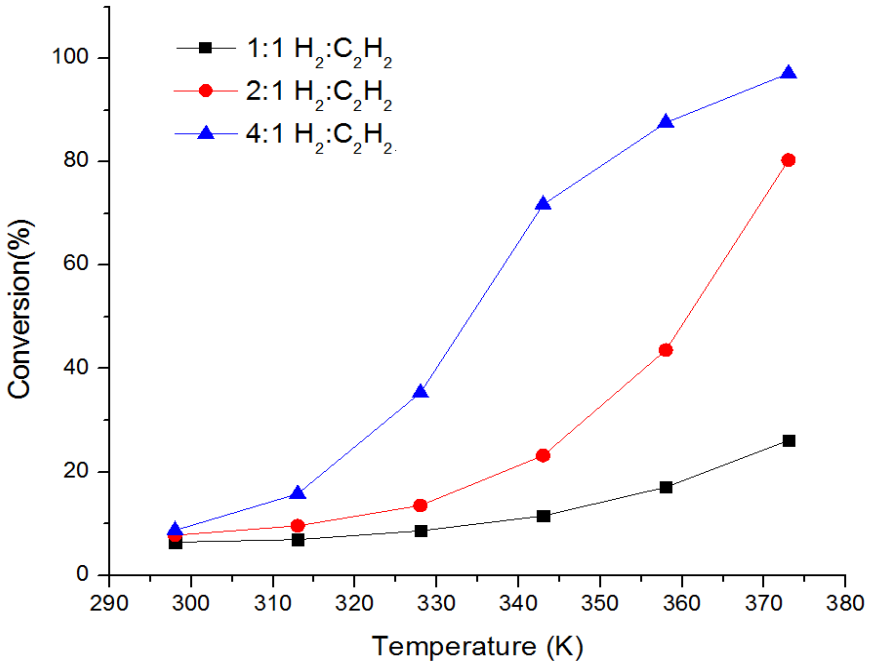

Figure 4.15: Conversion of Acetylene using the Pd-PE-MCM-41-Et Catalyst

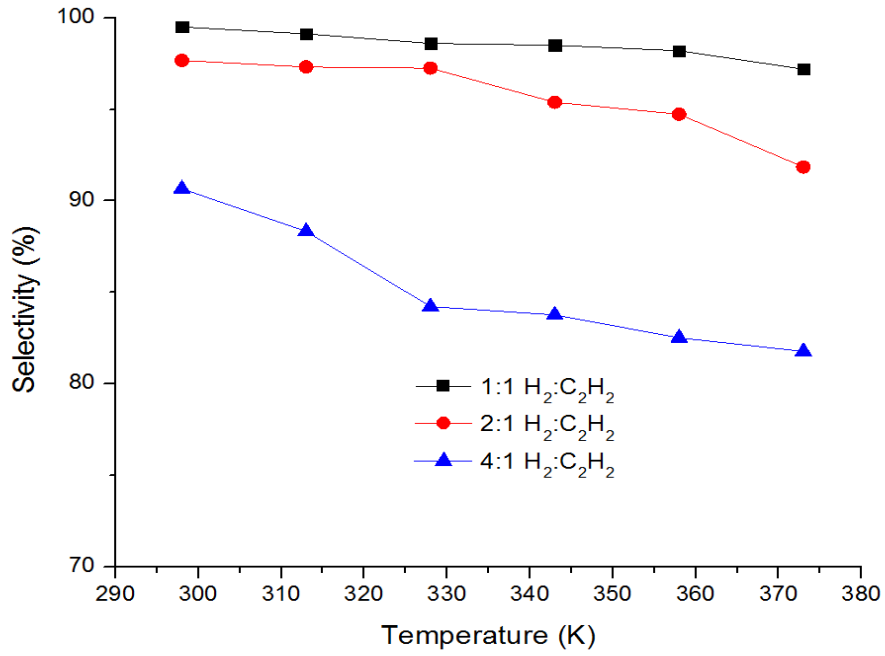

Figure 4.16: Selectivity of Ethylene using the Pd-PE-MCM-41-Et Catalyst

Finally, the water washed Pd-PE-MCM-41 catalysts was calcined at 550 °C for 6 hours in order to remove all surfactants. The removal of both $CTMA^+$ and DMDA was confirmed by TGA, FTIR, and nitrogen adsorption. In both the FTIR and TGA, the only peaks shown correspond to SiO_2 and surface hydroxyl groups. The removal of $CTMA^+$ and DMDA can be seen by the significant increase in surface area and pore volume due to the removal of the remaining surfactants within the mesopores.

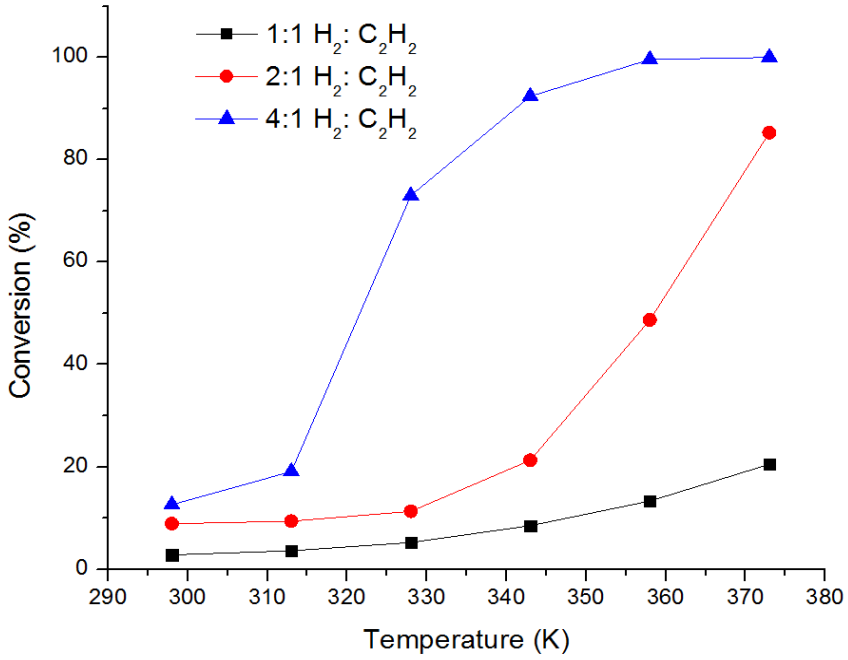

Figure 4.17: Conversion of Acetylene using the Pd-PE-MCM-41-CR Catalyst

Figure 4.17 shows that with the presence of the one to one ratio of hydrogen to acetylene, the conversion was increased slowly with increasing temperature. This shows that surfactants play a key role in the conversion to ethylene. However, when the ratio is increased, the conversion also increased significantly. This shows that not only does DMDA have a role on the conversion, but so does $CTMA^+$. Comparing the results of Pd-PE-MCM-

41-Et shows that as conversion is increased, with increasing temperature, the selectivity tends to suffer.

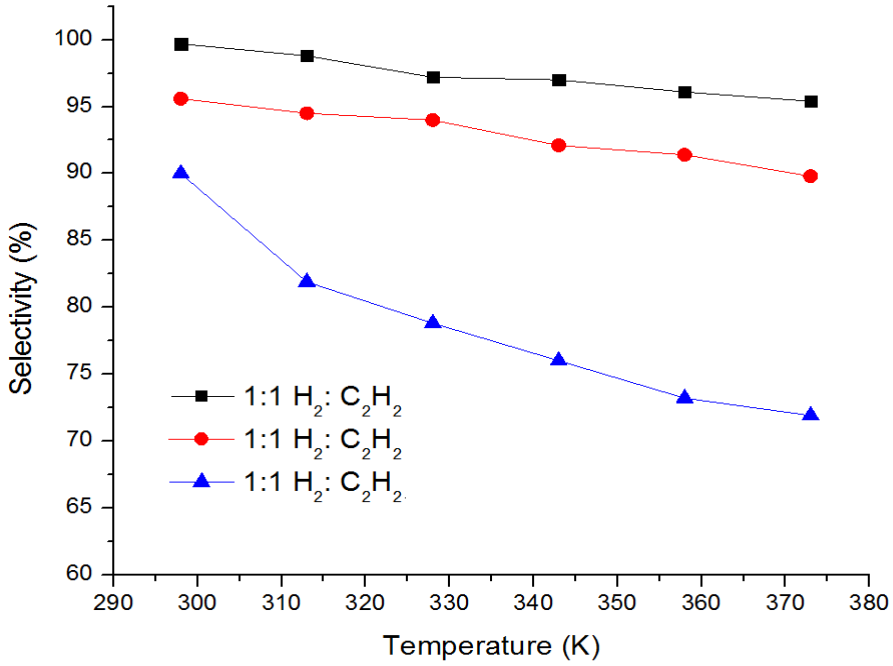

Figure 4.18: Selectivity of Ethylene using the Pd-PE-MCM-41-CR Catalyst

Not only was the conversion important, but also the selectivity is key in determining the overall success of the catalytic reaction. The selectivity, as seen in Figure 4.18, has shown that at low conversions the selectivity will be higher than with increased temperatures. For example, at 85% selectivity, the conversion is 89% while at 25% conversion the selectivity is 95%.

In order to understand both the activity and selectivity of the three palladium-supported catalysts, they must be compared to each other. As expected, the conversion increased with increasing temperatures from room temperature to as high as 373 K. In the Pd-PE-MCM-41-W catalyst, the conversion reached as high as 100% in a 2:1 ratio of H_2:

C_2H_2 at 373 K, whereas the Pd-PE-MCM-41-Et and Pd-PE-MCM-41-CR catalysts showed a conversion of 80% and 85%, respectively. The increase in conversion with temperature agrees with many examples in the literature, which is due to the enhancement of the rate of acetylene activation on the surface of the catalyst. It should also be stated that a blank experiment was run, consisting of just the pore expanded MCM-41 silica, which showed no activity towards hydrogenation of acetylene. This insinuates the crucial need for the palladium nanoparticles in the reaction. At 373 K, the selectivity started to show a decrease in the water washed catalyst at a 2:1 ratio of hydrogen to acetylene. However, the ethanol washed and calcined catalysts showed selectivities of 75% and 71%, respectively.

One way to explain the above results would be that the nitrogen containing compound, DMDA, which is only present in the water wash catalyst, often influences the electron density of the metallic nanoparticles.[104] This change in the electron density will affect the adsorption of the reactants, and desorption of the products. By this effect not being seen in both Pd-PE-MCM-41-Et and Pd-PE-MCM-41-CR catalysts, this hypothesis is strongly supported. This hypothesis is further supported by the fact that Wang et al found that activity and selectivity was highly influenced by the presence of N, O organic functionalities on the silica surface.[104]

It is important to understand how active the catalysts are and if they are subject to deactivation. Therefore, the deactivation was looked at via time on steam (TOS) behaviour. To do this, the catalyst was used under the same conditions (hydrogen ratio, temperature) for a long period of time. This will display whether or not the catalyst will lose its activity or selectivity over time.

Figure 4.19 shows that at 373 K with a $H_2/C_2H_2 = 2$, not only does the conversion decrease as a function of time, but so does the selectivity. By increasing the ratio of hydrogen to acetylene to 4 to 1, the conversion was not affected at 12 hours, but the selectivity decreased by 14%, showing that the catalyst was subject to deactivation. This can be due to several factors including carbonaceous deposits and sintering of the metallic nanoparticles at higher temperatures that can lead to aggregation.[131] Two techniques, which would be quite helpful in exploring this, would be SEM as well as TEM after the catalysts were spent. This needs to be further explored, as outlined in the future work section.

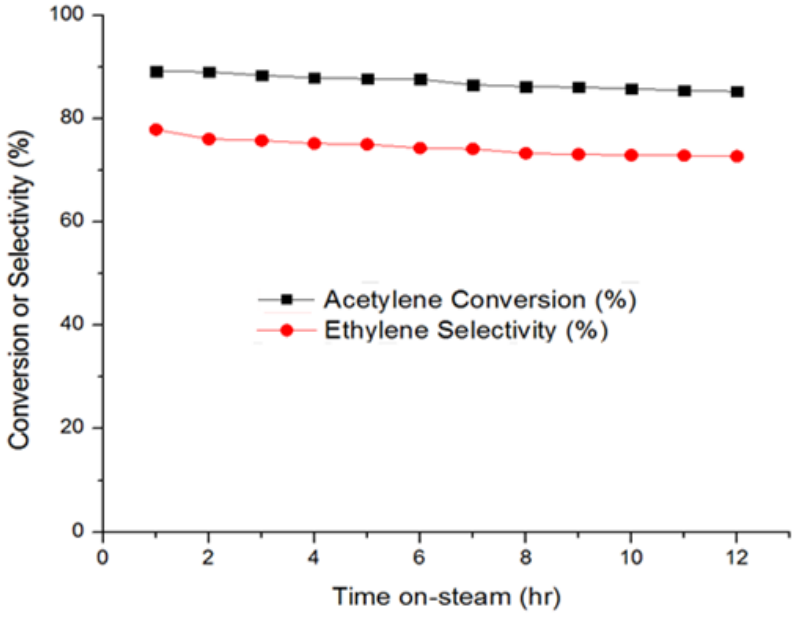

Figure 4.19: TOS of Pd-PE-MCM-41-W at 2:1 H_2:C_2H_2 at 373 K

However, in order to truly compare the results, one needs to compare the activation energies of the catalysts. In order to compare the activation energy, one must apply the Arrhenius equation, as seen below[132]:

$$k=Ae \quad (15)$$

where k is the rate constant, A is the pre-exponential factor, E_a is the activation energy, R is the universal gas constant, and T is the absolute temperature in kelvin. In order to determine, the activation energy, the Arrhenius equation must be given in straight-line form.[132] This is seen below:

$$\ln(k) = -ERT + \ln(A) \quad (16)$$

This means that when a reaction obeys the Arrhenius equation, the plot of ln (k) versus 1/T will give a straight line. This can further be used to calculate the activation energy. Therefore, activation energy can be determined by applying the following equation[131]:

$$E = -\text{slope}/R \quad (17)$$

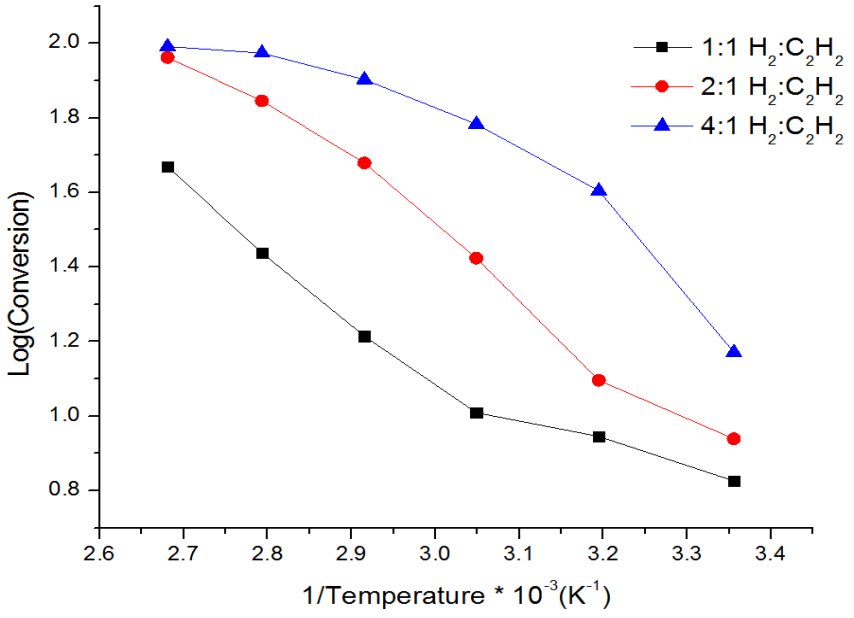

Figure 4.20: Log (Conversion) Vs. 1/T for the Pd-PE-MCM-41-W Catalyst

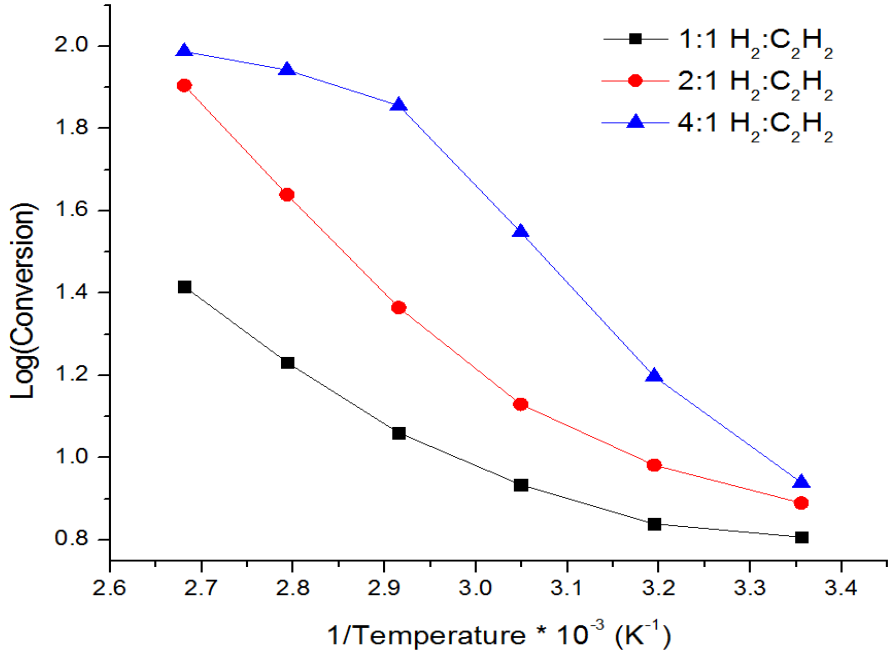

Figure 4.21: Log (Conversion) Vs. 1/T for the Pd-PE-MCM-41-Et Catalyst

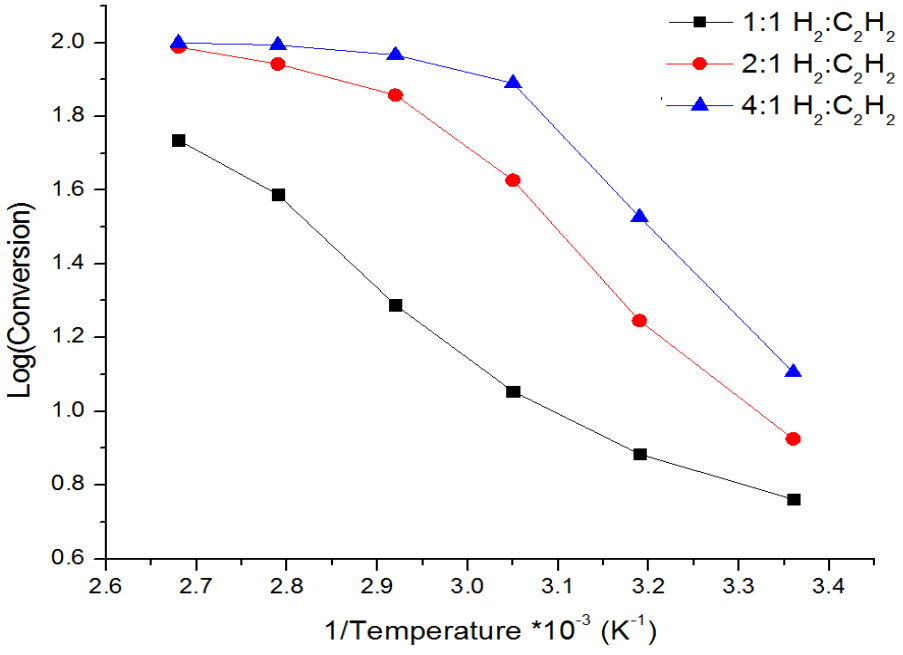

Figure 4.22: Log (Conversion) Vs. 1/T for the Pd-PE-MCM-41-CR

However, this equation does not represent the true activation energies of acetylene hydrogenation. Instead of using the true rate constants, the apparent rate constants, denoted as Q, were used as a function of conversion. Since the rate constants change with an increase in concentration, these values do not accurately portray the true rate constants as a change in concentration does change the rate constants. It should also be noted that the slopes of each line are not truly linear lines, which may further lead to lower apparent activation energies. This equation can be applied since the conditions for the reaction are held constant including flow rate, catalyst amount, etc. Therefore, conversion can also be defined as:

$$\text{Conversion} = \text{rate} * \tau \tag{18}$$

where rate is the rate constant and τ is residence time as defined blow

$$\tau = \text{system capacity for a particular system} \text{flow rate} \tag{19}$$

Since the residence time for the catalysts used will stay constant, it can be considered a constant, a, and used in the linear-form of the Arrhenius equation.

$$\ln(\text{rate}) = \ln(\text{rate}) + \ln(a) \tag{20}$$

Since it is used in a logarithm, it can be separated into two separate terms, as shown above, and therefore, it will not affect the slope of the Arrhenius equation and thus, not the apparent activation energy of the reaction.

In order to understand the effects of the activation energy, the thermodynamics of the reactions must be discussed. The activation energy is the minimum energy that must be used in a chemical system in order for a reaction to proceed.[132] When using a catalyst, it will

lower the transition state to a lower energy, thus the catalyst will increase the reaction rate to produce the desired product.

Table 4.7: Calculated Apparent Activation Energies for Palladium Supported Catalysts

	Pd-PE-MCM-41-W	**Pd-PE-MCM-41-Et**	**Pd-PE-MCM-41-CR**
1:1 H_2:C_2H_2	12.6	7.5	12.6
2:1 H_2:C_2H_2	14.3	12.7	13.7
4:1 H_2:C_2H_2	----	15.8	----

***All values reported in kJ/mol.** ---- Not reported due to non-linear behaviour

From Table 4.7, it can be seen that as the concentration of H_2 increases, the higher the apparent activation energy will be. One can also, seen previously Figures 4.12 and 4.15 as well as Table 4.7, see that as the amount of product formed is increased, the amount of energy required to overcome the energy barrier to be able to achieve high conversion is increased. Even though many assumptions are made for this calculation, it still gives a general idea of what is to be expected from the activation energies of the overall reaction. Previously, it was reported that hydrogenation reactions, such hydrogenation of benzene and acetylene, have an activation energy between 40-44 kJ/mol. This means that the apparent activation energy is under estimated by approximately 60% and will have to be further improved in order to have any significance.

The percent yield is calculated by multiplying the selectivity by the conversion. It is important to take into account the conversion of the hydrogenation of acetylene as not 100% conversion can be assumed in this case.

From these results it can be seen that as the conversion rose, the selectivity was found to suffer. However, with low conversions the selectivities remained high. To achieve a good yield, the selectivities must stay high while achieving a high conversion. However, for the catalyst Pd-PE-MCM-41-W, the highest yield able to be achieved was 91.6%. This occurred from maintaining a high selectivity with a good conversion. To achieve a good yield, the selectivity must be improved.

Upon washing with ethanol, the catalyst Pd-PE-MCM-41-Et showed a substantial decrease in the highest percent yield due to the effect of DMDA. The ability of DMDA to further help Pd^0 active sites played an important in the overall yields via the increase in electron density.

By using the catalyst, Pd-PE-MCM-41-CR, it did not improve upon its yield. However, it was improved upon in comparison to the ethanol washed catalyst. The highest achieved percent yield for the calcined catalyst was 75.5%, which corresponded to a conversion of 85.3% with a selectivity of 88.4%. This means that the removal of CTMA plays an important role in hydrogenation to acetylene.

The turnover frequency (TOF) were calculated and are shown in Figures 4.23-4.25. The turnover frequency was determined by taking the moles of ethylene and dividing it by the moles of catalysts times percent dispersion as a function time.[128] The moles of product were determined by calibrating the GC and knowing the amount of catalysts used for the reaction. In order to determine the time of the reaction, the number of loops in GC needed to be known, which will subsequently give the TOF per unit of time.

□□□=□□□ □□ □□□□□□□□□□□ □□ □□□□□□□□□*%

□□□□□□□□□□□*□□□□(□) (21)

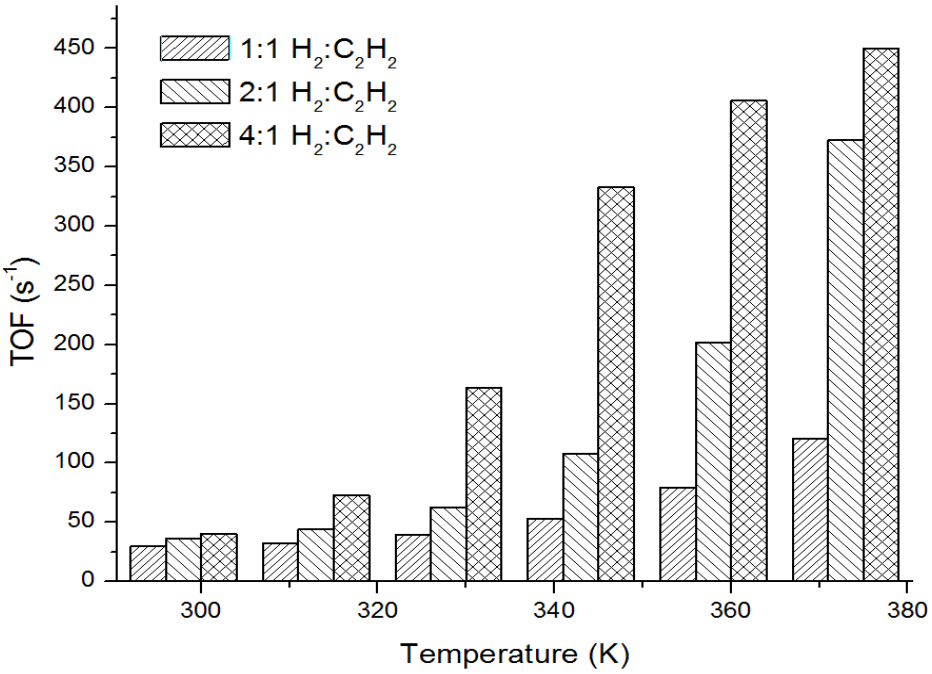

Figure 4.23: Calculated TOF for the Catalyst Pd-PE-MCM-41-W

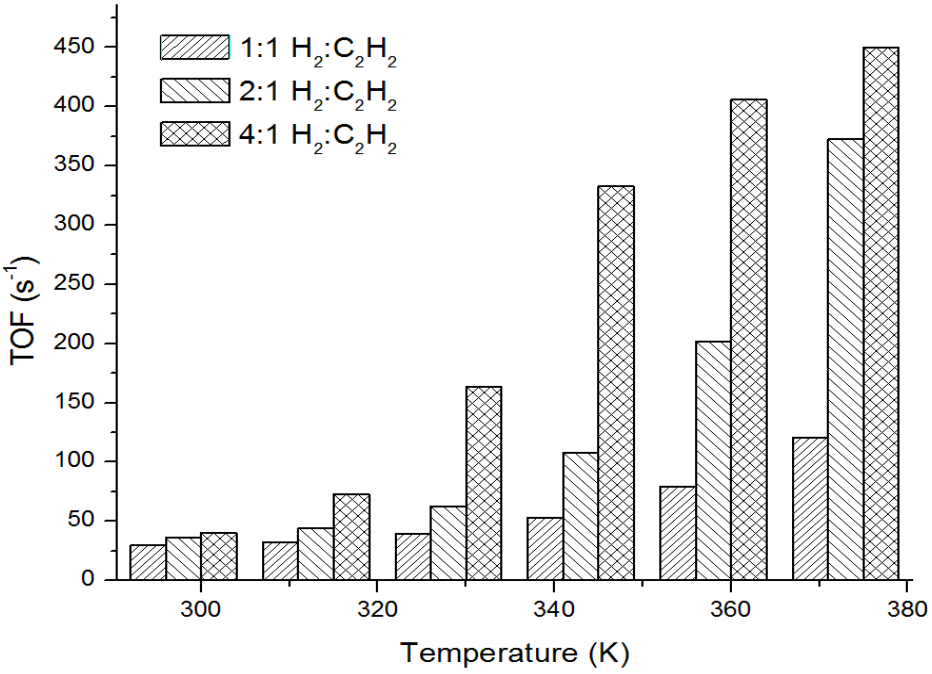

Figure 4.24: Calculated TOF for the Catalyst Pd-PE-MCM-41-Et

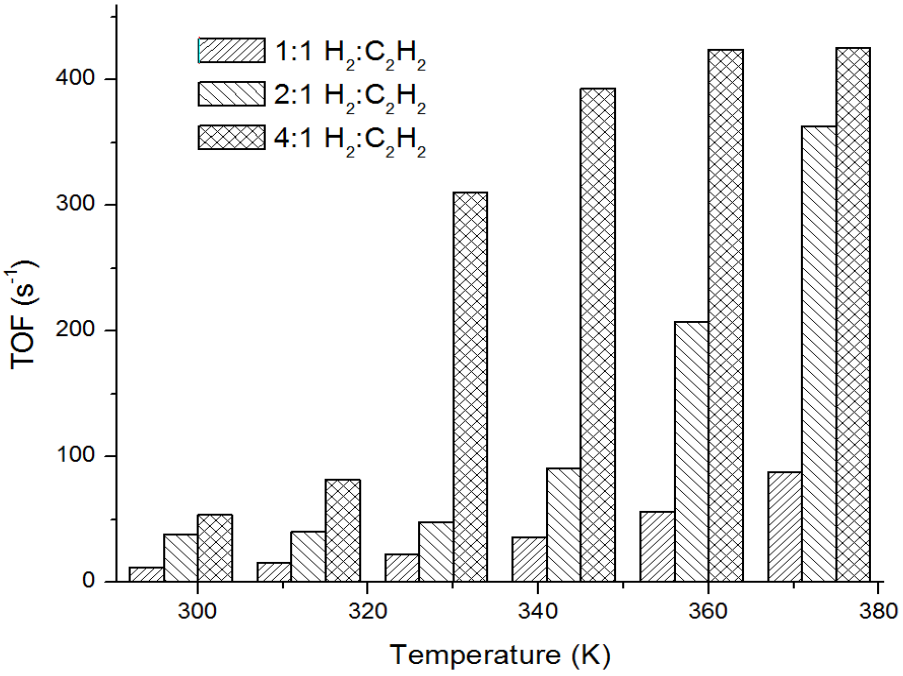

Figure 4.25: Calculated TOF for the Catalyst Pd-PE-MCM-41-CR

From these results it can be seen that the activity of the catalyst Pd-PE-MCM-41-W is much higher due to the role of DMDA within the selective hydrogenation of acetylene. This is particularly profound in the one to one ratio of hydrogen to acetylene; it shows that the TOF is much higher for the water washed catalyst as compared to both the ethanol washed catalyst as well as the calcined catalyst. The water washed catalyst is reported at just over 4 s^{-1} while both the ethanol washed and calcined are calculated to be at ~100 s^{-1} and ~ 125 s^{-1}, respectively at 313 K. Upon increasing the ratio of hydrogen to acetylene to two to one, the maximum TOF is achieved at 373 K, with just over 500 s^{-1}. However, the TOF for the water washed catalyst is maintained with no large increases. But, in comparison to the ethanol washed and calcined catalysts, they both have large increases between 343-373 K, reaching maximum TOF at just over 450 s^{-1} for the ethanol washed catalyst and just under 450 s^{-1} for the calcined catalyst. Upon increasing the hydrogen to acetylene ratio to four to one, it was found that TOFs increased much more quickly due to the rapid increase in conversion. Maximum TOF was achieved at 373 K for the water washed catalyst. For the ethanol washed catalyst, the maximum TOF was seen at 373 K, with large increases, which shows the prominent effect that temperature displays on the activity of the catalysts. Finally, the calcined catalyst shows a maximum activity at 373 K. However, even though good TOF is displayed, TOF does not take into account the selectivity of the catalysts. The selectivities were found to be quite low, especially with a rise in conversion at increased temperatures and ratios of hydrogen to acetylene. In order to address this issue, the metal complexation and reduction of both Au and PdAu supported nanoparticles are looked at in sections 4.4 and 4.5.

4.4 Selective Hydrogenation over Gold Nanoparticles

In order to see the effect of Au nanoparticles on the PdAu supported nanoparticles, the Au supported catalysts were also studied. The Au supported nanoparticles were prepared through a complexation technique that gave a 0.012% loading of Au by mass. This catalyst was then washed with copious amounts of ethanol in order to remove DMDA, which resulted in a loading of 0.029% Au by mass. The samples were then calcined at 550 °C in air which resulted in a 1.11% loading of Au by mass. It should be noted, however, that the loadings of both the water washed and ethanol washed samples were not as expected as most of the gold was lost through filtration. This could be due to the weak electrostatic interactions of the gold with amines, resulting in most of the gold not being deposited within the pores of the PE-MCM-41.

To test this hypothesis, the adsorption of gold must first be compared to a theoretical study done in 2013 by Lewoczko et al. They found that the adsorption energy of gold on long chain amines increased as the alkyl chain of the amine decreased.[133] This shows that the longer the alkyl chain is, the weaker the interactions will be between the long alkyl chain amine groups and the gold nanoparticles.[133] This explains why most of the Au particles were lost when filtered, as shown via ICP analysis.

Even though this explains why the gold loading suffered, the adsorption of both hydrogen and hydrocarbons, particularly acetylene and ethylene, must also be understood. First, gold has a limited ability to chemisorb hydrogen, especially compared to palladium. It is also dependent upon the dissociation of hydrogen molecules. It is suggested that hydrogen reacts with low-coordinated Au atoms on the corner and edge sites, which have a more reactive d-band via increased electron density.[134] Therefore, the smaller the nanoparticle is, the more corner and edge sites there will be. This is a possible explanation for why gold

nanoparticles, in the range of 2-5 nm have been shown to be active for certain catalytic reactions.[134] For supported Au nanoparticles, it is suggested that the adsorption of hydrogen is an activated process via the dissociation of hydrogen molecules.[133]

For the adsorption of alkynes and alkenes, it was demonstrated that the high selectivity of gold is due to the much stronger adsorption of alkyne versus that of the alkene. Upon the selective hydrogenation to the alkene, the strongly adsorbed acetylene prevents the re-adsorption of the alkene to further hydrogenate the alkene to the alkane.[134] Total hydrogenation to the alkane only occurs once the concentration of the alkyne is low enough to allow adsorption of the alkene. Catalytic hydrogenations of the C_2 alkyne attributed the high selectivity to the preferential adsorption at the edges of nanoparticles, thus making particle size distribution very important.[134]

In terms of the catalytic reactions, all three catalysts were inactive at low temperatures. However, upon increasing the temperature to 573 K, the conversion was found to increase to approximately 10% while maintaining a high selectivity. However, this creates a need for the consumption of energy as well as an increase in the cost of developing these catalysts. An assumption based on the method of catalyst preparation is that since catalyst metal impregnation and complexation tends to lead to larger particle sizes, the particle size is much larger than what is required to be active.[132] Since the mean of the palladium nanoparticles were all found to be above 10 nm, it is fair to assume that the gold nanoparticles would be even bigger.

Even though the use of gold supported catalysts showed little to no activity, there are many other uses for gold in catalysts. In particular, it provides two main uses. Firstly, most

catalysts are subject to deactivation by decreasing the number of active sites, a decrease in the number of quality active sites, and the degradation in the porous structure of the support. One of the most common paths of deactivation is through thermal degradation; larger metallic particles can grow and coalesce to form larger nanoparticles.[133] Secondly, palladium based catalysts have been known to suffer in terms of selectivity while maintaining high activity. In order to address both these issues, the alloying of palladium with a group XI (Cu, Ag, Au) metal should be able to help.[134] In this case, the alloying of palladium with gold occurred and will be discussed in section 4.5.

4.5 Selective Hydrogenation Over PdAu Nanoparticles

Even though the conversion of the Pd based catalysts were quite high, the selectivity tended to suffer. In order to get better selectivity of the catalysts, an enhancer, gold, was added to the catalysts. The PdAu supported on PE-MCM-41 were prepared via complexation technique which resulted in a 0.035% Au with 0.088% Pd by mass. This sample was then subsequently washed with ethanol to remove DMDA, This resulted in a 0.35% Au with 0.17% Pd by mass. However, the Au loading content was much lower than originally anticipated due to the lower adsorption of gold and amines in the PE-MCM-41-Et washed catalyst. This is likely due to the weak electrostatic interactions of gold with long chain amine functionalities, as they would be much weaker than that of palladium and amine groups, as evident by minimal loss of palladium. The PdAu-PE-MCM-41-W catalyst was then calcined at 550 °C, which resulted in the loss of both $CTMA^+$ and DMDA. This gave a catalyst loading of 1.6% Au with 0.37% Pd by mass.

First and foremost, the PdAu supported catalysts must be characterized. The first method of characterization is through the use of hydrogen TPR. The TPR profile for the PdAu-PE-MCM-41 should show two peaks; one for reduction to Pd^0 and one for the reduction to Au^0 from Pd^{2+} and Au^{3+}. However, no peaks for the reduction of gold occurred. This could mean one of two things; firstly, it is possible that the reduction of Au^{3+} to Au^0 did not occur and that only the reduction of Pd^{2+} to Pd^0 occurred. This is possible as chemisorption on gold has been found to not occur.[133] The second possibility that could occur is that the palladium and gold form bimetallic alloys and thus the one peak would represent both the reduction of palladium and gold nanoparticles. The second case is the most plausible case, particularly since the uptake properties of hydrogen would not be expected to change. The TPR profile showed a T_{max} at 190°C for both PdAu-PE-MCM-41-W and PdAu-PE-MCM-Et while no TPR peak was observed for PdAu-PE-MCM-41-CR.

Secondly, the catalysts needed to be characterized in terms of the metallic properties. The amount of adsorbed hydrogen per gram, the dispersion of the atoms, and the metallic surface area are shown below in Table 4.8. From this, it is shown that if H_2 uptake on gold does not occur, then this only shows only the surface palladium uptake of hydrogen, which would account for the smaller apparent size of the metallic nanoparticles.

Table 4.8: Textural Properties of Palladium-Gold Catalysts

Catalyst	Uptake of H_2	Dispersion (%)	Metal Area	Particle Size
PdAu-PE-MCM-41-W	4.7	15.6%	0.86	6.3
PdAu-PE-MCM-41-Et	4.9	16.2%	0.89	7.6
PdAu-PE-MCM-41-CR	5.2	17.3%	0.95	8.4

***Units of Uptake of H_2 are µmol/g and metal area is m^2/g**

Finally, the PdAu catalysts were characterized via N_2 adsorption, and it was shown that there was no significant change to the surface area, pore volume, and pore size. The textural properties showed a type IV adsorption isotherm, indicative of a mesoporous material. As there was no change to the overall shape of the adsorption isotherm, this indicates that the structural integrity was of the mesoporous silica was maintained.

Table 4.9: Textural Properties of the Supported PdAu Catalysts

	S_A (m^2/g)	V_p (cm^3/g)	d_p (nm)
PdAu-PE-MCM-41-W	61.9	0.11	6.2
PdAu-PE-MCM-41-Et	527.3	1.22	7.4
PdAu-PE-MCM-41-CR	1025.7	2.05	8.5

Once the catalysts have been characterized, it is important to mention the catalytic results. In order to keep the results consistent, the same amount palladium was kept in all trials. To do so, 140 mg ($1.16 * 10^{-4}$ mmol pd) of the catalyst PdAu-PE-MCM-41-W was used in the hydrogenation of acetylene. The water washed catalyst showed superior selectivity for the 1:1 ratio of hydrogen to acetylene; this catalyst showed a selectivity of no less than 98%, as seen in Figure 4.27. However, the conversion suffered only achieving a

conversion of 44%, as seen in Figure 4.26. Upon heating to a max of 493 K, it was shown that the maximum conversion able to be achieved was 64%. The conversion levelled out at 448 K, meaning that the maximum conversion at a one to one ratio is 64% due the acetylene molecules being in excess.

In order to address this issue, the ratio of hydrogen to acetylene was increased to 2 to 1; this should allow for 100% conversion to ethylene. However, this may expose problems to selectivity by over hydrogenating acetylene to ethane, and not stopping at ethylene. Even though this could have potentially reduced the selectivity of ethylene, it occurred only slightly. At 100% conversion, the selectivity was 97.75%, as shown in Figure 4.26 and Figure 4.27. However, using the four to one ratio of hydrogen to acetylene showed a decrease in the selectivity to as low as 92% while maintaining high conversions. This is drastically improved upon the addition of gold, as without using gold as enhancer, the selectivity reached a low of 58%.

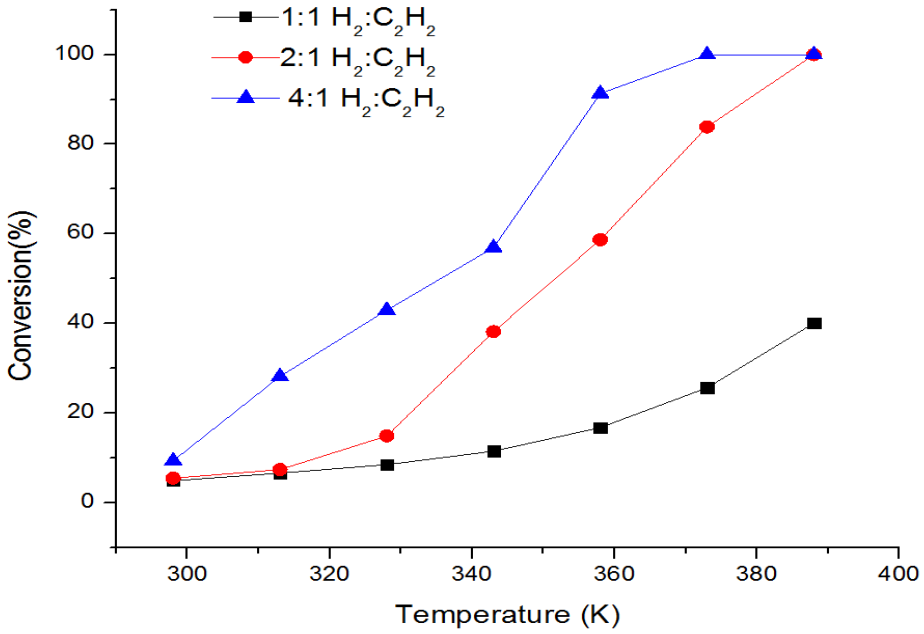

Figure 4.26: Conversion of Acetylene using the PdAu-PE-MCM-41-W Catalyst

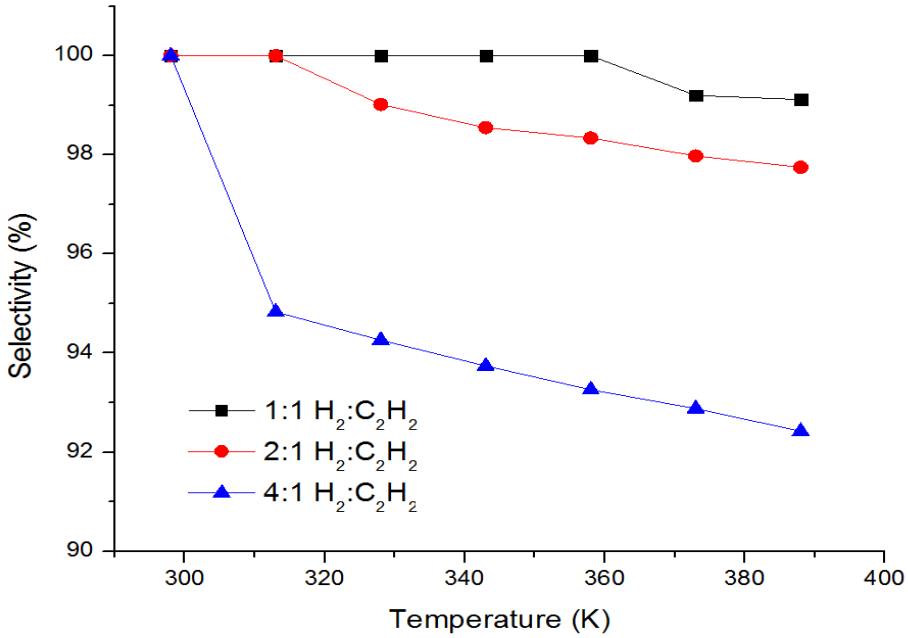

Figure 4.27: Selectivity of Ethylene using the PdAu-PE-MCM-41-W Catalyst

Upon switching to the ethanol washed catalyst, PdAu-PE-MCM-41-Et, conversion only reached 45% at one to one ratio of hydrogen to acetylene while maintaining a high selectivity of 92% at 388 K. By increasing the ratio, the conversion reached 100%, but the selectivity was found to suffer reaching just under 80%, as seen in Figure 4.28 and Figure 4.29. However, it is observed that the selectivity was found to increase with an increase in conversion from 343 K to 388 K. This effect can be attributed to the electronic properties of palladium-gold catalyst and the impact of the $CTMA^+$ through a stronger electrostatic interaction.

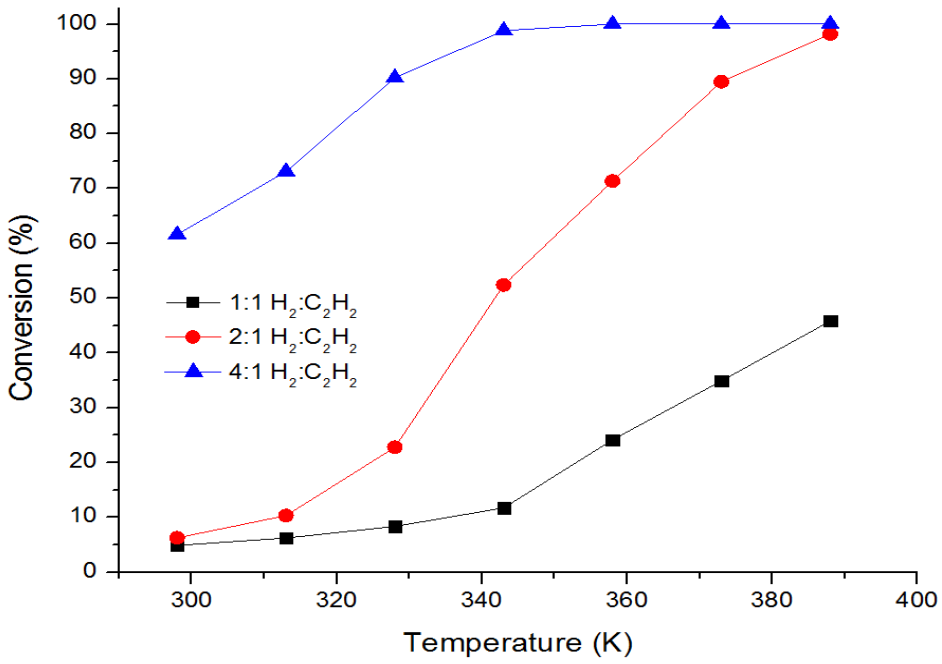

Figure 4.28: Conversion of Acetylene using the PdAu-PE-MCM-41-Et Catalyst

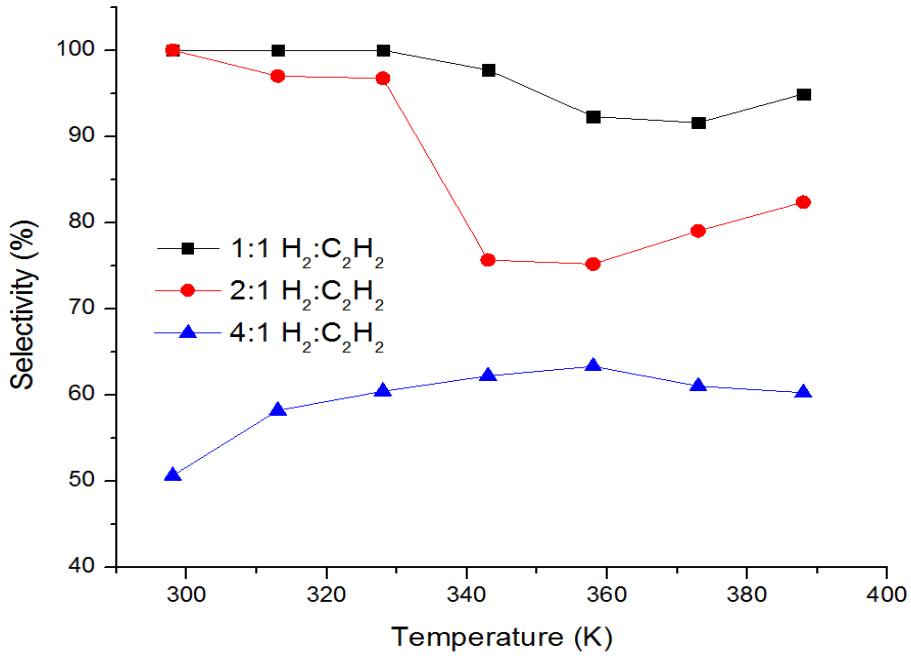

Figure 4.29: Selectivity of Ethylene using the PdAu-PE-MCM-41-Et Catalyst

The catalysts were then calcined upon treatment at 550 °C, and this catalyst was found to have better conversion and selectivity than the ethanol washed catalyst. It was found that PE-MCM-41-CR only reached 23% conversion in a one to one ratio, but upon switching to a 2:1 and a 4:1 ratio of hydrogen to acetylene, the conversions were found to be significantly increased, as seen in Figures 4.30 and 4.31. In comparison to the ethanol washed catalyst, all of the textural properties (surface area, pore size, etc) were increased, allowing for a much more reactive species, thus generating higher selectivities.

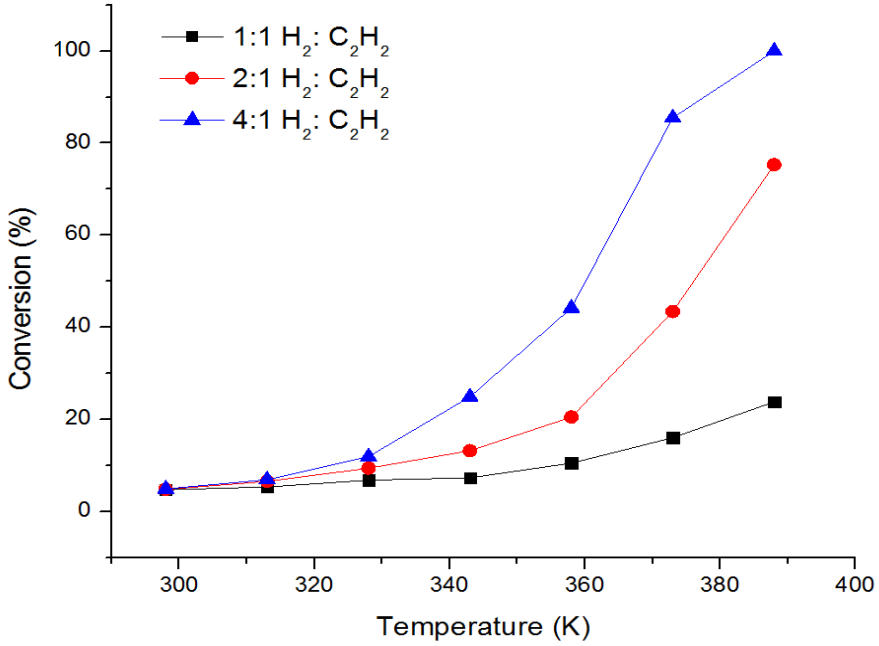

Figure 4.30: Conversion of Acetylene using the PdAu-PE-MCM-41-CR Catalyst

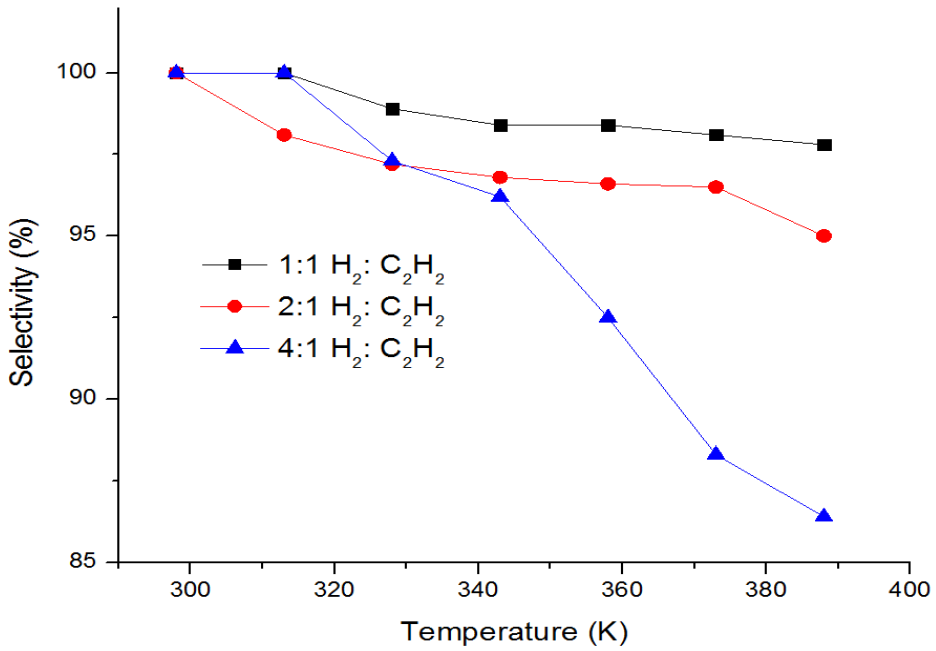

Figure 4.31: Selectivity of Ethylene using the PdAu-PE-MCM-41-CR Catalyst

The deactivation of the PdAu catalysts was studied and it was found that the conversion was maintained while it was found that selectivity was starting to drop slightly at 12 hours, as shown in Figure 4.32. This can be due to carbonaceous deposits or sintering of the nanoparticles, although temperatures would be too low for aggregation of the particles via sintering. This means the catalysts do not go under a deactivation mechanism via the formation of carbonaceous deposits, green oil, or the over hydrogenation of acetylene to ethane. If carbonaceous deposits were present on the catalyst, there would have be a significant change in both the conversion and selectivity towards ethylene.

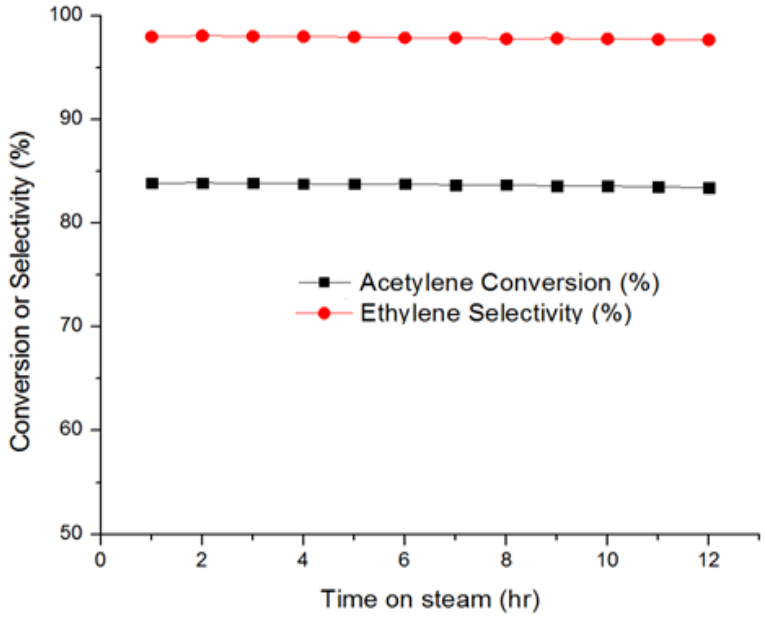

Figure 4.32: TOS of PdAu-PE-MCM-41-W at 2:1 H_2:C_2H_2 at 373 K

Even though it is important to explain and compare the catalysts in terms of conversion and selectivity, it is also important to understand the apparent activation of the energy required for the catalytic activity. As explained in Section 4.3, apparent activation energy is the amount of energy required to surpass the barrier needed to complete the reaction. However, this number does not represent the true value of hydrogenation reactions (40-44 kJ/mol), but it may give an indication that this reactions activation energy is much lower. The apparent activation energy barrier is lowered via the introduction of a catalyst by lowering the minimum kinetic energy that is required in order for the reaction to proceed. By doing so, this will increase the number of collisions that will occur with the required kinetic energy, which will help create product molecules that can be separated from the catalyst. The linear form for the Arrhenius equation was plotted, as seen in Figures 4.33-4.35 and the apparent activation energies were determined, as shown in Table 4.10.

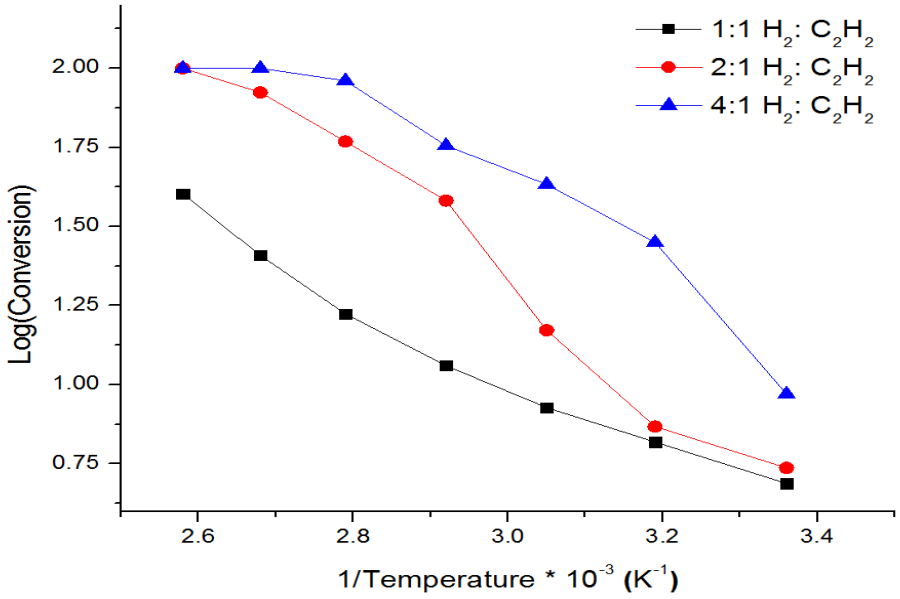

Figure 4.33: Log (Conversion) Vs. 1/T for the PdAu-PE-MCM-41-W Catalyst

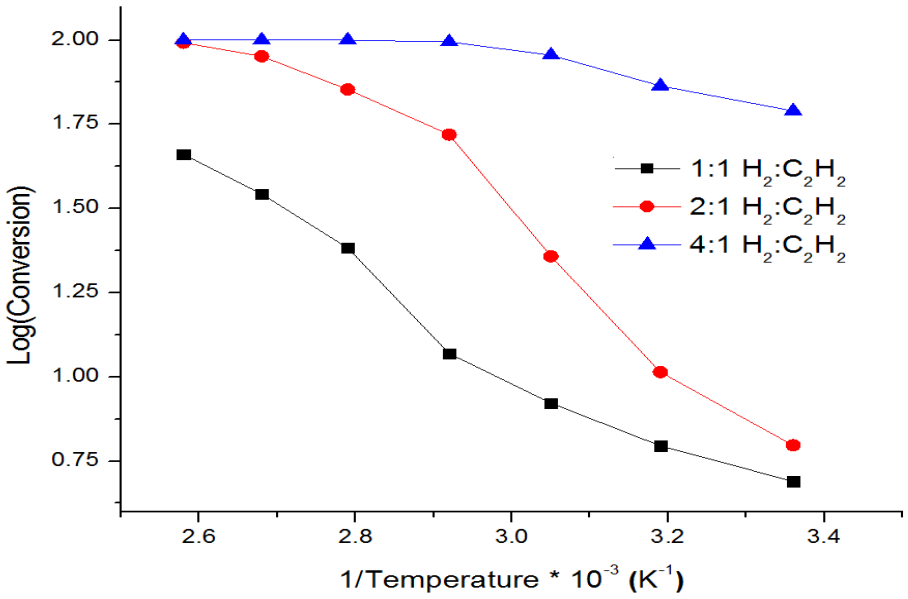

Figure 4.34: Log (Conversion) Vs. 1/T for the PdAu-PE-MCM-41-Et Catalyst

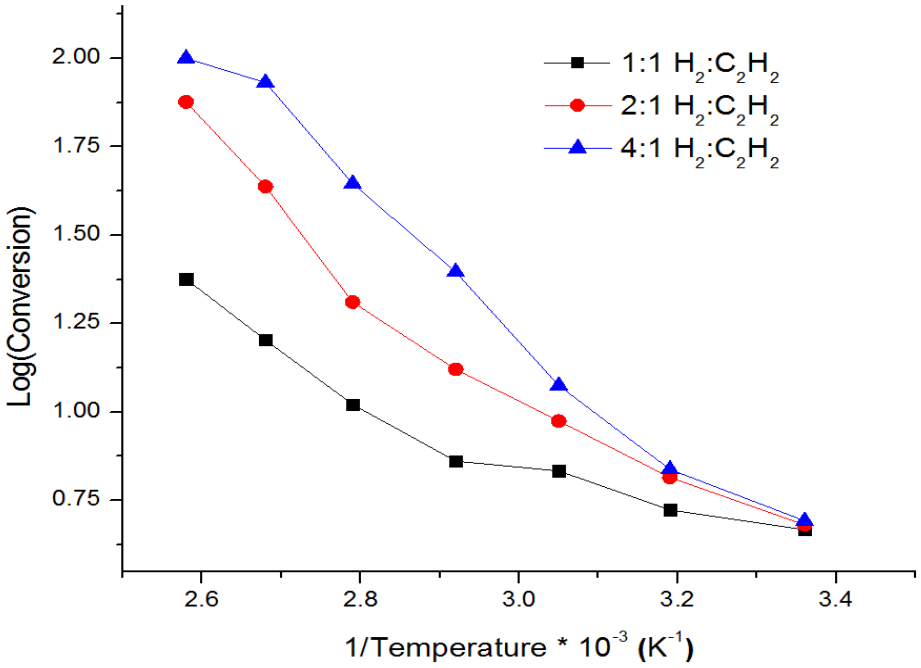

Figure 4.35: Log (Conversion) Vs. 1/T for the PdAu-PE-MCM-41-CR Catalyst

From the tabulated apparent activation energies, it is seen that as the conversion is increased, the higher the apparent activation energy is, which describes the kinetic energy of the reactants that are needed to complete this reaction. This shows that the PE-MCM-41-W catalyst required the most amount of energy in the 2:1 ratio of hydrogen to acetylene since it achieved the highest conversion. By comparing the PdAu activation energies to the Pd activation energies, it can be seen that the PdAu activation energies were much higher as the slopes were much greater. This is based on the vast increase in the conversion of these catalysts due to the higher overall conversions of the Pd-PE-MCM-41 catalysts. Even though the apparent activation energies were closer to the true values of activation energy, they are still under estimated by about 50% and must be further improved on.

One aspect that is not taken into account for these catalysts is the selectivity achieved in the catalytic reaction. In order to account for the selectivity in these reactions, the percent yields were looked at as both selectivity and conversion must be considered.

Table 4.10: Calculated Activation Energies of the Supported PdAu Catalysts

	PdAu-PE-MCM-41-W	PdAu-PE-MCM-41-Et	PdAu-PE-MCM-41-CR
1:1 H_2: C_2H_2	14.1	16.2	10.8
2:1 H_2: C_2H_2	22.0	20.3	18.4
4:1 H_2: C_2H_2	****	****	22.4

****Cannot be calculated due to non-linear behaviour. All values reported in kJ/mol.**

Another way to compare the activity of the catalysts is through the overall percent yield of acetylene to ethylene. The percent yield is calculated by multiplying the conversion by the selectivity. For the catalyst PdAu-PE-MCM-41-W, it can be seen that the percent yields were much higher, reaching as high as 97.8% due to the increased electron density. The increase in selectivity from the monometallic palladium catalyst is due to the decrease in the number of sites available for the formation of the beta palladium hydride. As well, there was also a decrease in the number of multi-coordination sites available, attributing to the presence of gold and the formation of a bimetallic palladium-gold alloy.

The catalysts TOF are shown below in Figures 4.36-4.38. The TOF is the calculated activity of the catalysts per time unit, which based on the number of surface atoms. This will help to compare the activity of the catalysts at different temperatures. From this, it can be seen that the TOF of the Pd-PE-MCM-41 catalysts are significantly higher than the PdAu-PE-MCM-41 catalysts. This is due to the amount of gold used in each reaction is taken into

consideration and calculated in the TOF. However, since gold does not contribute to the overall conversion, as demonstrated by using Au-PE-MCM-41 catalysts, it would be best to compare the overall TOFs using only Pd of both Pd-PE-MCM-41 and PdAu-PE-MCM-41 catalysts. By doing so, the overall numbers were very similar to that of Pd-PE-MCM-41, thus meaning that no significant change to the TOF was achieved upon the introduction of gold into the palladium matrix in PE-MCM-41.

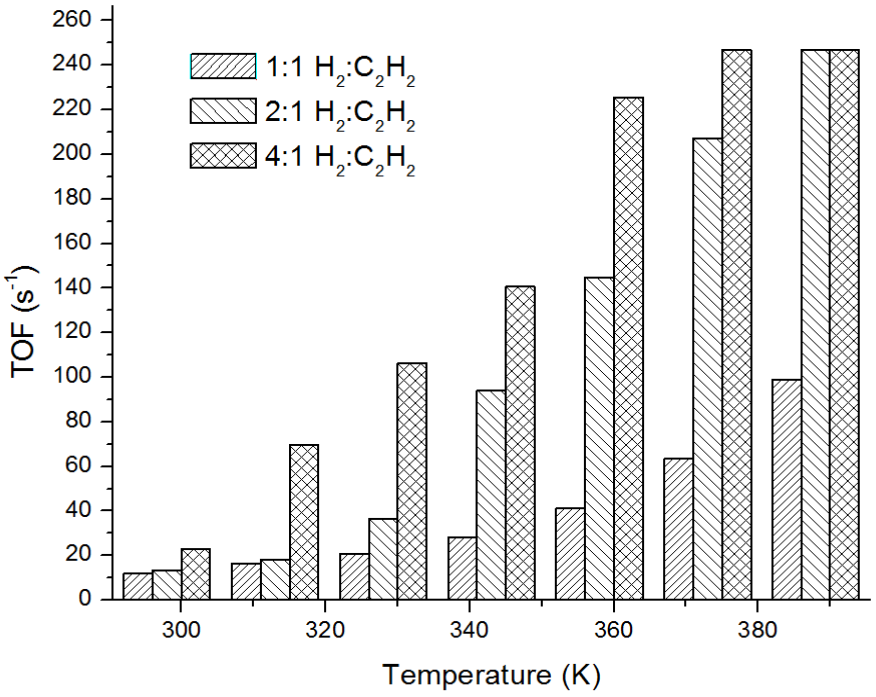

Figure 4.36: Calculated TOF for the Catalyst PdAu-PE-MCM-41-W

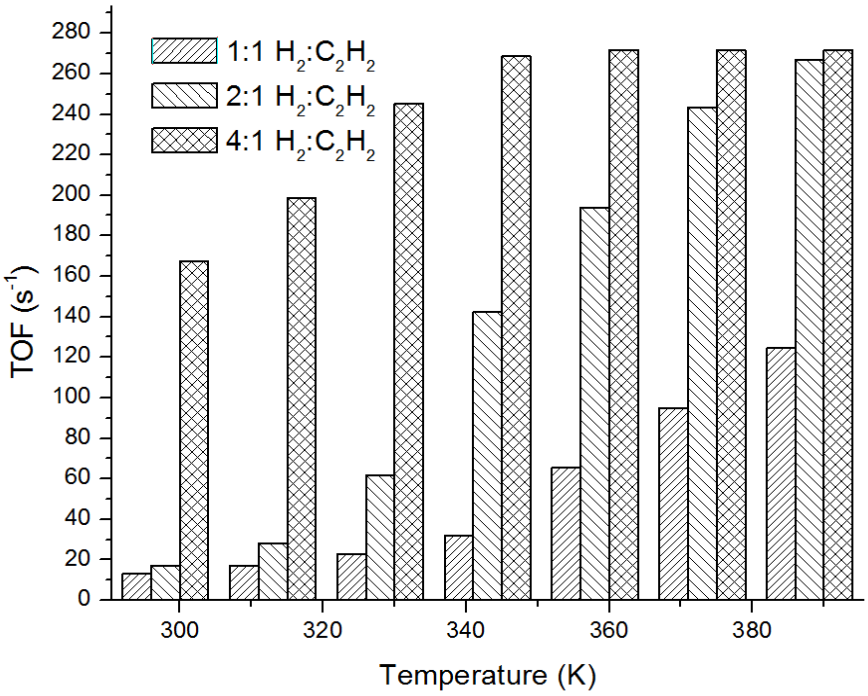

Figure 4.37: Calculated TOF for the Catalyst PdAu-PE-MCM-41-Et

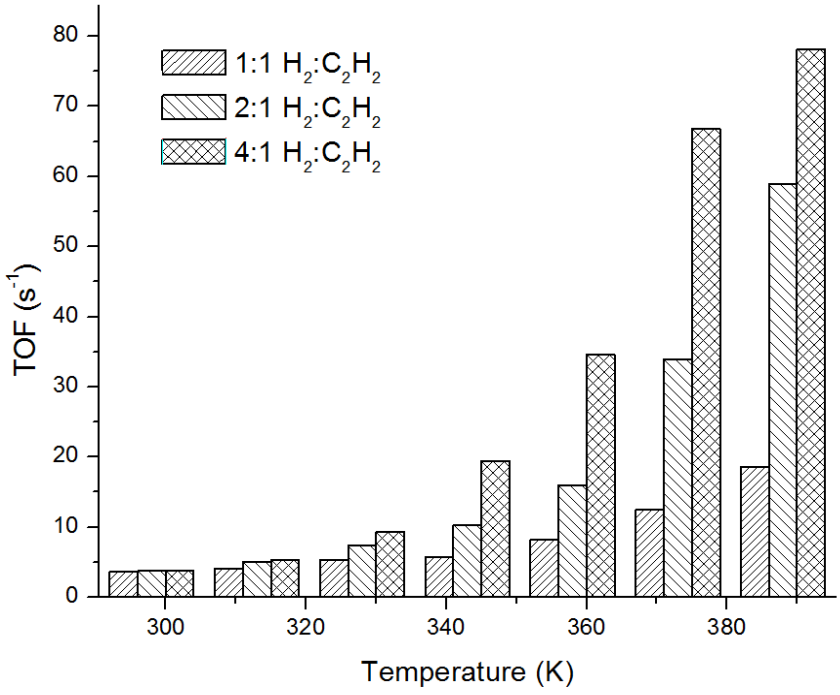

Figure 4.38: Calculated TOF for the Catalyst PdAu-PE-MCM-41-CR

From these results it can be seen that the activity of the catalyst Pd-PE-MCM-41-W shows much higher activity due to the role of DMDA in which the electron density of palladium is increased. However, when comparing the TOF of the PdAu-PE-MCM-41-W to the catalyst PdAu-PE-MCM-41-Et, there is not much difference between the two except for the fact that the four to one ratio of hydrogen to acetylene rises much faster due to the high conversion at lower temperatures. The water washed catalyst is reported at just over 250 s^{-1} at its highest conversion, while the ethanol washed showed a TOF of 275 s^{-1}. The difference is attributed not only to the metal loading of the catalyst, but also to metal dispersion. But one thing that the TOF does not take into account is the selectivity as the water washed catalyst selectivity reached 92% while the ethanol washed catalyst reached as low at 50%. Therefore, both must be taken into account when comparing. The calcined catalyst, however, showed very little activity at low temperatures, but began to achieve high conversions at high temperatures (388 K) in the two to one ratio of hydrogen to acetylene. Upon switching to the four to one ratio, the TOFs steadily increased, reaching a maximum of 80 s^{-1}. It should be noted that the reason for the significant decrease in the TOF values is due to the gold loading in the bimetallic Pd-Au supported catalysts. However, the gold nanoparticles do not contribute significantly towards the TOFs and may not need to be included in the calculation.

Chapter 5: Conclusions and Future Work

5.1 Conclusion

The selective hydrogenation of acetylene has been a key industrial reaction for the mass production and purification of ethylene. However, many problems were found with the catalysts used for this reaction including deactivation, formation of side products including green oil, both selectivity and conversion issues, and energy consumption. In order to help overcome these issues, both monometallic and bimetallic species were supported on PE-MCM-41-W, PE-MCM-41-Et, and PE-MCM-41-CR.

The two surfactants with PE-MCM-41, DMDA and $CTMA^+$, are proposed to repel each other, allowing easier access for the palladium nanoparticles into the pores. They create a channel in which the metallic cations interact strongly with the amine functionalities, thus driving the palladium nanoparticles into the pores. The presence of DMDA has been shown to have a positive influence on the catalytic performance of acetylene

First and foremost, group X (Ni, Pt, Pd) elements have been shown to be excellent catalysts, particular in hydrogenation reactions. For that reason the use of palladium supported nanoparticles were studied. The catalysts Pd-PE-MCM-41-W, Pd-PE-MCM-41-Et, and Pd-PE-MCM-41-CR were characterized and were found to have large pore sizes, surface areas, and pore volumes. The reactions were carried out via a flow-through reactor using a mixture of three gases: nitrogen, acetylene, and 10% hydrogen in nitrogen flowing at 80 mL/minute. The hydrogenation reaction was run with 2% acetylene and the remaining gas mixture using increasing amounts of hydrogen to acetylene (1, 2, and 4). The catalyst Pd-PE-MCM-41-W showed insufficient activity at the one to one ratio, while maintaining good

selectivity. Upon increasing the hydrogen to acetylene ratio, the conversion increased substantially, reaching 100% conversion at high temperatures. However, the selectivity suffered when the ratio was increased, particularly in the four to one ratio of hydrogen to acetylene, reaching as low as 93% at high conversion. The catalyst Pd-PE-MCM-41-Et again showed insufficient activity at equal concentrations of hydrogen and acetylene. However, the conversion was much lower, as compared to the Pd-PE-MCM-41-W. The presence of DMDA has been shown to have a positive influence on the catalytic performance of acetylene. This shows that DMDA played a key role in the selective hydrogenation to acetylene, likely due to the increased electron density. Upon increasing the hydrogen to acetylene ratio, the conversion was seen to reach ~100% at high temperatures in the 4:1 ratio. However, the selectivity decreased to just under 60%. This decrease was much more drastic than that of the water washed catalysts. This is likely due to the weakening of the repulsion forces, creating a harder path to selectively hydrogenate acetylene. Finally the catalyst, Pd-PE-MCM-41, was investigated in order to see the effect of no surfactants in the support and what role they played in the catalytic behaviour. The one to one ratio of hydrogen to acetylene showed little activity, barely reaching 20% conversion with high selectivity. However, upon increasing the hydrogen concentration, the conversions increased significantly upon introduction to higher temperatures. Even though the conversions were high, the selectivities suffered since there are no repulsive forces to prevent from reaching the palladium active sites. Furthermore, the TOF were then determined and they were found to reach approximately 10 s^{-1} for the Pd-PE-MCM—41-W catalyst, while both the Pd-PE-MCM-41-Et and Pd-PE-MCM-41-CR catalysts showed an activity just over 9 s^{-1} at high conversion.

In terms of the supported gold catalysts, it was shown that loading of gold was very difficult due to minimal adsorption with long alkyl chain amines. This resulted in the DMDA not creating a driving force to deposit the gold ions into the pores. The catalysis results were shown to not be very active. One hypothesis is that due to the expected particle size of greater than 10 nm, it is also expected that gold was inactive since gold has found to be active in the 2-5 nm range.

Finally, the palladium-gold bimetallic supported catalysts were explored in order to see the effects of alloying and to address low selectivity issues. The catalyst PdAu-PE-MCM-41-W showed a conversion of only 40% at a 1:1 ratio of H_2/C_2H_2. This is likely due to not enough hydrogen molecules being able to attach to the palladium-gold active sites. Upon increasing the ratio of hydrogen to acetylene, a much higher conversion was able to be achieved at higher temperatures (100% conversion) while maintaining very high selectivities. The selectivities at 388 K were found to be 98% and 92% for the two to one and four to one ratios of hydrogen to acetylene, respectively. Upon ethanol extraction of the DMDA from within the pores, the selectivity was found to substantially drop while maintaining high conversion. This is clearly seen to be the effect of DMDA on the conversion and the selectivity. The catalyst was then calcined at high temperature in order to remove the remaining $CTMA^+$. From the conversion and selectivity, it can clearly be seen that $CTMA^+$ does not play a significant role in either the selectivity or the conversion. In fact, upon the removal of $CTMA^+$, it was shown that the selectivity of 71% was increased to a selectivity of 86% at 100% conversion. The TOF of the catalysts were then calculated by assuming that only palladium adsorbed hydrogen, which was shown in the chemisorption of the gold supported catalysts.

5.2 Future Work

Even though a vast amount of work was undertaken and completed, a lot of possibilities still remain with regards to this project. With regard to the palladium catalysts, the first issue to be addressed would be to optimize the loading of the catalysts with the palladium salt, K_2PdCl_4. This would help to eliminate unnecessary costs, thus providing a more valuable catalyst for possible industrial use. The next piece of work that needs to be completed would be to see if there is an effect on the method of preparation of the catalysts. The technique used in the current study was complexation, but other techniques, such as adsorption from solution, co-precipitation, and chemical vapour deposition have been used. This should be explored in order to be able to control the particle size of the palladium nanoparticles. Another possibility would be to prepare the support, with palladium as part of the support. Adding in acidic or basic sites through the addition of other elements, such as aluminum oxide, would be interesting to determine the effect the basicity or acidity would have on the catalytic results. The deactivation rate and catalyst regeneration should be looked at to see how viable this catalyst might be.

In terms of characterization of the catalysts, many other techniques should be completed. The effect of particle size must be understood, and therefore, TEM of the remaining catalysts must be completed. The TEM, or STEM, of the reduced and spent catalysts should be studied in order to see the effect of the catalytic process on the metallic nanoparticles. As well, TEMs should be completed on the regenerated catalysts to see if the regeneration process is viable.

In order to accurately determine the effects of DMDA, one thing that must be done is that the calcined PE-MCM-41 should be grafted with DMDA. Different ratios of grafted DMDA should also be completed. Once grafted, the silica should be loaded with palladium and the catalytic reactions must be run. The grafted amines should also be loaded with palladium and group X (Ni, Pt, Pd) elements, to form a bimetallic alloy and the hydrogenation of acetylene using these catalysts should be run.

Finally, the effects of the support and the physical properties of it must be understood. The effect of the structural properties, such as pore size, pore volume, and surface area must be understood. One way to do this would be to alter these properties. Varying surfactant or co-surfactant lengths as well as the introduction of auxillary organics, which will cause the pore size to swell, can alter the physical properties. Furthermore, different types of silica supports should be tested and understood. For example, the use of SBA-15 instead of MCM-41 should be studied. Finally, the morphological effects must be understood; therefore, the different shapes of the M41S family should be explored including MCM-48 and MCM-50.

In terms of the gold supported catalysts, the first thing that must be considered should be particle size and particle size distribution. Upon the determination of the metallic particle size, a method or technique must be developed in order to control particle size as it typically needs to be between 2-5 nm to be active, otherwise it will possess the properties of bulk gold.

In terms of the supported bimetallic palladium-gold system, there is much work to be completed. Since PdAu supported catalysts were such a success, they must be further understood. First and foremost, the catalysts must be characterized in terms of TEM to

determine their particle size distribution. Furthermore, the reaction conditions must be optimized, particularly regarding the loading of both metals and the amount of catalyst used. Finally, since gold is one of the most expensive metals and its cost is continually rising, the use of other metals and enhancers should be considered. One such example would be to use either silver or copper instead of gold to significantly reduce the costs but hopefully maintain similar activity and selectivity.

Finally, when dealing with bimetallic alloys, it is important to understand if an alloy was formed or if they are two separate monometallic species. Two such ways are through x-ray photoelectron spectroscopy (XPS) and x-ray diffraction (XRD). XPS analyzes the surface and its elements can be detected. By comparing the electron volts of both metals separately, it should be evident on whether a charge transfer occurred, resulting in the formation of an alloy. XRD of the bimetallic species should clearly show different peaks than that of the two separate monometallic species, indicating an alloy was formed. However, the ratio between the bimetallic must be greater than 1:1 to determine if an alloy was formed.

.

References

1) Huang, W.; Pyrz, W.; Lobo, R. F.; Chen, J. G. *Appl. Catal., A.* **2007,** *333,* 254

2) Chen, J. Q.; Bozzano, A.; Glover, B.; Fuglerud, T.; Kvisle, S. *Catal. Today* **2005,** *106,* 103

3) Kim, W. J.; Moon, S. H. *Catal. Today* **2012,** *185,* 2.

4) Liu, J.; Yang, Q.; Zhao, X.S.; Zhang, L. *Microporous Mesoporous Mater.* **2007**, *106,* 62.

5) Williford, R. E.; Li, X. S.; Addleman, R. S.; Fryxell, G. E.; Baskaran, S.; Birnbaum, J. C.; Coyle, C.; Zemanian, T.S.; Wang, C.; Courtney, A.R. *Microporous Mesoporous Mater.* **2005**, *85,* 260.

6) Rouquerol, J.; Avnir, D.; Fairbridge, C.W.; Everett, D.H.; Haynes, J.H.; Pernicone, N.; Ramsay, J.D.F; Sing, K.S.W.; Unger, K.K. *Pure Appl. Chem.* **1994**, *66,* 1739.

7) Sing, K. S.W.; Everett, D.H.; Haul, R.H.W.; Moscou, L.; Pierotti, R.A.; Rouquerol, J.; Siemieniewska, T. *Pure Appl. Chem.* **1985,** *57,* 603.

8) He, Z.; Zhu, Z.; Li, J.; Zhou, J.; Wei, N. *J. Hazard. Mater.* **2011,** *190,* 133.

9) Kresge, C. T.; Leonowicz, M. E.; Roth, W. J.; Vartuli, J. C.; Beck, J. S. *Nature* **1992,** *359,* 710.

10) Pinnavaia, T. J. *Science* **1983,** *220,* 365.

11) Mastalir, A.; Rac, B.; Kiraly, Z.; Molnar, A. *J. Mol. Catal. A: Chem.* **2007,** *264,* 170.

12) Papp, A.; Molnar, A.; Mastalir, A. *Appl. Catal. A.* **2005,** *289,* 256.

13) Sobczak, I. *Catal. Today* **2009,** *142,* 258.

14) Panpranot, J.; Pattamakomsan, K.; Goodwin Jr, J. G.; Praserthdam, P. *Catal. Commun.* **2004,** *5,* 583.

15) Joseph, T.; Kumar, K. V.; Ramaswamy, A. V.; Halligudi, S. B. *Catal. Commun.* **2007,** *8,* 629.

16) Das, D. D.; Sayari, A. *J. Catal.* **2007,** *246,* 60.

17) Zhao, X. S.; Lu, G. Q. *J. Phys. Chem. B.* **1998,** *102,* 1556.

18) Belmabkhout, Y.; Guerrero, R. S.; Sayari, A. *Adsorption* **2011,** *17,* 395.

19) Miyamoto, M.; Takayama, A.; Uemiya, S.; Yogo, K. *J. Chem. Eng. Jpn.* **2012,** *45,*395.

20) Liu, X.; Du, Y.; Guo, Z.; Gunasekaran, S.; Ching, C. B.; Chen, Y.; Leong, S. S. J.; Yang, Y. *Microporous Mesoporous Mater.* **2009,** *122,* 114.

21) Spange, S.; Graser, A.; Muller, H.; Zimmermann, Y.; Rehak, P.; Jager, C.; Fuess, H.; Baehtz, C. *Chem Mater.* **2001,** *13,* 3698

22) Wan, Y.; Yang, H.; Zhao, D. *Acc. Chem. Res.* **2006,** *39,* 423.

23) Davis, M. E.; Lobo, R. F. *Chem. Mater.* **1992,** *4,* 756.

24) Aguiar, P. M. R. M.D.; Novaes, A. C.; Guarino, A. W. S. *Quim Nova.* **2002,** *25,* 1145

25) Selvam, P.; Bhatia, S. K.; Sonwane, C. G. *Ind. Eng. Chem. Res.* **2001,** *40,* 3237**.**

26) Koh, C. A.; Nooney, R.; Tahir, S. *Catal. Lett.* **1997,** *47,* 199.

27) Liu, J.; Yang, Q.; Zhao, X. S.; Zhang, L. *Microporous Mesoporous Mater.* **2007,** *106,* 62.

28) Liu, S.; Cool, P.; Collart, O.; Van Der Voort, P.; Vansant, E. F.; Lebedev, O. I.; Van Tendeloo, G.; Jiang, M. *J. Phys. Chem. B.* **2003**, *107,* 10405

29) Diaz, I.; Alvarez, C. M.; Mohino, F.; Pariente, J. P.; Sastre, E. *Microporous Mesoporous Mater.* ***2001,*** *44,* 295.

30) Marler, B.; Oberhagemann, U.; Vortmann, S.; Gies, H. *Microporous Mater.* **1996,** *6,* 375.

31) Pacheco, G.; Zhao, E.; Garcia, A.; Sklyarov, A.; Fripiat, J. J. *J. Mater. Chem.* **1998,** *8,* 219.

32) Schuth, F. *Chem. Mater.* **2001,** *13,* 3184.

33) Vaudry, F.; Khodabandeh, S.; Davis, M. E. *Chem. Mater.* **1996,** *8,* 1451.

34) Zhao, E.; Hardcastle, S. E.; Pacheco, G.; Garcia, A.; Blumenfeld, A. L.; Fripiat, J. J. *Microporous Mesoporous Mater.* **1999,** *31,* 9.

35) Tanev, P. T.; Pinnavaia, J. T. *Science* **1995,** *267,* 865.

36) Zhang, W.; Froba, M.; Wang, J.; Tanev, P. T.; Wong, J.; Pinnavaia, J. T. *J. Am. Chem. Soc.* **1996,** *118,* 9164.

37) Patarin, J.; Lebeau, B.; Zana, R. *Curr. Opin. Colloid Interface Sci.* **2002,** *7,* 107.

38) Sousa, A. D; Souza, K.C.D.; Mohallem, N. D.S.; Sousa, R.G.D; Sousa, E. M. B. *Advances in Diverse Industrial Applications of Nanocomposites*.Ch.9 Pp.178 Intech. Rijeka, Croatia. **2011.**

39) Windsor, P.A.; Gray, G. W. *Liquid Crystals and Plastic Crystals*, vol. 1. Ellis Horwood, Chichester, **1974**.

40) Ekwall, P. Brown, G. H. (Ed.) *Advances in Liquid Crystals,* vol.1, Academic, New York, **1975**.

41) Quo, H.; Margolese, D. I.; Stucky, G. D. *Chem. Mater.* **1996,** *8,* 1147.

42) Richer, R.; Mercier, L. *Chem. Mater.* **2001,** *13,* 2999.

43) Soller-Illia, G. J. A. A.; Sanchez, C.; Lebeau, B.; Patarin, J. *Chem. Rev.* **2002,** *102,* 4093

44) Beck, J. S.; Vartulia, J. C.; Roth, W. J.; Leonowicz, M. E.; Kresge, C. T.; Schmitt, K. D.; Chu, C. T. W.; Olson, D. H.; Sheppard, E. W.; McCullen, S. B.; Higgins, J. B.; Schlenker, J. L. *J. Am. Chem. Soc.* **1992,** *114,* 10834.

45) Stucky, G. D.; Monnier, A.; Schuth, F.; Huo, Q.; Margolese, D.; Kumar, D.; Krishnamurty, M.; Petroff, P.; Firouzi, A.; Janicke, M.; Chmelka, B. F. *Mol. Cryst.. Liq. Cryst.* **1994,** *240,* 187.

46) Huo, Q.; Margolese, D. I.; Stucky, G. D.; *Chem. Mater.* **1996,** *8,* 1147.

47) Zhang, J.; Luz, Z.; Goldfarb, D. *J. Phys. Chem. B.* **1997,** *101,* 7087.

48) Monnier, A.; Schuth, F.; Huo, Q.; Kumar, D.; Margolese, D.; Maxwell, R. S.; Stucky, G. D.; Krishnamurty, M.; Petroff, P.; Firouzi, A.; Janicke, M.; Chmelka, B. F. *Science* **1993,** *261,* 1299

49) Lin, H. P.; Mou, C. Y. *Acc. Chem. Res.* **2002,** *35,* 927.

50) Kim, J. M.; Sakamoto, Y.; Hwang, Y. K.; Kwon, Y. U.; Terasaki, O.; Park, S. E.; Stucky, G. D. *J. Phys. Chem. B.* **2002,** *106,* 2552.

51) Campos, J. M.; Lourenco, J. P.; Cramail, H.; Ribeiro, M.R. *Prog. Polym. Sci.* **2012**, *37,* 1764.

52) Hoffmann, F.; Cornelius, M.; Morell, J.; Froba, M. *Angew. Chem. Int. Ed.* **2006,** *45,* 3216.

53) Sattler, K. D. *Handbook of Nanophysics: Functional Nanomaterials* CRC Press. Florida, **2011**.

54) Tanev, P. T. Pinnavaia, J. T. *Chem. Mater.* **1996,** *8,* 2068.

55) Prouzet, E.; Pinnavaia, J. T. *Angew. Chem. Int. Ed.* **1997,** *36,* 516.

56) Busio, M.; Janchen, J.; Van Hoof, J. H. C. *Microporous Mater.* **1995,** *5,* 211.

57) Janicke, M. T.; Landry, C. C.; Christiansen, S. C.; Kumar, D.; Stucky, G. D.; Chmelka, B. F. *J. Am. Chem. Soc.* **1998,** *120,* 6940.

58) Chen, Y. W.; Lin, H. Y. *J. Porous Mater.* **2002,** *9,* 175.

59) Thanabodeekij, N.; Tanglumlert, W.; Gulari, E.; Wongkasemjit, S. *Appl. Organometal. Chem.* ***2005,*** *19,* 1047

60) Vartuli, J. C.; Roth, W. J.; Beck, J. S.; McCullen, S. B.; Kresge, C. T. *The Synthesis and Properties of M41S and Related Mesoporous Materials.* Vol. 1, Springer-Verlag, Berling, Germany, **1998**.

61) Kleitz, F.; Schmidt, W.; Schuth, F. *Microporous Mesoporous Mater.* **2003,** *65,* 1.

62) Mokaya, R.; Jones, W.; Luan, Z.; Alba, M. D.; Klinowski, J. *Catal. Letter.* **1996,** *37,* 113.

63) Keene, M. T. J.; Gougeon, R. D. M.; Denoyel, R.; Harris, R. K.; Rouquerol, J.; Llewellyn, P. L. *J. Mater. Chem.* **1999,** *9,* 2843.

64) Chen, C. Y.; Burkett, S.; Li, H. X.; Davis, M. E. *Microporous Mater.* **1993,** *2,* 23.

65) Kim, J. M.; Ryoo, R. *Chem. Mater.* **1999,** *11,* 487.

66) Kawi, S.; Lai, M. W. *Chem. Commun.* **1998,** 1407.

67) Lu, X. B.; Zhang, W. H.; He, R. *Chin. Chem. Lett.* **2002,** *13,* 480.

68) Buchel, G.; Denoyel, R.; Llewellyn, P. L.; Rouquerol, J. *J. Mater. Chem.* **2001,** *11,* 589.

69) Clark, T.; Ruiz, J. D.; Fan, H.; Brinker, J. C.; Swanson, B. I.; Parikh, A. N. *Chem. Mater.* **2000,** *12,* 3879.

70) Jabariyan, S.; Zanjanchi, M. A. *Ultrason. Sonochem.* **2012,** *19,* 1087.

71) Chorkendorff, I.; Niemantsverdriet, J. W. *Concepts of Modern Catalysis and Kinetics.* 2nd edition, Wiley-VCH GmbH & Co. KgaA, Weinheim, 2007.

72) Pollard, D. J.; Woodley, J. M. *Trends Biotechnol.* **2007,** *25,* 66.

73) Bornscheuer, U. T.; Kazlauskas, R. J. *Angew. Chem. Int. Ed.* **2004,** *43,* 6032.

74) Averill, B.A.; Eldredge, P. *Chemistry: Principles, Patterns, and Applications.* 1st edition. Pearson Benjamin Cummings. **2007**

75) Vasudevan, D. M.; Sreekumari, S.; Vaidyanathan, K. *Textbook of Biochemistry for Dental Students.* 2nd edition, Jaypee Brothers Medical Publishers Ltd. New Delhi, India, **2011**.

76) Gonzalo, D. G.; Mihovilovic, M. D.; Fraaije, M. W. *Chembiochem* **2010,** *11,* 2208.

77) Trost, B. M. *Angew. Chem. Int. Ed.* **1995,** *34,* 259.

78) McElroy, M. B.; Salawitch, R. J.; Wofsy, S. C.; Logan, J. A. *Nature* **1986,** *321,* 759.

79) Hutchings, G. J. *J. Mater. Chem.* **2009,** *19,* 1222.

80) Marnellos, G.; Stoukides, M. *Nature* **1998,** *282,* 98.

81) Erisman, J. W.; Sutton, M. A.; Galloway, J.; Klimont, Z.; Winiwarter, W. *Nat. Geosci.* **2008,** *1,* 636.

82) Hvolbaek, B.; Janssens, T. V. W.; Clausen, B. S.; Falsig, H.; Christensen, C. H.; Norskov, J. K. *Nano Today* **2007,** *2,* 14.

83) Astruc, D. *Nanoparticles and Catalysis.* Wiley-VCH GmbH & Co. KgaA, Weinheim, **2008**.

84) Daniel, M. C.; Astruc, D.; *Chem. Rev.* **2004,** *104,* 293.

85) Faraday, M. *Philos. Trans.* **1857,** *151,* 183.

86) Brust, M.; Walker, M.; Bethell, D.; Schiffrin, D. J.; Whyman, R. J. *J. Chem. Soc. Chem. Commun.* **1994,** *801.*

87) Rapino, L. D.; Nord, F. F. *J. Am. Chem. Soc.* **1941,** *63,* 2745.

88) Haruta, M.; Kobayashi, T.; Sano, H.; Yamada, N. *Chem. Letter.* **1987,** *405.*

89) Haruta, M. *CATTECH* **2002,** *6,* 102.

90) Hirai, H.; Nakao, Y.; Toshima, N. J. *Macromol. Sci. Chem.* **1978,** *A12,* 1117.

91) Mu, X. D.; Evans, G. D.; Kou, Y. *Catal. Lett.* **2004,** *97,* 151.

92) Martino, A.; Yamanaka, S. A.; Kawola, J. S.; Ly, D. A. *Chem. Mater.* **1997,** *9,* 423.

93) Paulus, U. A.; Endruschat, U.; Feldmeyer, G. J.; Schmidt, T. J. *J. Catal.* **2000,** *195,* 383.

94) Papp, S.; Dekany, I. *Colloid Polym. Sci.* **2001,** *279,* 449.

95) Andres, R. P.; Bielefeld, J. D.; Henderson, J. I.; Janes, D. B.; Kolagunta, V. R.; Kubink, C. P.; Mahoney, W.; Osifchin, R. G.; Reifenberger, R. *Science* **1996,** *273,* 1690.

96) Bell, A. T. *Science* **2003,** *299,* 1688.

97) Maury, C. M.; Chizallet, C.; Sautet, P.; Raybaud, P. *ACS Catal.* **2012,** *2,* 1346.

98) Lee, D. K. *Korean J. Chem. Eng.* **1990,** *7,* 233.

99) Praserthdam, P.; Ngamsom, B.; Bogdanchikova, N.; Phatanasri, S.; Pramotthana, M. *Appl. Catal. A.* **2002,** *230,* 41.

100) Banares, M. A. *Catal. Today* **1999,** *2,* 319.

101) Albers, P.; Pietsch, J.; Parker, S. F. *J. Mol. Catal. A: Chem.* **2001,** *173,* 275.

102) Feng, X. J.; Lu, X. B.; He, R. *Appl. Catal. A.* **2004,** *28,* 347.

103) Scott, R. W. J.; Sivadinarayana, C.; Wilson, O. M.; Yan, Z.; Goodman, D. W.; Crooks, R. M. *J. Am. Chem. Soc.* **2005,** *127,* 1380.

104) Wang, K.; Chen, Y.; Li, X.; Ding, H. *Catal. Lett.* **2009,** *127,* 392.

105) Wang, H.; Wang, J. G.; Shen, Z. R.; Liu, Y. P.; Ding, D. T.; Chen, T. H. *J. Catal.* **2010,** *275,* 250.

106) Marzan, L. M. L.; Kamat, P. V. *Nanoscale Materials* Kluwer Academic Publishers. New York, Boston, Dordecht, London, Moscow, **2004.**

107) Hashmi, A. S. K; Hutchings, G. J. *Angew. Chem. Int. Ed.* **2006**, *45,* 7896.

108) Hartfelder, U.; Kartusch, C.; Makosch, M.; Rovezzi, M.; Sa, J.; Bokhoven, J. A. V. *Catal. Sci. Technol.* **2013**, *3,* 454.

109) Sarkany, A. *React. Kinet. Catal. Lett.* **2009**, *96,* 43

110) Hvolbaek, B.; Janssens, T. V. W.; Clausen, B. S.; Falsig, H.; Christensen, C. H.; Norskov, J. K. *Nano Today* **2007**, *2,* 14.

111) Gutierrez, L. F.; Hamoudi, S.; Belkacemi, K. *Catalysts.* **2011,** *1,* 97

112) Jia, J.; Haraki, K.; Kondo, J. N.; Domen, K.; Tamaru, K. *J. Phys. Chem. B.* **2000**, *104,* 11153.

113) Schwank, J. *Gold. Bull.* **1985,** *18,* 1.

114) Hutchings, G. J. *Chem. Commun.* **2008,** 1148.

115) Ksar, F.; Ramos, L.; Keita, B.; Nadjo, L.; Beaunier, P.; Remita, H. *Chem. Mater.* **2009**, *21,* 3677.

116) Evangelisti, C.; Schiavi, E.; Aronica, L. A.; Caporusso, A. M.; Vitulli, G.; Bertinetti, L.; Martra, G.; Balerna, A.; Mobilio, S. *J. Catal.* **2012,** *286,* 224.

117) Frevel, L. K.; Kressley, L. J.; *Selective Hydrogenation of Acetylene In Ethylene And Catalyst Therefor* Dow Chemical Company, **1957.**

118) Nutt, M. O.; Hughes, J. B.; Wong, M. *Environ. Sci. Technol.* **2005,** *39,* 1346.

119) Choudhary, T. V.; Sivadinarayana, C.; Datye, A. K.; Kumar, D.; Goodman, D. W. *Catal. Lett.* **2002,** *86,* 1.

120) Sayari, A.; Shee, D.; Al-Yassir, N.; Yang, Y. *Top. Catal.* **2010**, *53,* 154.

121) Sing, K. S. W. *Pure. Appl. Chem.* **1982**, *54,* 2201.

122) Brunauer, S.; Emmett, P. H.; Teller, E. *J. Am. Chem. Soc.* **1938**, *60*, 309.

123) Barrett, E. P.; Joyner, L. G.; Halenda, P. P. *J. Am. Chem. Soc.* **1951**, *73,* 373.

124) Kruk, M.; Jaroniec, M; Sayari, A. *Langmuir* **1997**, *13,* 6267.

125) Hsu, H.-C.; Shown, I.; Wei, H.-Y.; Chang, Y.-C.; Du, H.-Y.; Lin, Y.-G.; Tseng, C.-A.; Wang, C.-H.; Chen, L.-C.; Lin, Y.-C.; Chen, K.- H. *Nanoscale* **2013**, *5,* 262.

126) Scott, R. W. J.; Wilson, O. M.; Crooks, R. M. *Chem. Mater.* **2004**, *16,* 5682.

127) Zhu, H.; Qin, Z.; Shan, W.; Shen, W.; Wang, J. *J. Catal.* **2004**, *225,* 267.

128) Kim, S. K.; Kim, C.; Lee, J. H.; Kim, J.; Lee, H.; Moon, S. H. *J. Catal.* **2013**, *306,* 146.

129) Sangeetha, P.; Shanthi, K.; Rao, K. S. R.; Viswanathan, B.; Selvam, P. *Appl Catal., A.* ***2009****, 353,* 160.

130) Mostoufi, N.; Ghoorchian, A. Sotudeh-Gharebagh, R. *Int. J. Chem. Reactor Eng.* **2005**, *3,* Article A14.

131) Moulinn, J. A.; van Diepen, A. E.; Kapteijn, F.; *Appl. Catal., A.* **2001**, *212,* 3

132) Masterton, W. I.; Hurley, C. N. *Chemistry: Principles and Reactions.* Cenage Learning. Belmont, California, USA. **2009.**

133) Lewoczko, A. D.; BelBruno, J. J. *Phys. Chem. Chem. Phys.* **2013**, *15,* 4707.

134) McEwan, L.; Julius, M.; Roberts, S.; Fletcher, J. C. Q. *Gold. Bull.* **2010**, *43,* 298.